Appendix A

Motion tracking measurements results

A.1 Laser Trackers

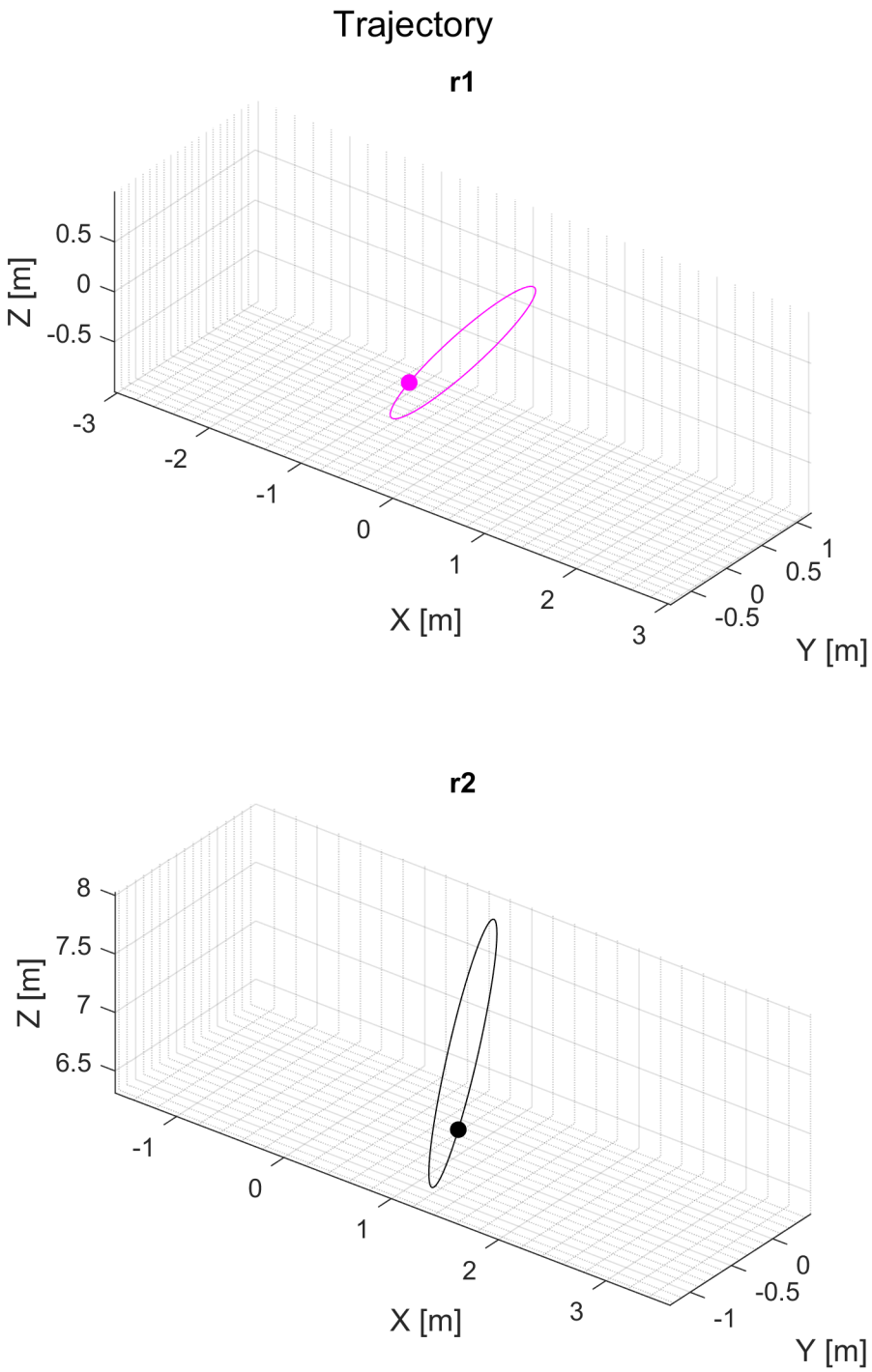

Figure A.1: Laser tracker simulation, dynamic calibration by circular movement, trajectory.

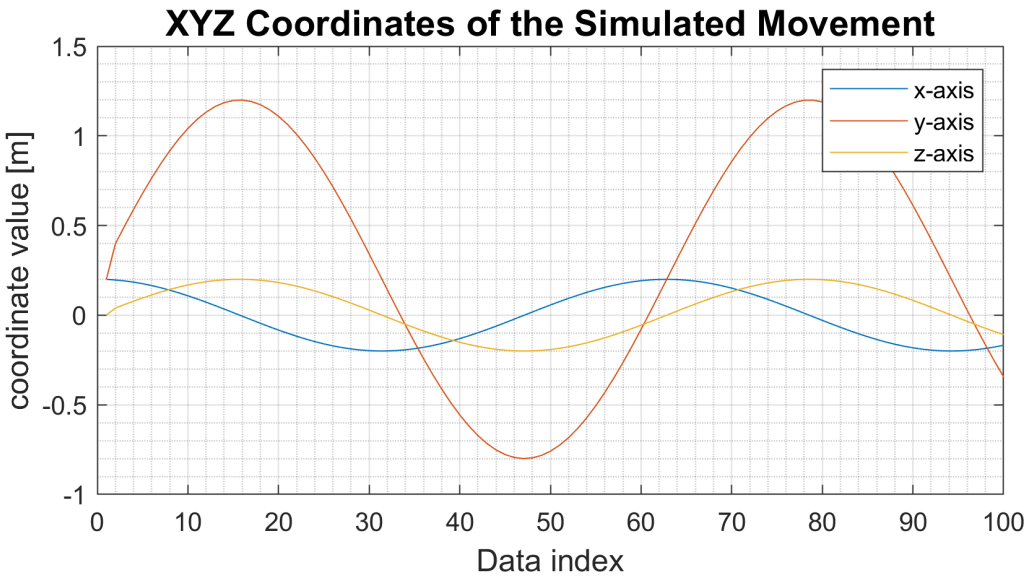

Figure A.2: Laser tracker simulation, dynamic calibration by circular movement, position vector.

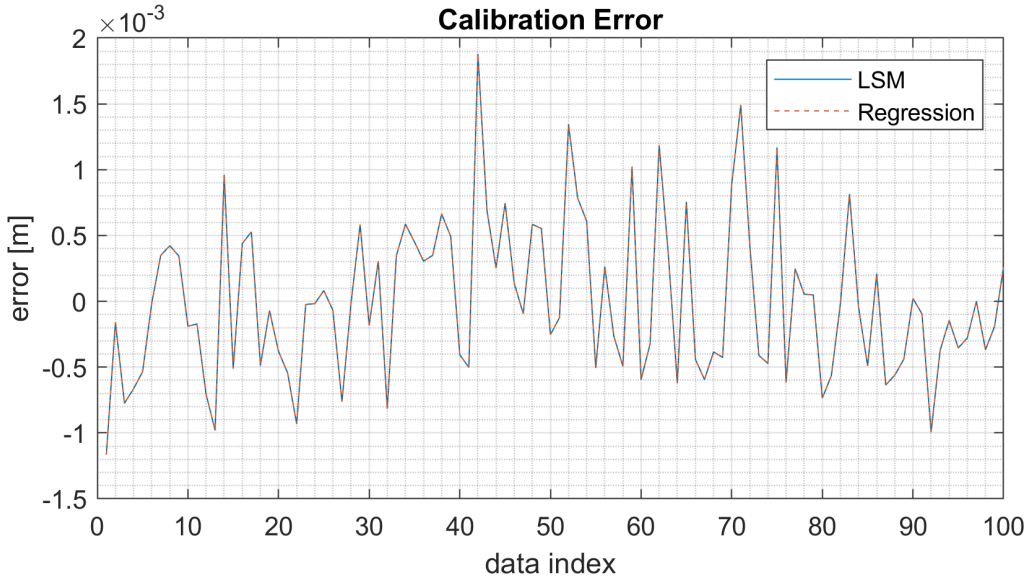

Figure A.3: Laser tracker simulation, dynamic calibration by circular movement with maximum noise, calibration error.

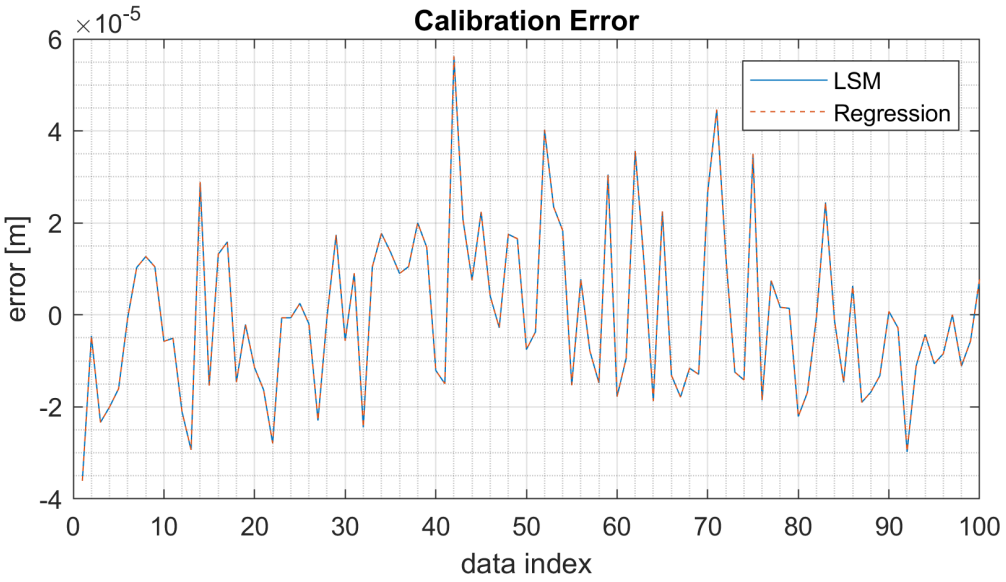

Figure A.4: Laser tracker simulation, dynamic calibration by circular movement with minimum noise, calibration error.

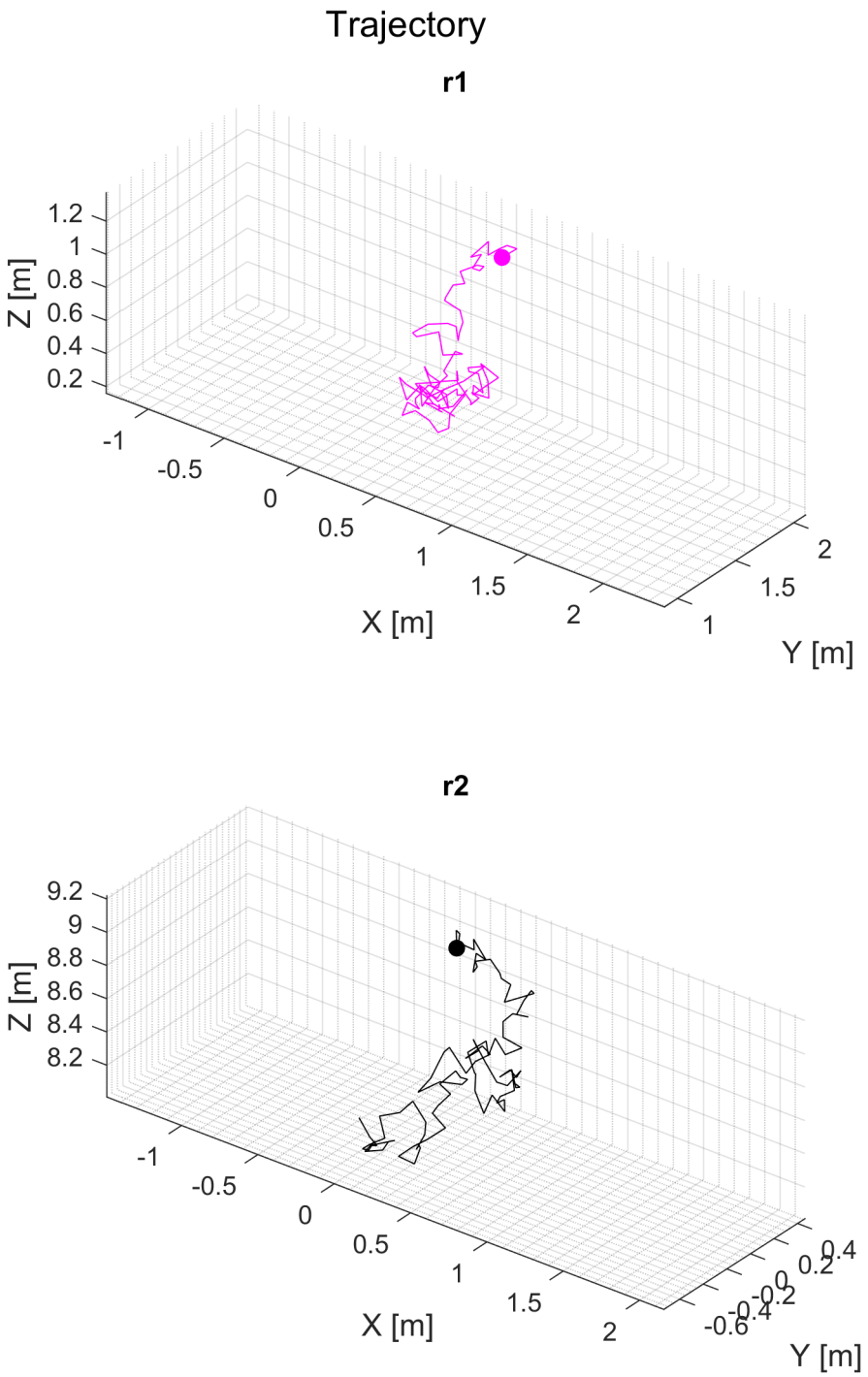

Figure A.5: Laser tracker simulation, dynamic calibration by random movement, trajectory.

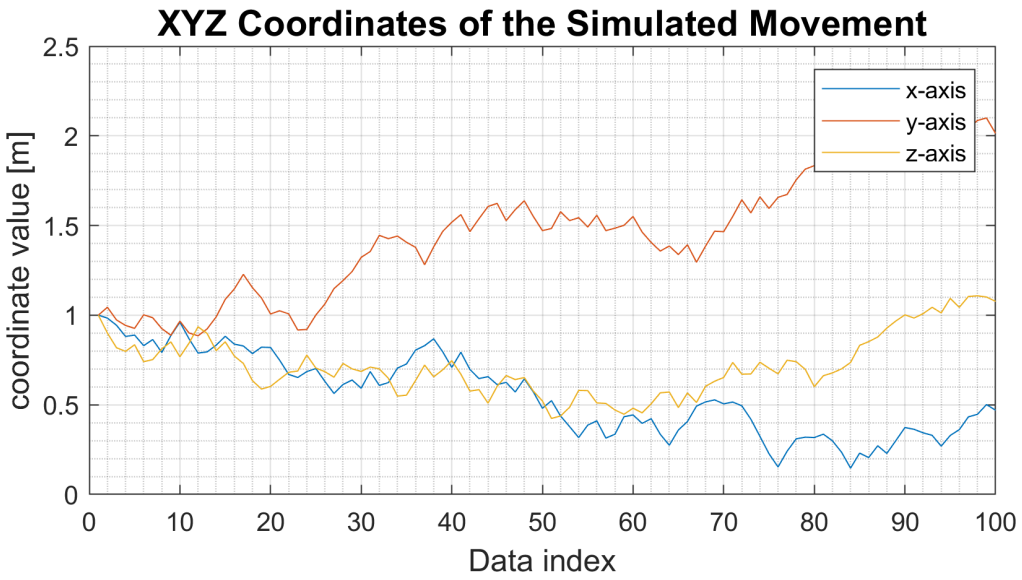

Figure A.6: Laser tracker simulation, dynamic calibration by random movement, position vector.

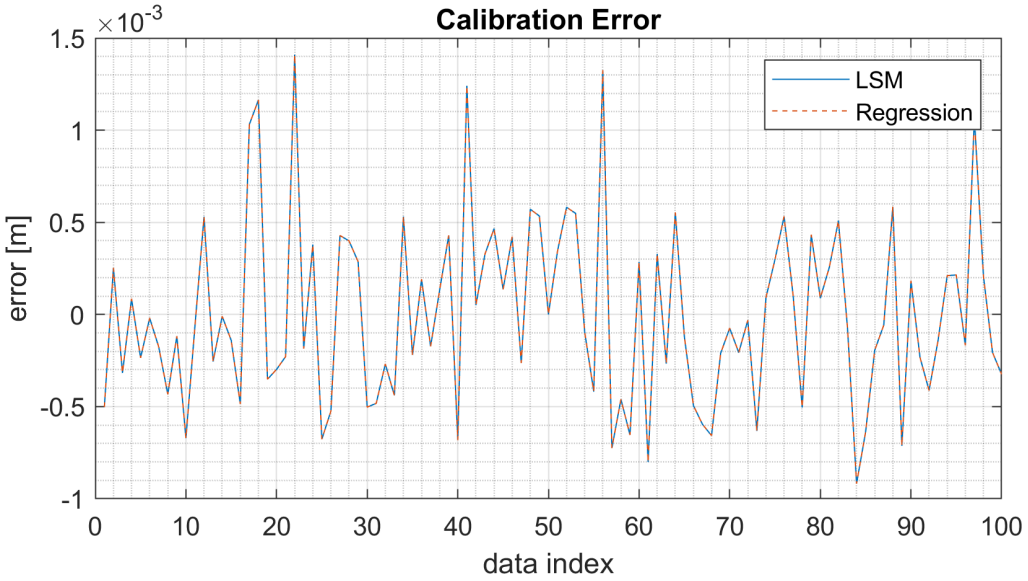

Figure A.7: Laser tracker simulation, dynamic calibration by random movement with maximum noise, calibration error.

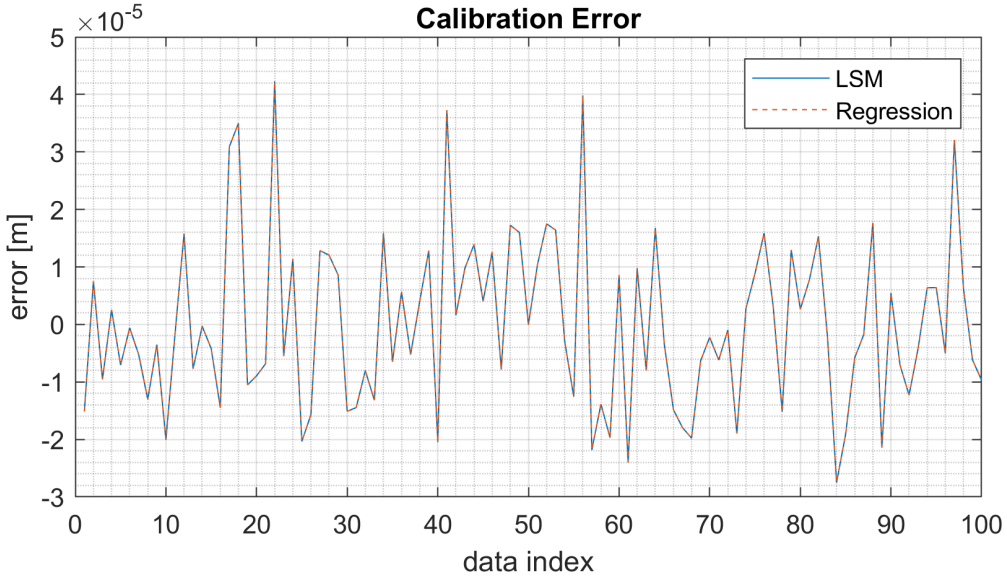

Figure A.8: Laser tracker simulation, dynamic calibration by random movement with minimum noise, calibration error.

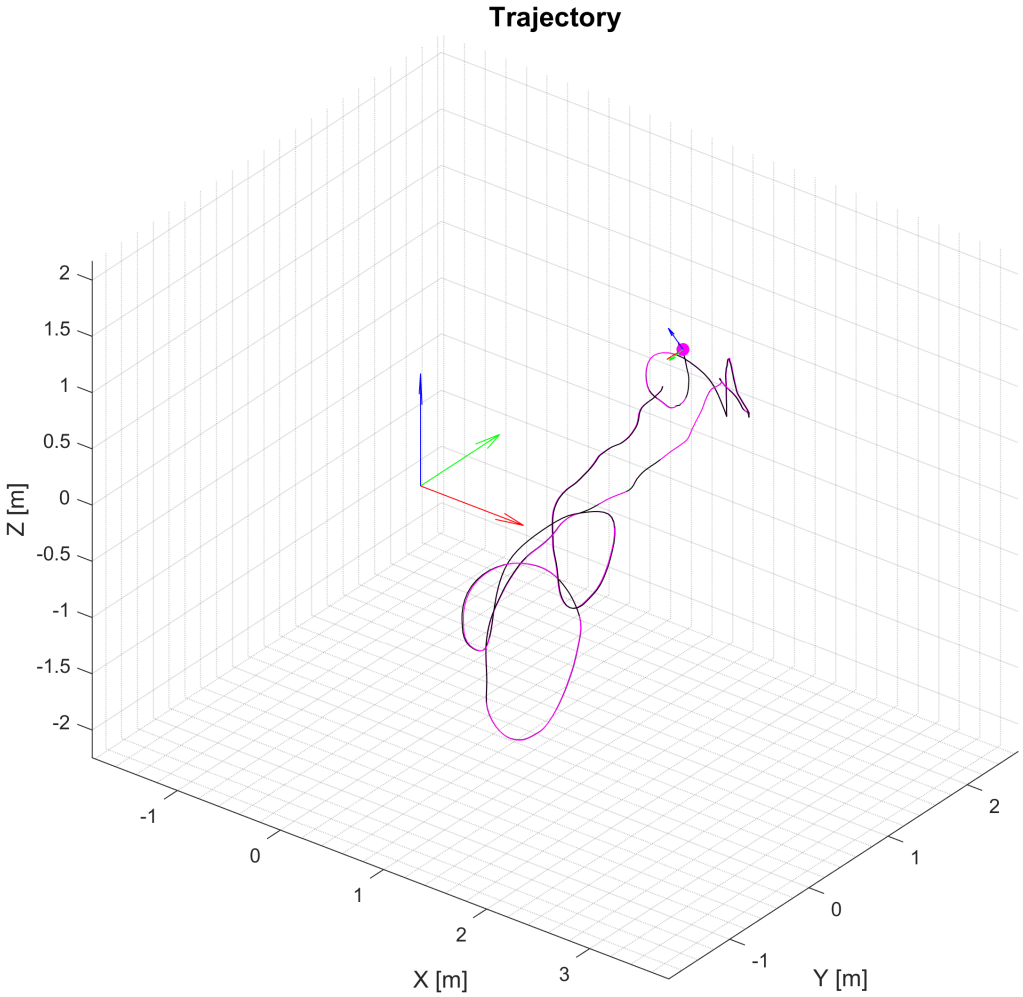

Figure A.9: Laser tracker measurements, dynamic calibration, trajectory.

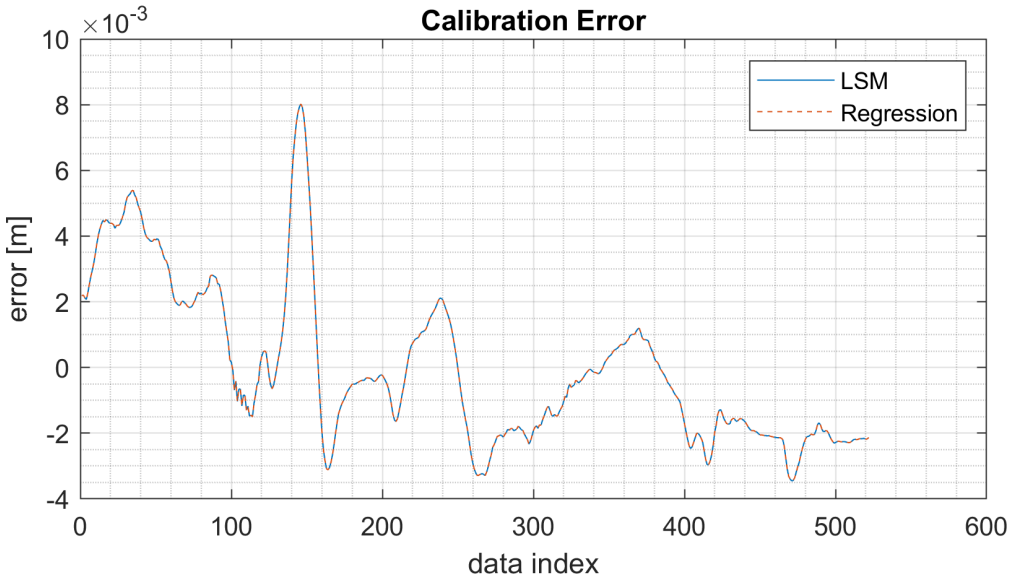

Figure A.10: Laser tracker measurements, dynamic calibration, calibration error.

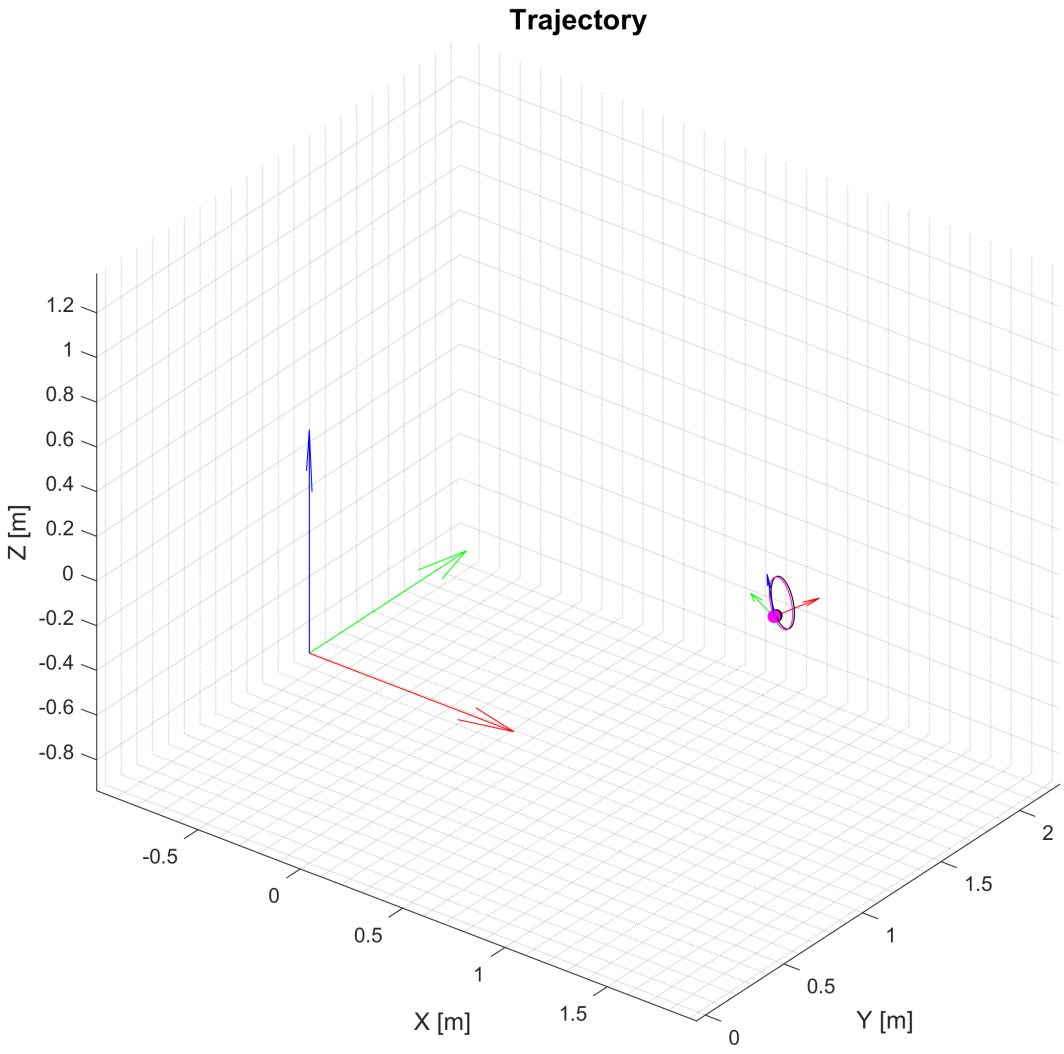

Figure A.11: Laser tracker measurements, circular movement with common reflector, trajectory. Data based on dynamic calibration are not coincident.

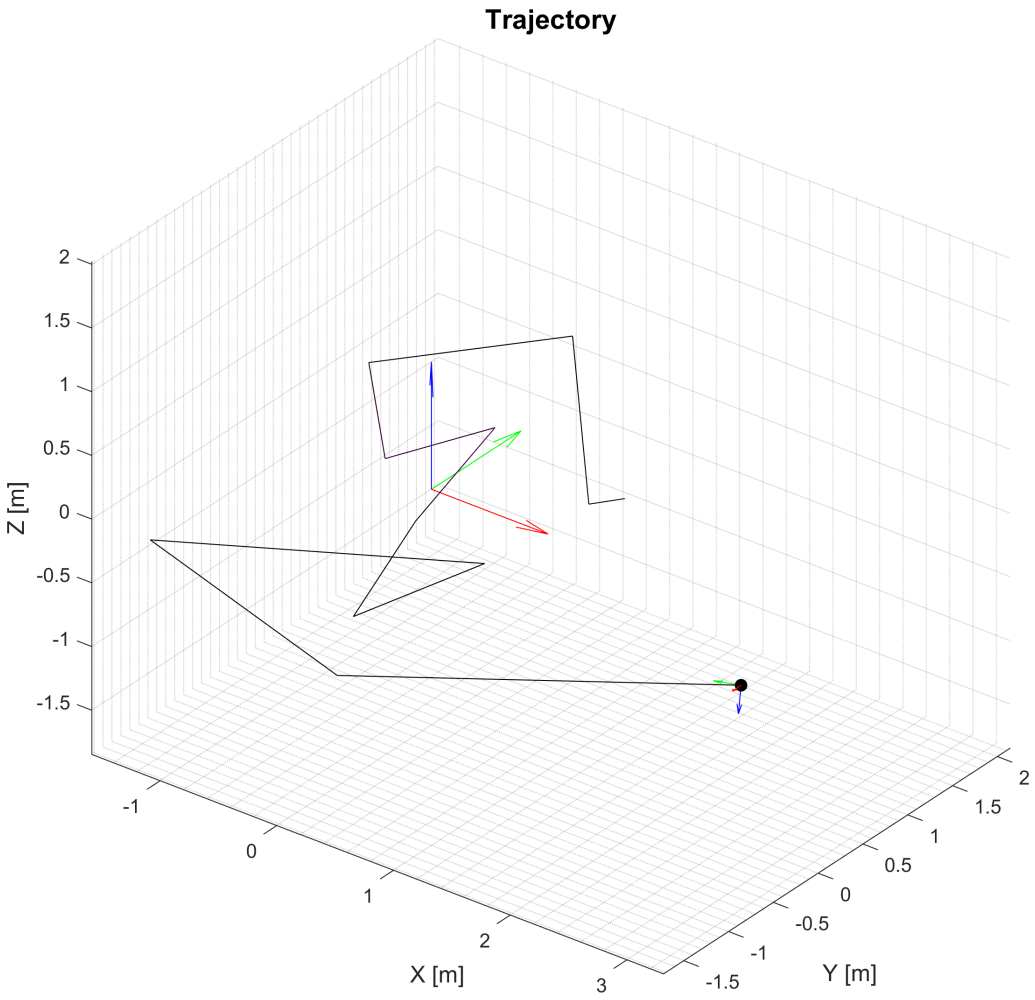

Figure A.12: Laser tracker measurements, static calibration, trajectory.

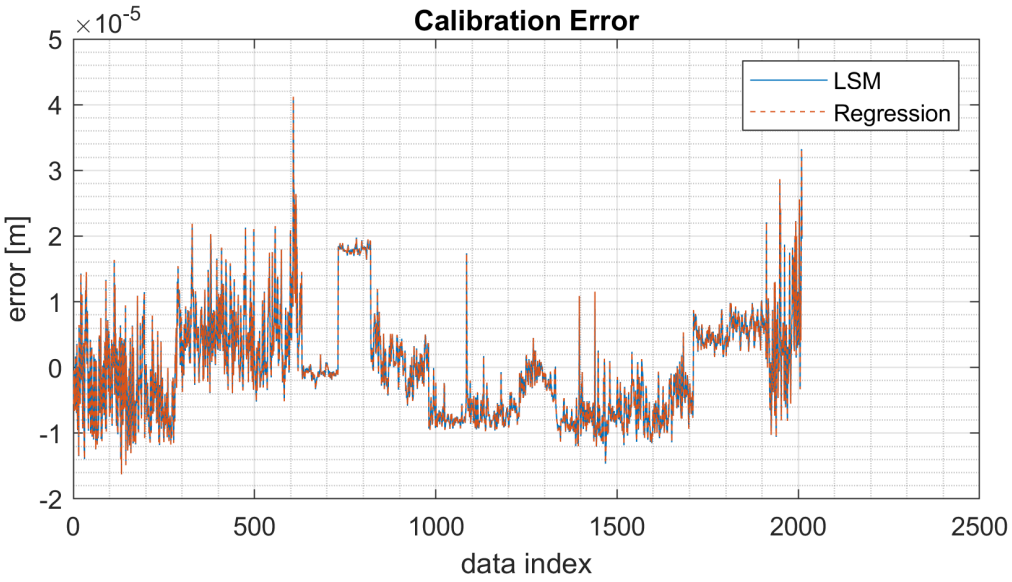

Figure A.13: Laser tracker measurements, static calibration, calibration error.

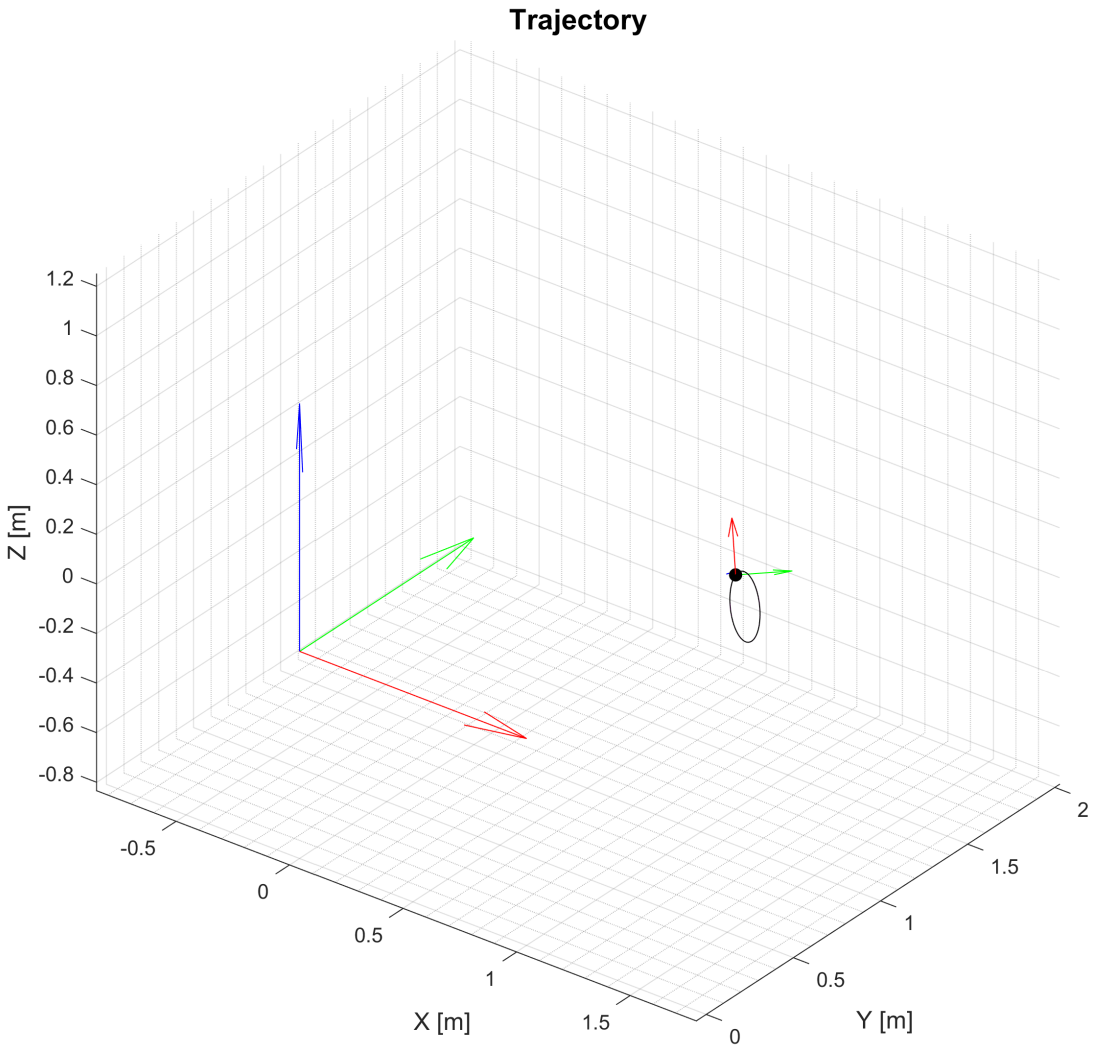

Figure A.14: Laser tracker measurements, circular movement with common reflector, trajectory. Data based on static calibration are coincident.

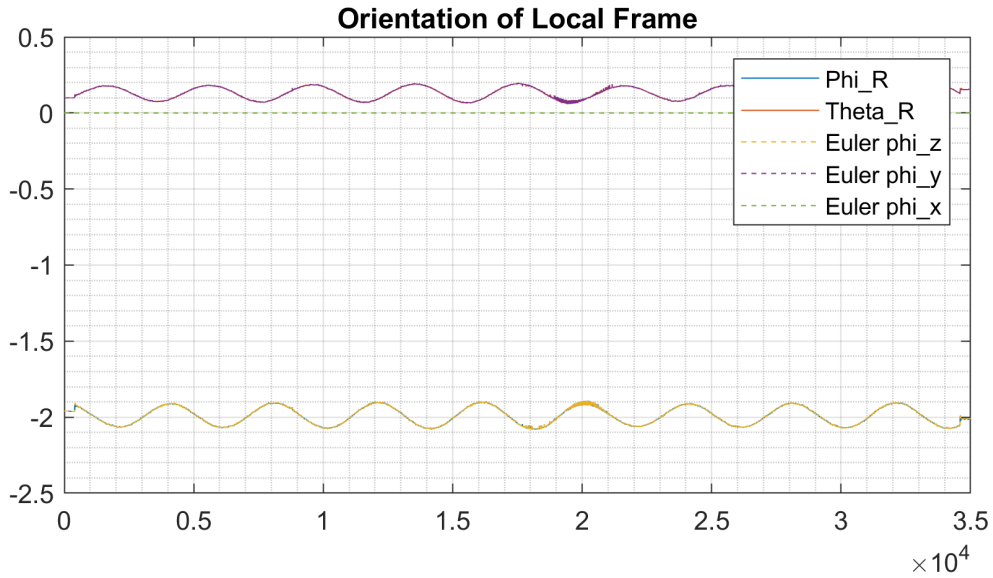

Figure A.15: Laser tracker measurements, circular movement with common reflector, orientation. Rotation around x-axis is not defined.

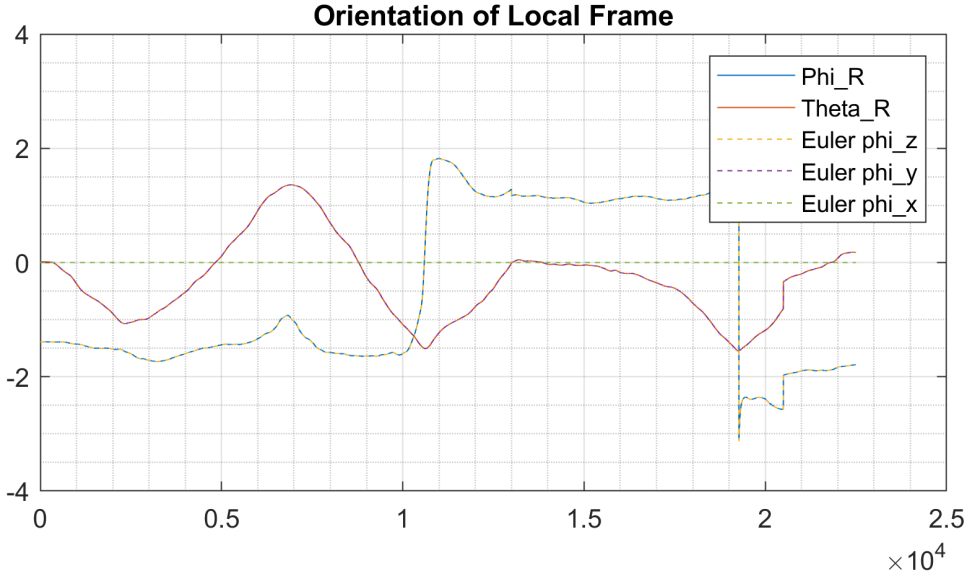

Figure A.16: Laser tracker measurements, random movement, orientation. Rotation around x-axis is not defined.

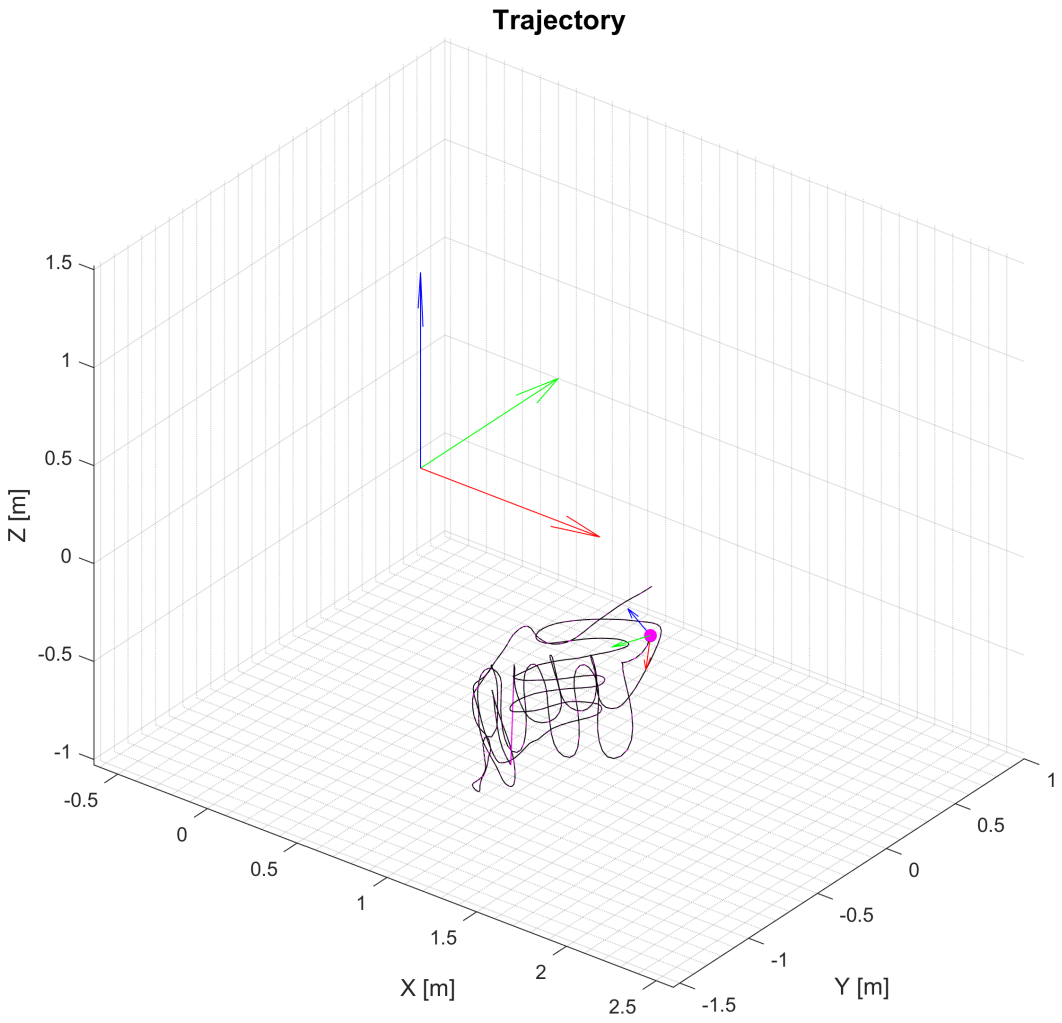

Figure A.17: Laser tracker measurements, random movement 1 with common reflector, trajectory.

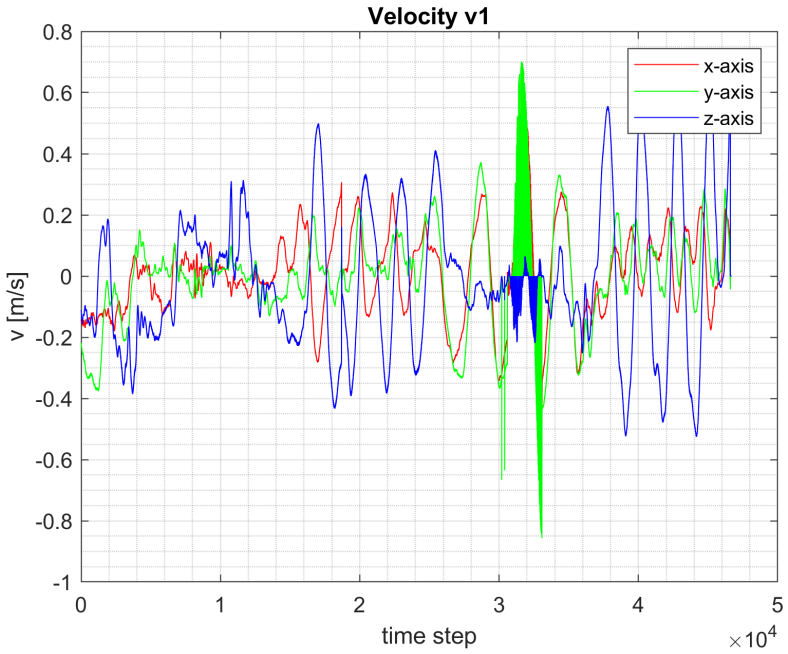

Figure A.18: Laser tracker measurements, random movement 1, velocity measured by tracker 1. The dense parts of the diagram are oscillations due to laser tracker's loss of signal.

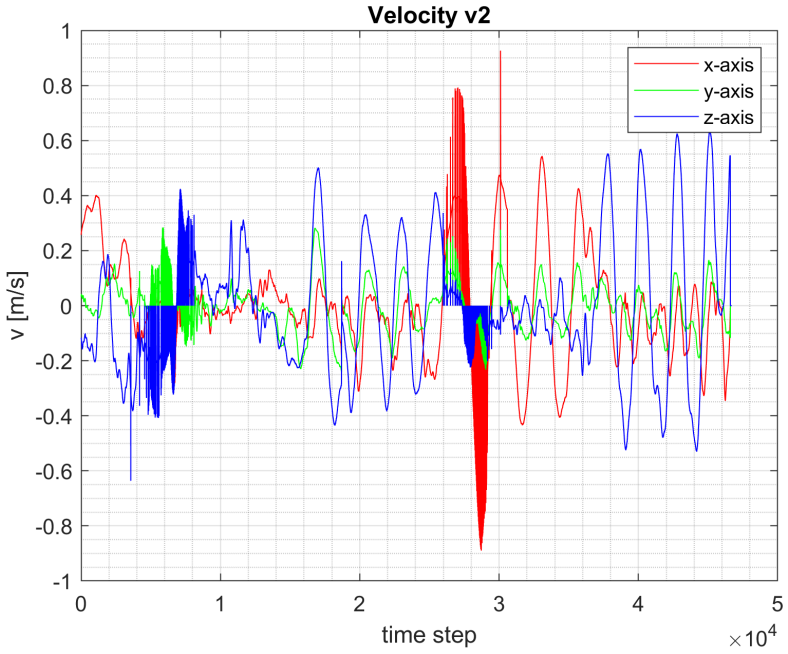

Figure A.19: Laser tracker measurements, random movement 1, velocity measured by tracker 2. The dense parts of the diagram are oscillations due to laser tracker's loss of signal.

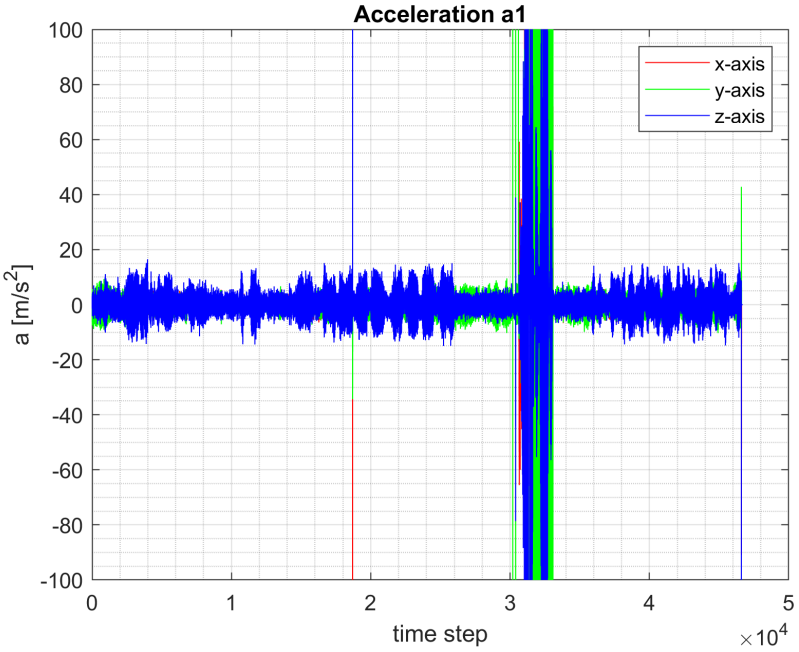

Figure A.20: Laser tracker measurements, random movement 1, acceleration measured by tracker 1. The dense parts of the diagram are oscillations due to laser tracker's loss of signal.

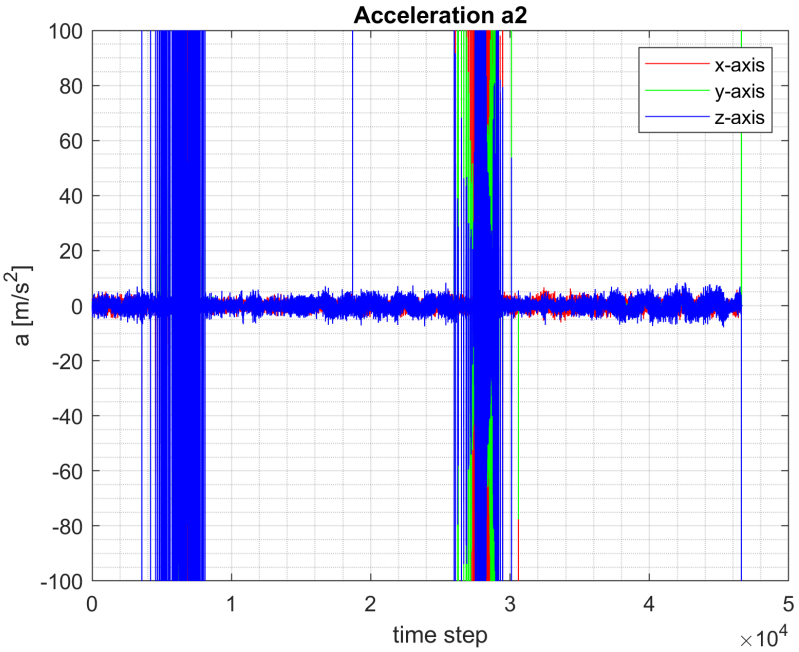

Figure A.21: Laser tracker measurements, random movement 1, acceleration measured by tracker 2. The dense parts of the diagram are oscillations due to laser tracker's loss of signal.

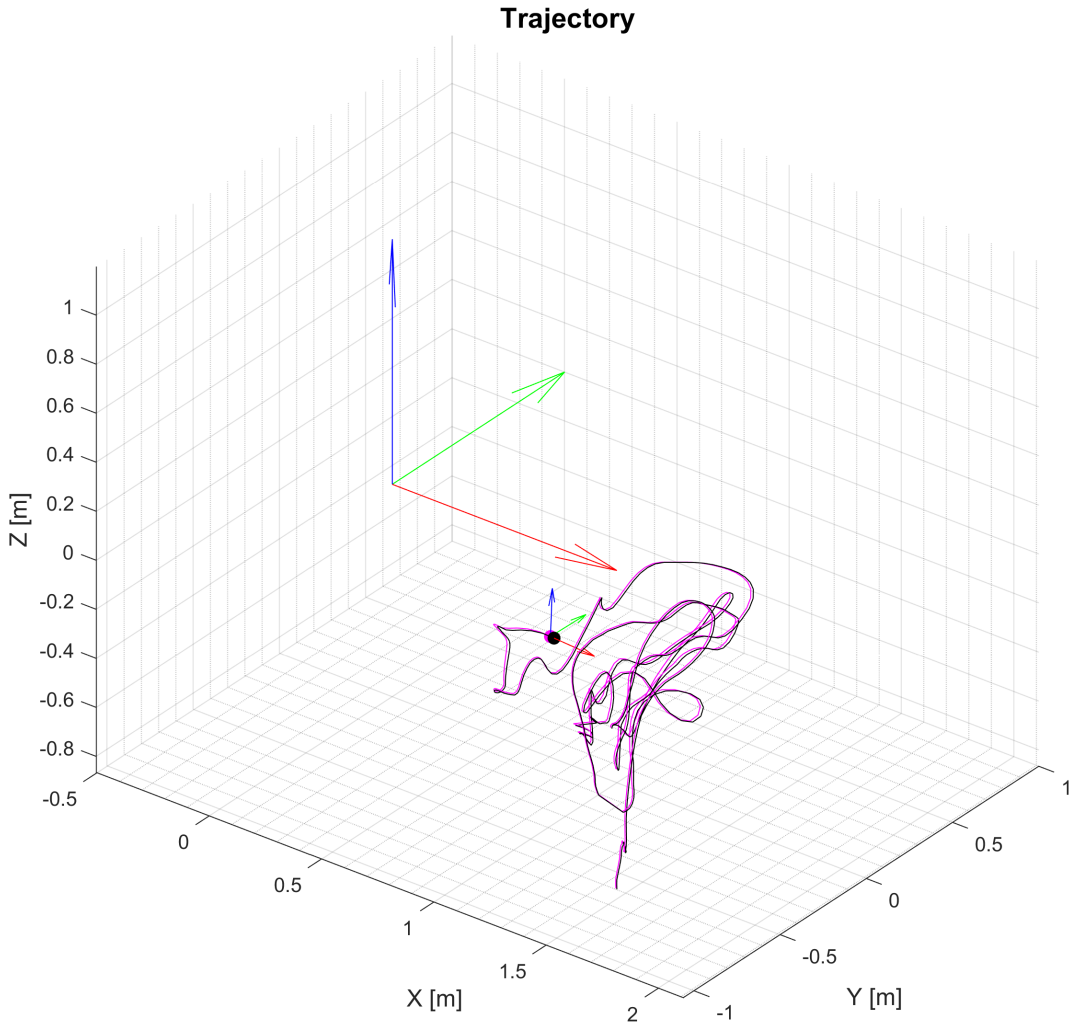

Figure A.22: Laser tracker measurements, random movement 2 with common reflector, trajectory.

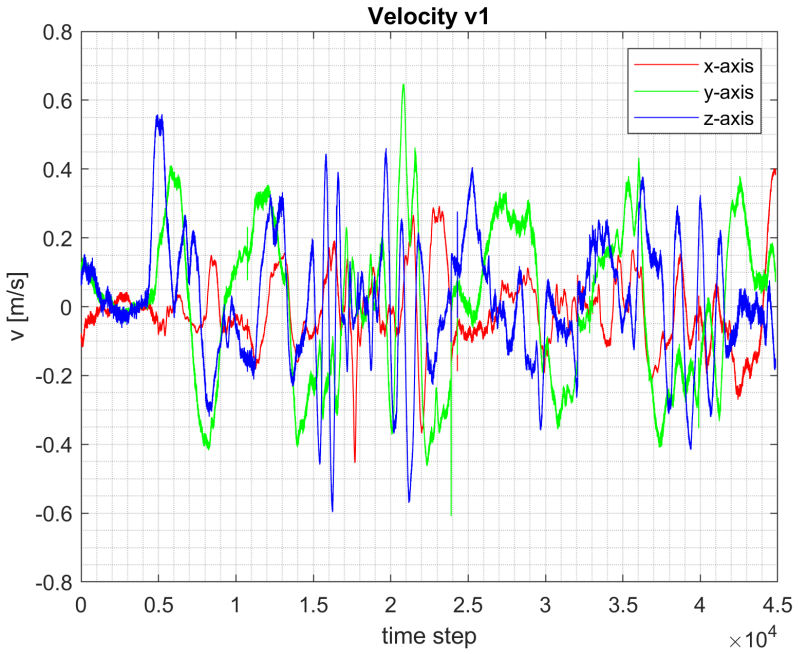

Figure A.23: Laser tracker measurements, random movement, velocity measured by tracker 1.

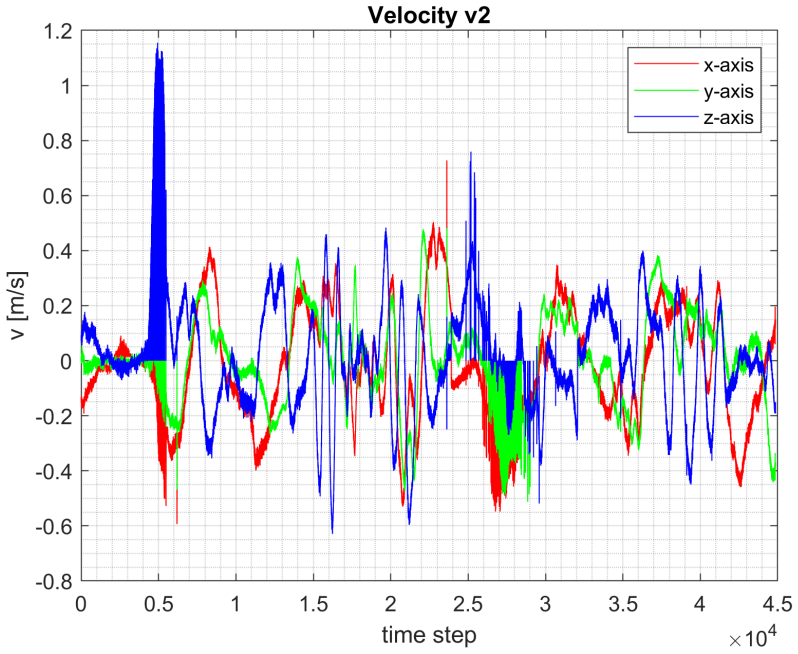

Figure A.24: Laser tracker measurements, random movement, velocity measured by tracker 2. The dense parts of the diagram are oscillations due to laser tracker's loss of signal.

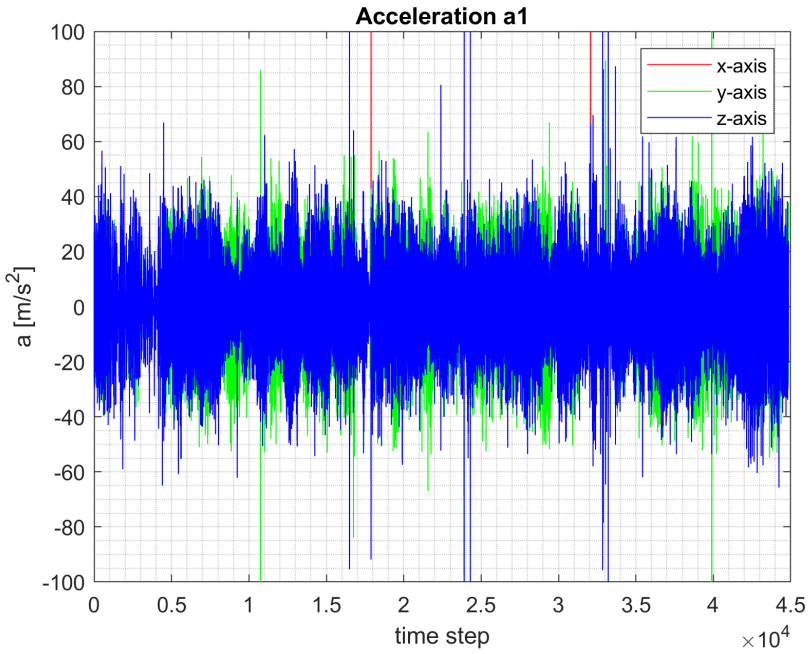

Figure A.25: Laser tracker measurements, random movement, acceleration measured by tracker 1.

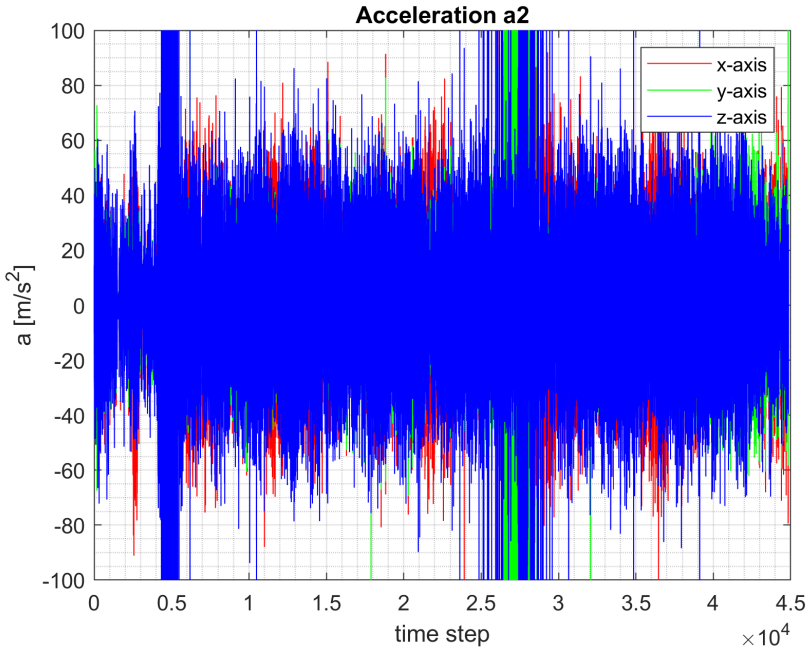

Figure A.26: Laser tracker measurements, random movement, acceleration measured by tracker 2. The dense parts of the diagram are oscillations due to laser tracker's loss of signal.

A.2 MMR IMU sensor

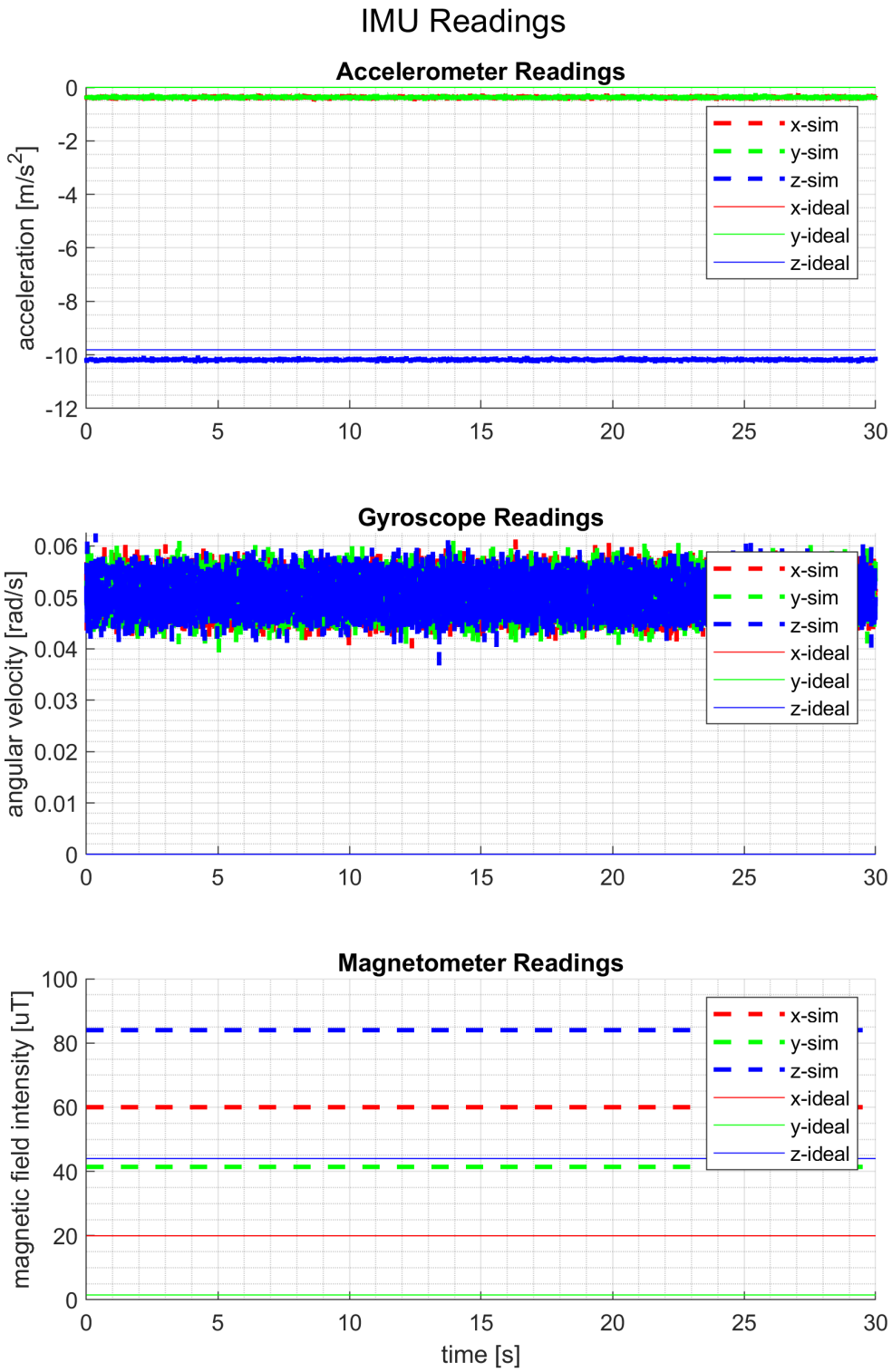

Figure A.27: MMR and ideal IMU simulations, steady state, sensor readings. Deviation of MMR data from an ideal IMU is visible.

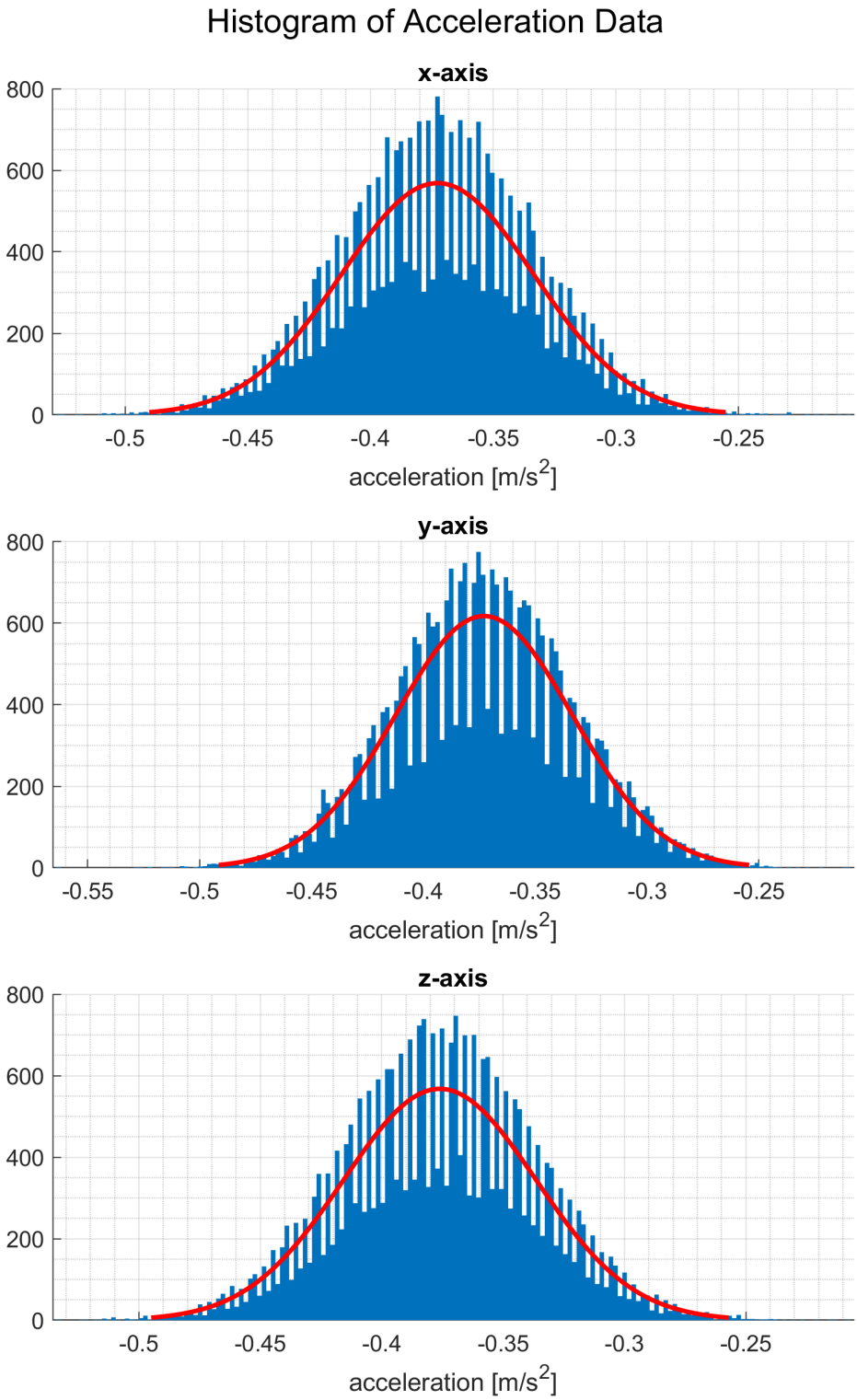

Figure A.28: MMR IMU simulation, steady state, histogram of measured acceleration with Gaussian fit. Offset from ideal zero measurements is shown, noise appears to be Gaussian.

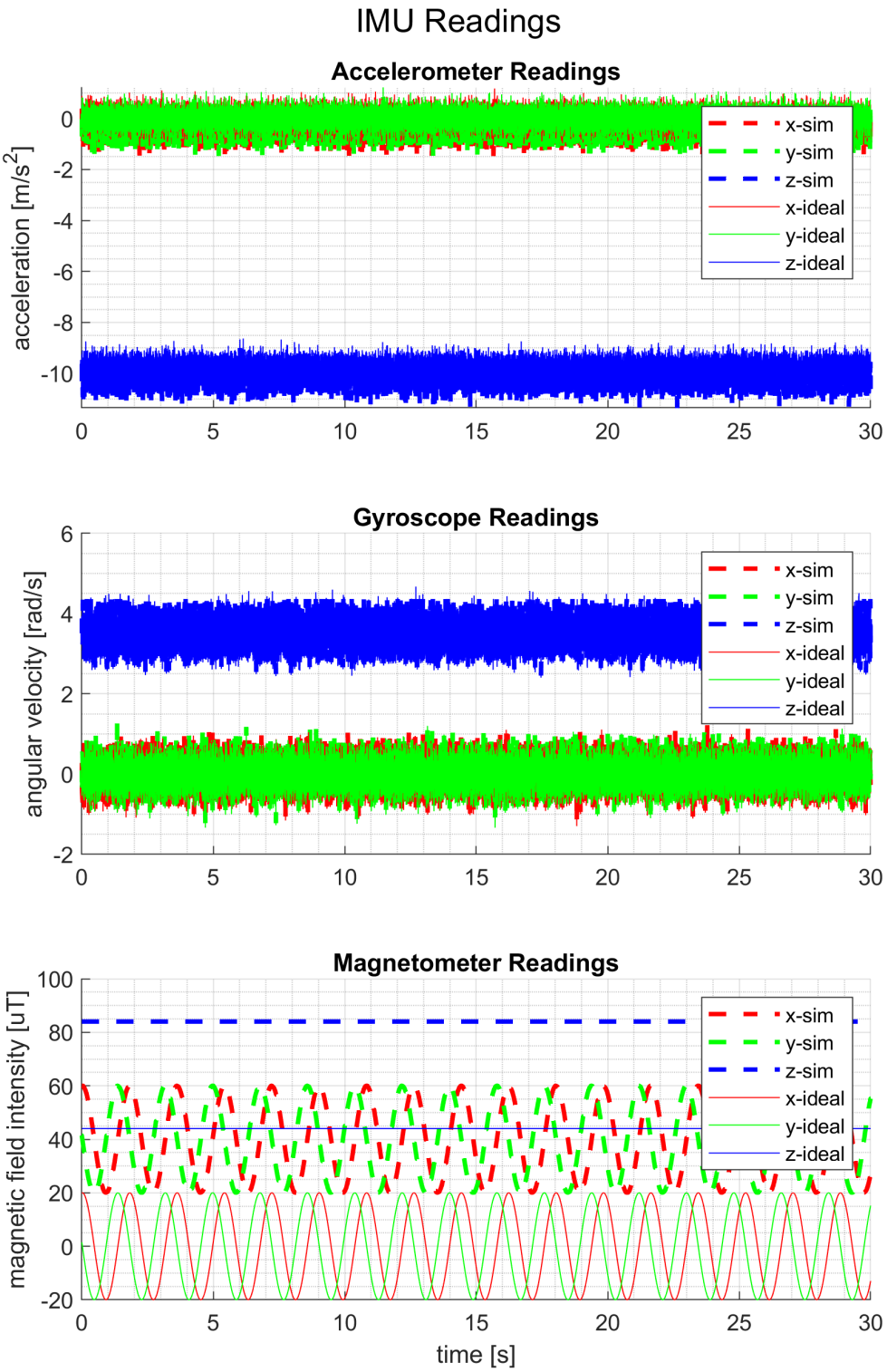

Figure A.29: MMR and ideal IMU simulations, rotation about z-axis, with added Gaussian noise, sensor readings. Deviation of MMR data from an ideal IMU is visible.

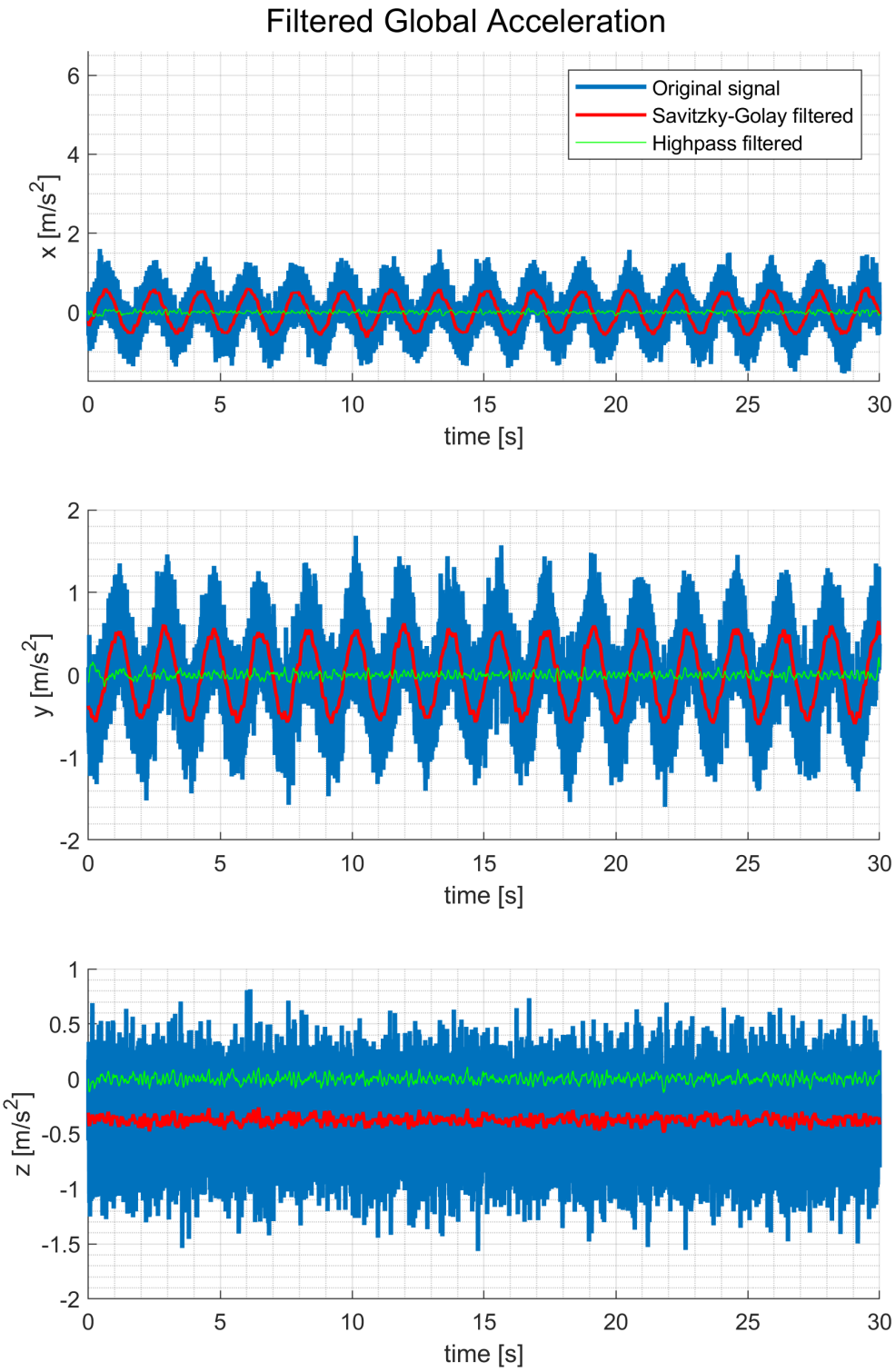

Figure A.30: MMR IMU simulation, rotation about z-axis, with added Gaussian noise, global acceleration. Undesirable oscillation in x- and y-axis is visible, possibly filtered out.

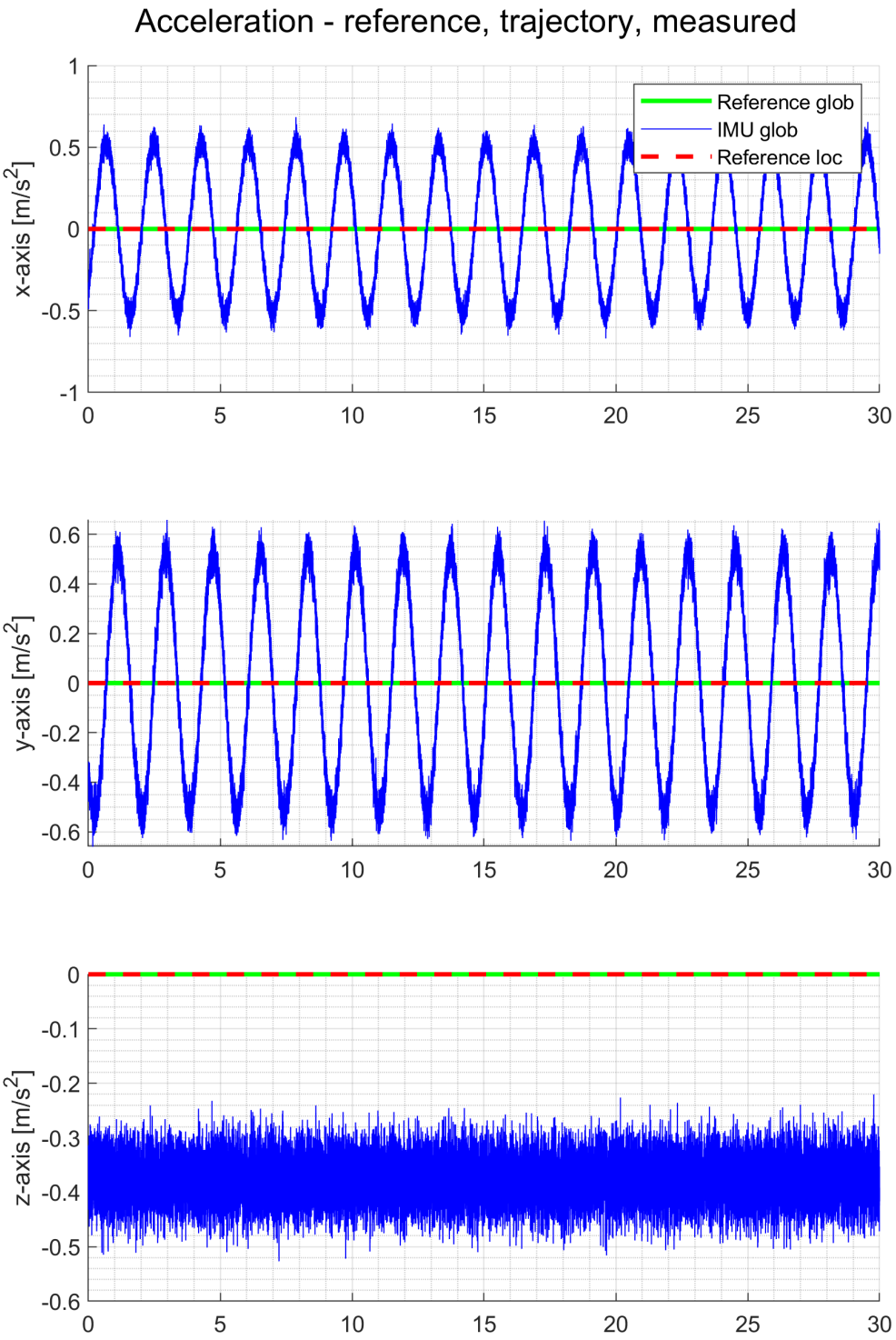

Figure A.31: MMR IMU simulation, rotation about z-axis, with added Gaussian noise, acceleration. Undesirable oscillation in x- and y-axis is visible.

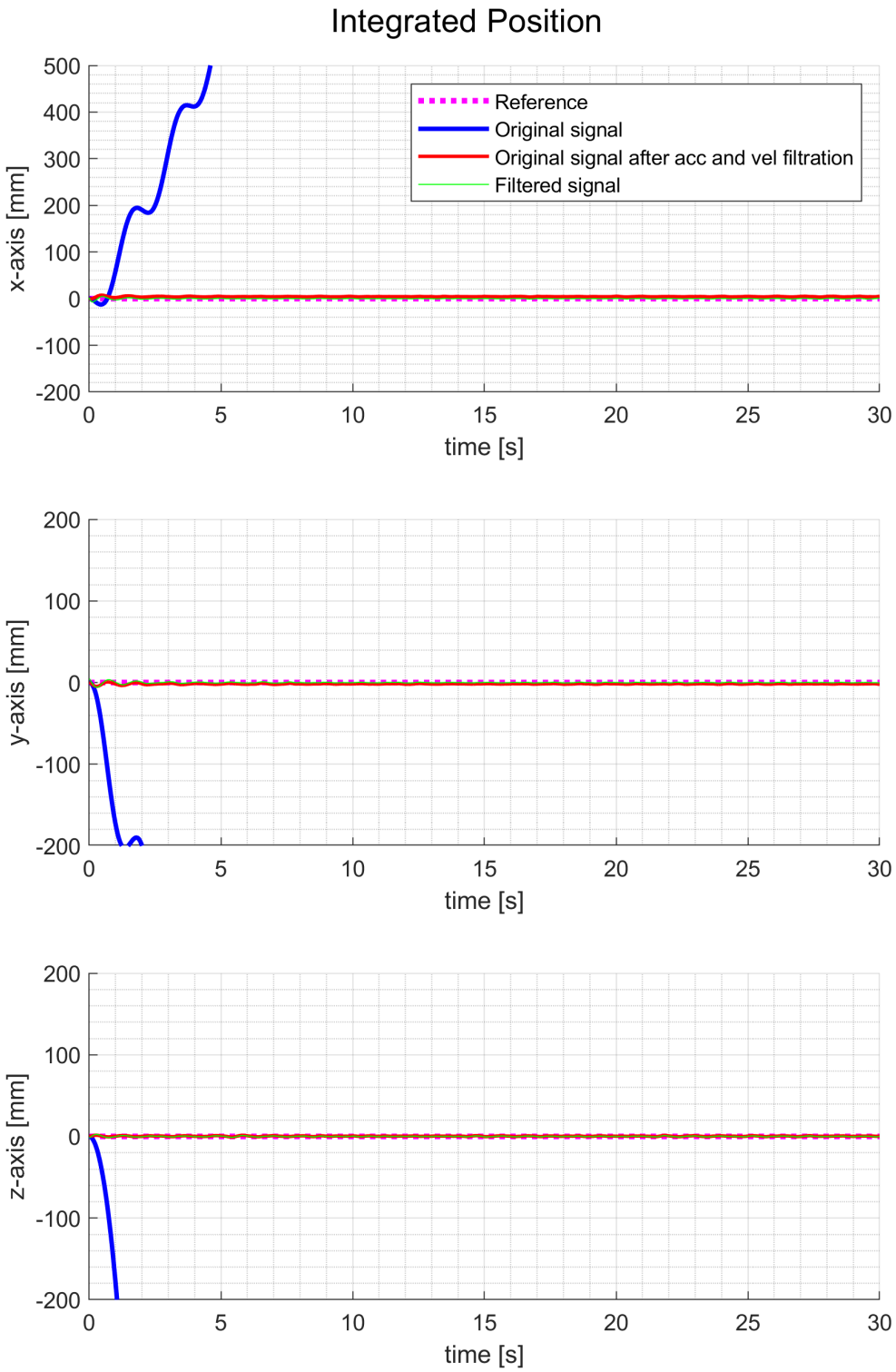

Figure A.32: MMR IMU simulation, rotation about z-axis, with added Gaussian noise, position. Original signal diverges, but coincides with reference when filtered.

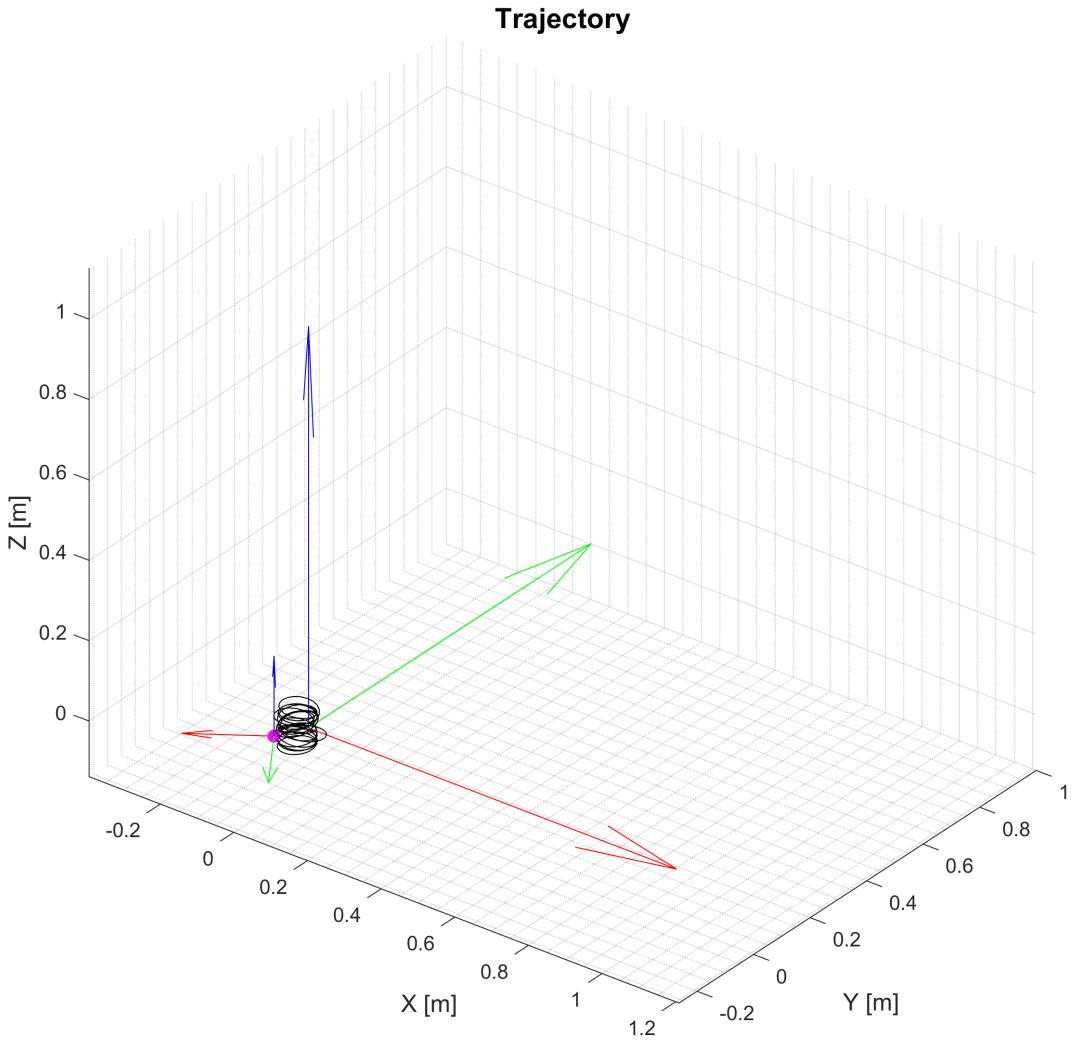

Figure A.33: MMR IMU simulation, rotation about z-axis, with added Gaussian noise, traveled trajectory. Without filtering, motion that was not present is generated due to double integration of errors.

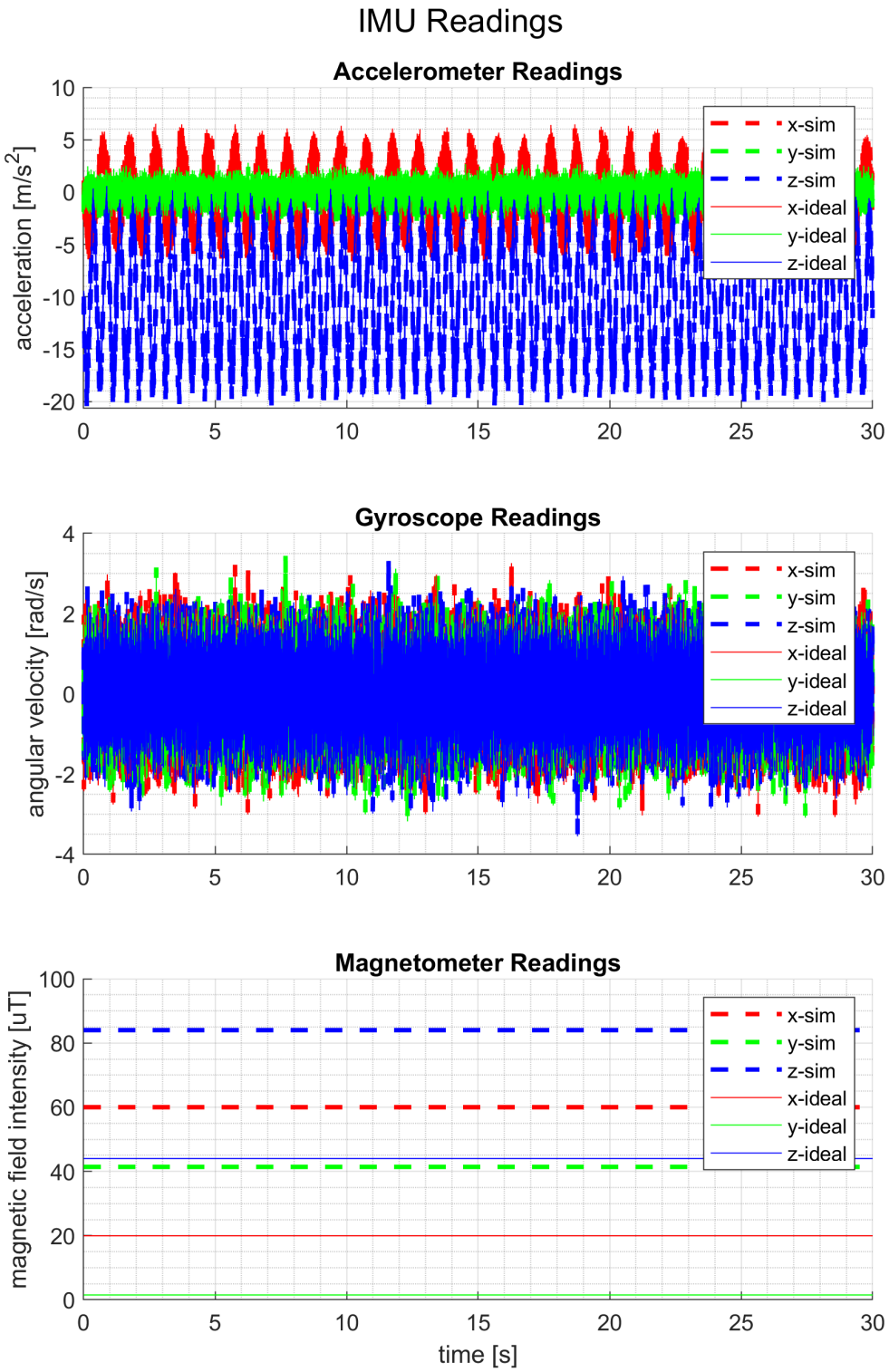

Figure A.34: MMR and ideal IMU simulations, harmonic motion in x- and z-axis, with added Gaussian noise, sensor readings. Deviation of MMR data from an ideal IMU is visible.

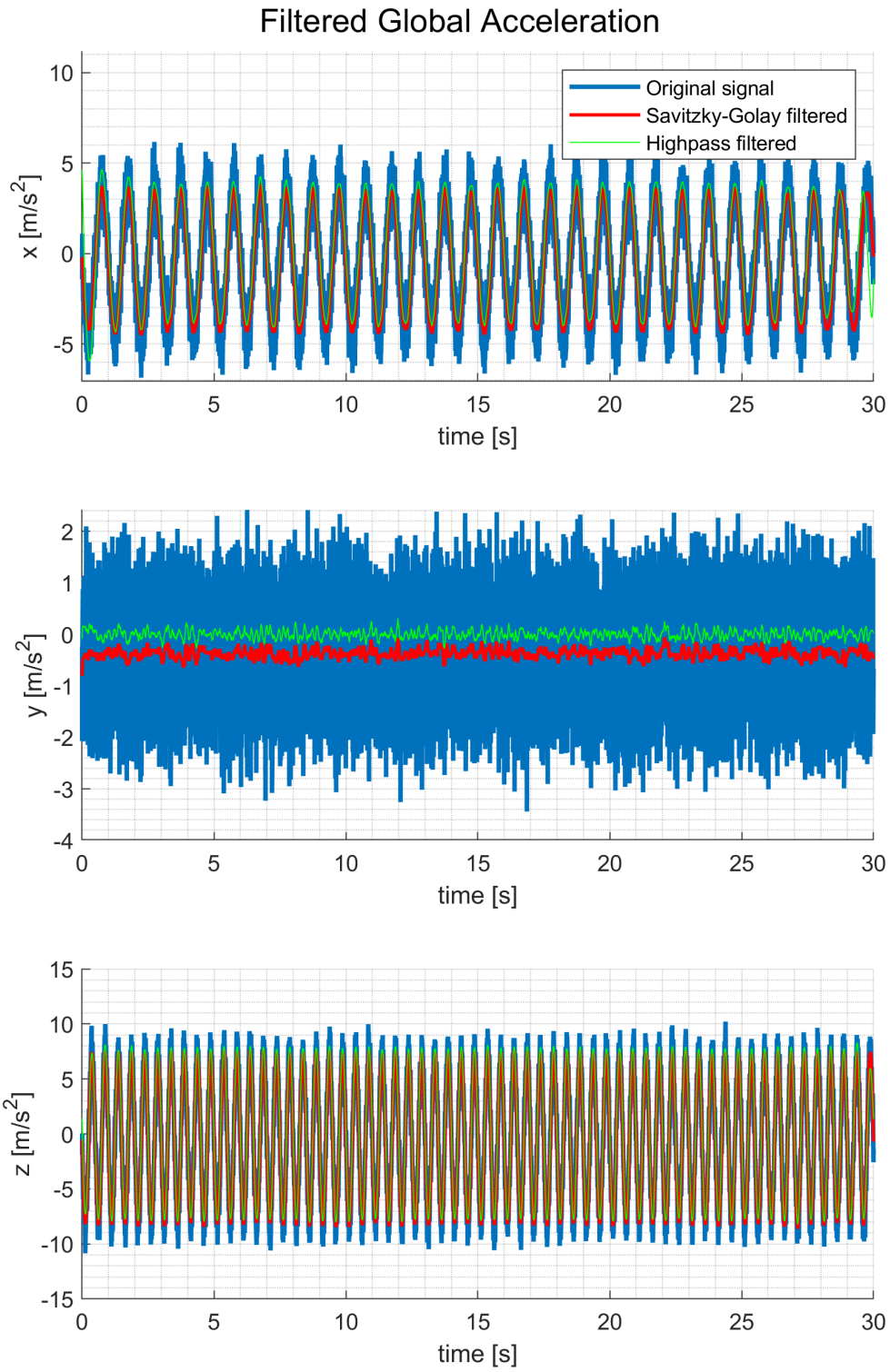

Figure A.35: MMR IMU simulation, harmonic motion in x- and z-axis, with added Gaussian noise, global acceleration. Large oscillation in y-axis is visible, possibly filtered out.

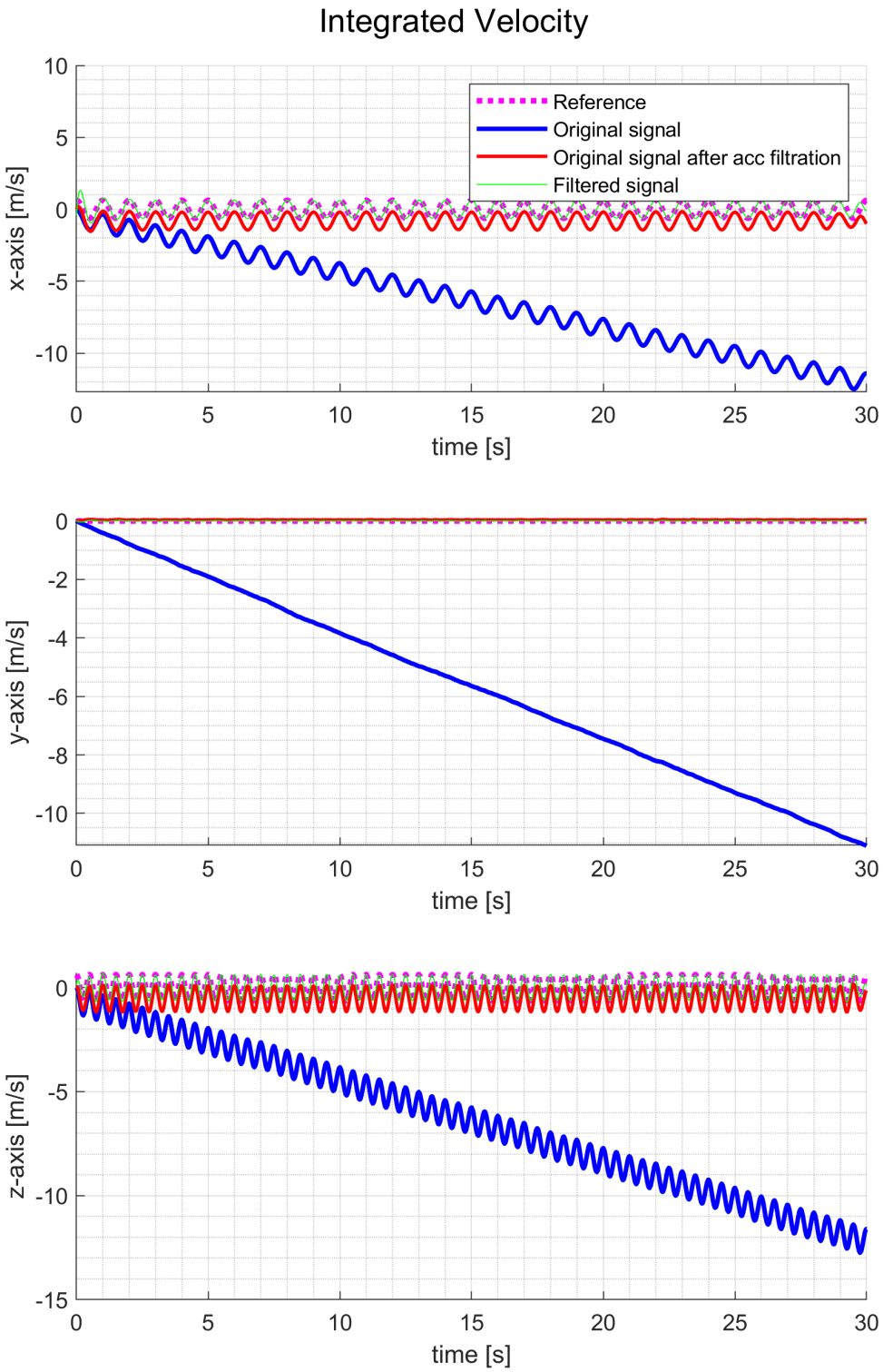

Figure A.36: MMR IMU simulation, harmonic motion in x- and z-axis, with added Gaussian noise, velocity. Original signal diverges, but coincides with reference when fully filtered.

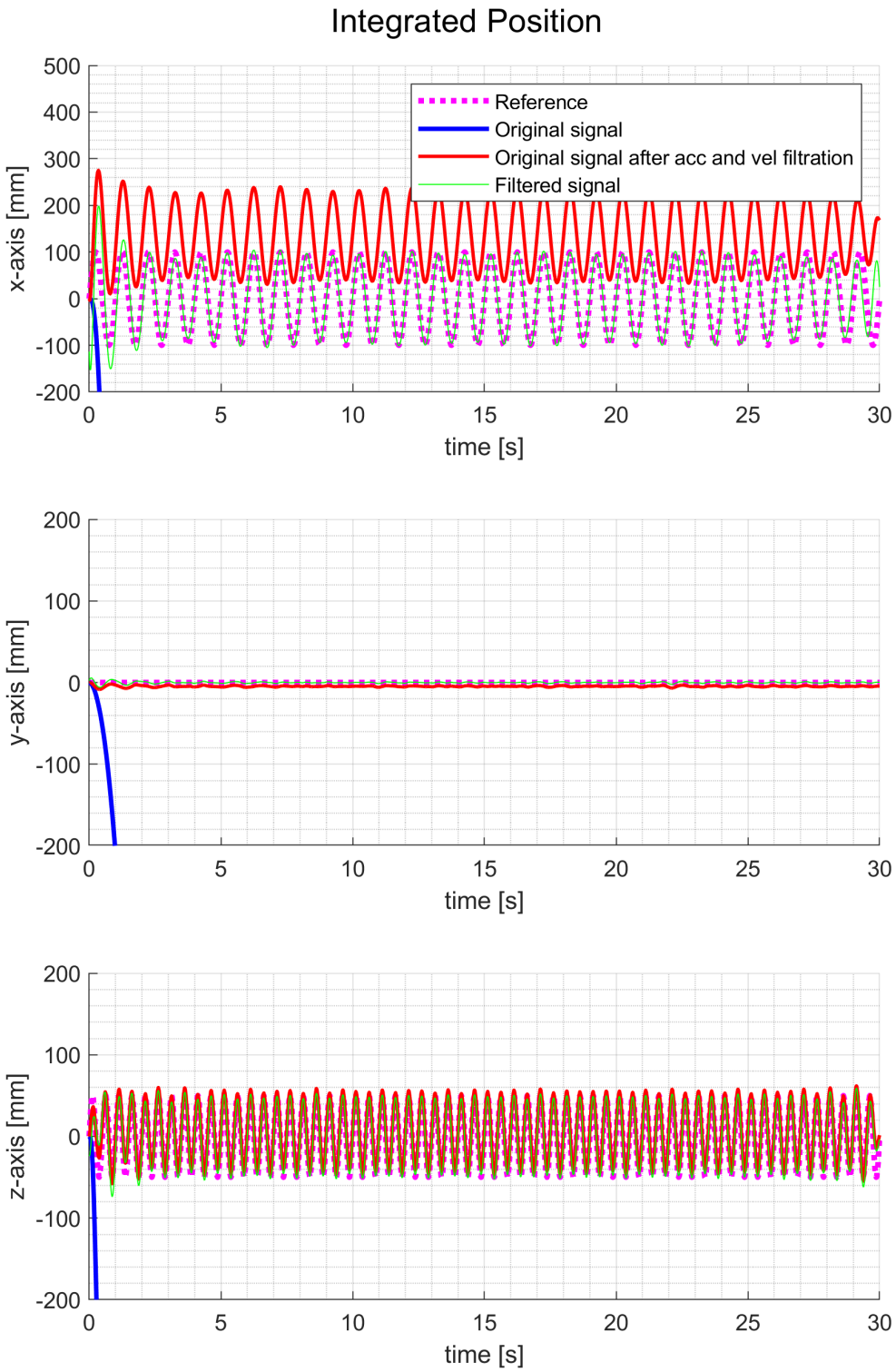

Figure A.37: MMR IMU simulation, harmonic motion in x- and z-axis, with added Gaussian noise, position. Original signal diverges, but coincides with reference when fully filtered.

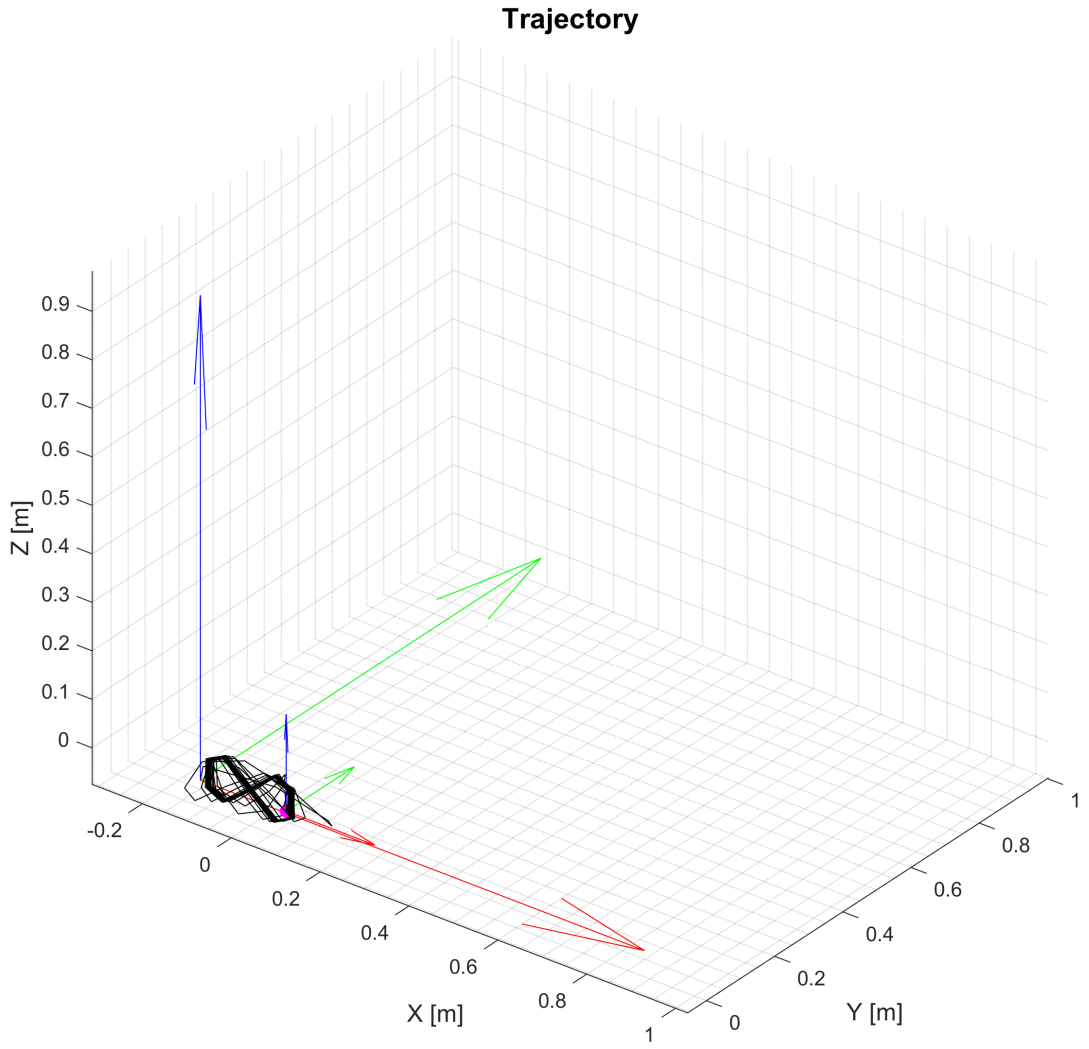

Figure A.38: MMR IMU simulation, harmonic motion in x- and z-axis, with added Gaussian noise, traveled trajectory. With filtering, the trajectory reflects real motion.

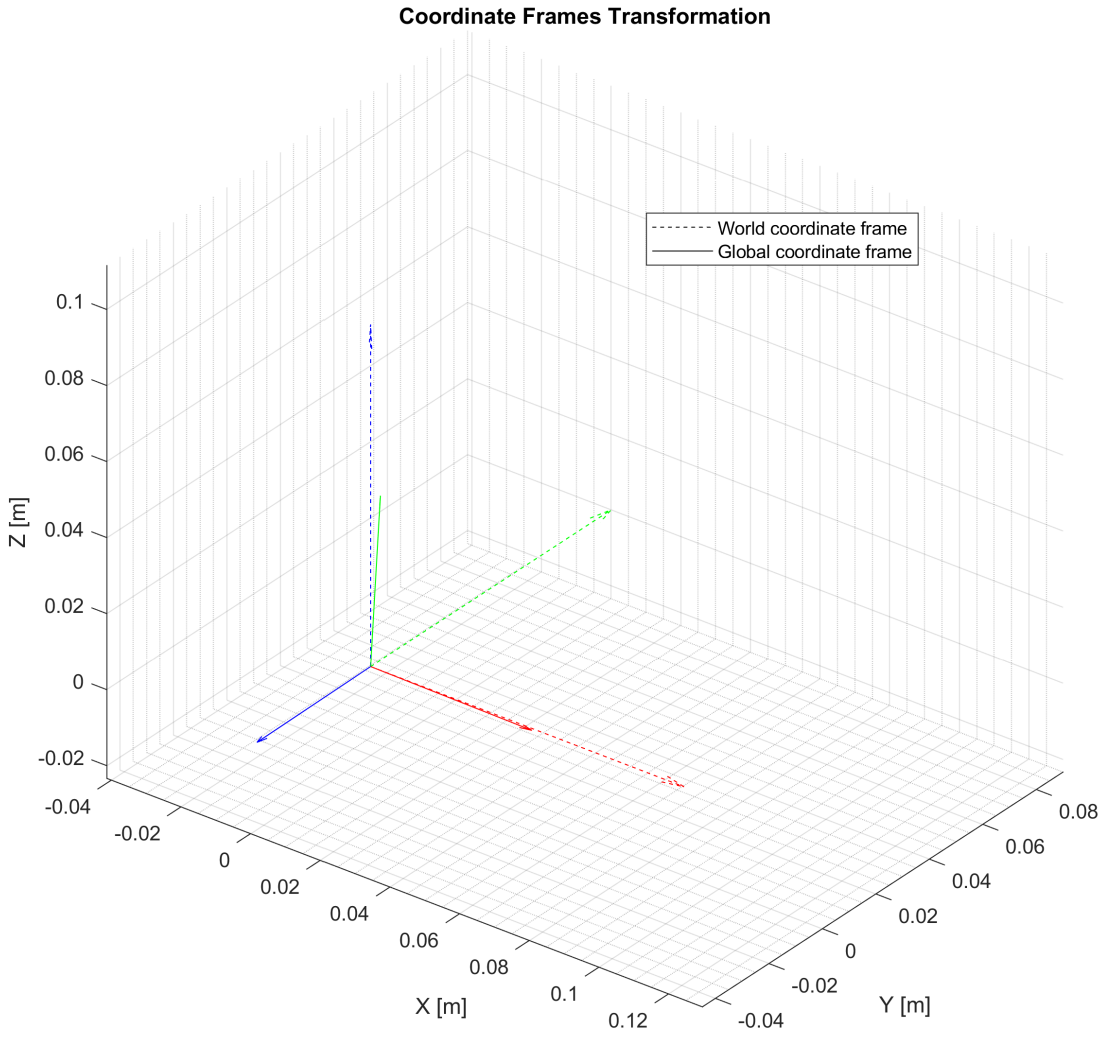

Figure A.39: MMR IMU experiment, transformation of coordinate frames.

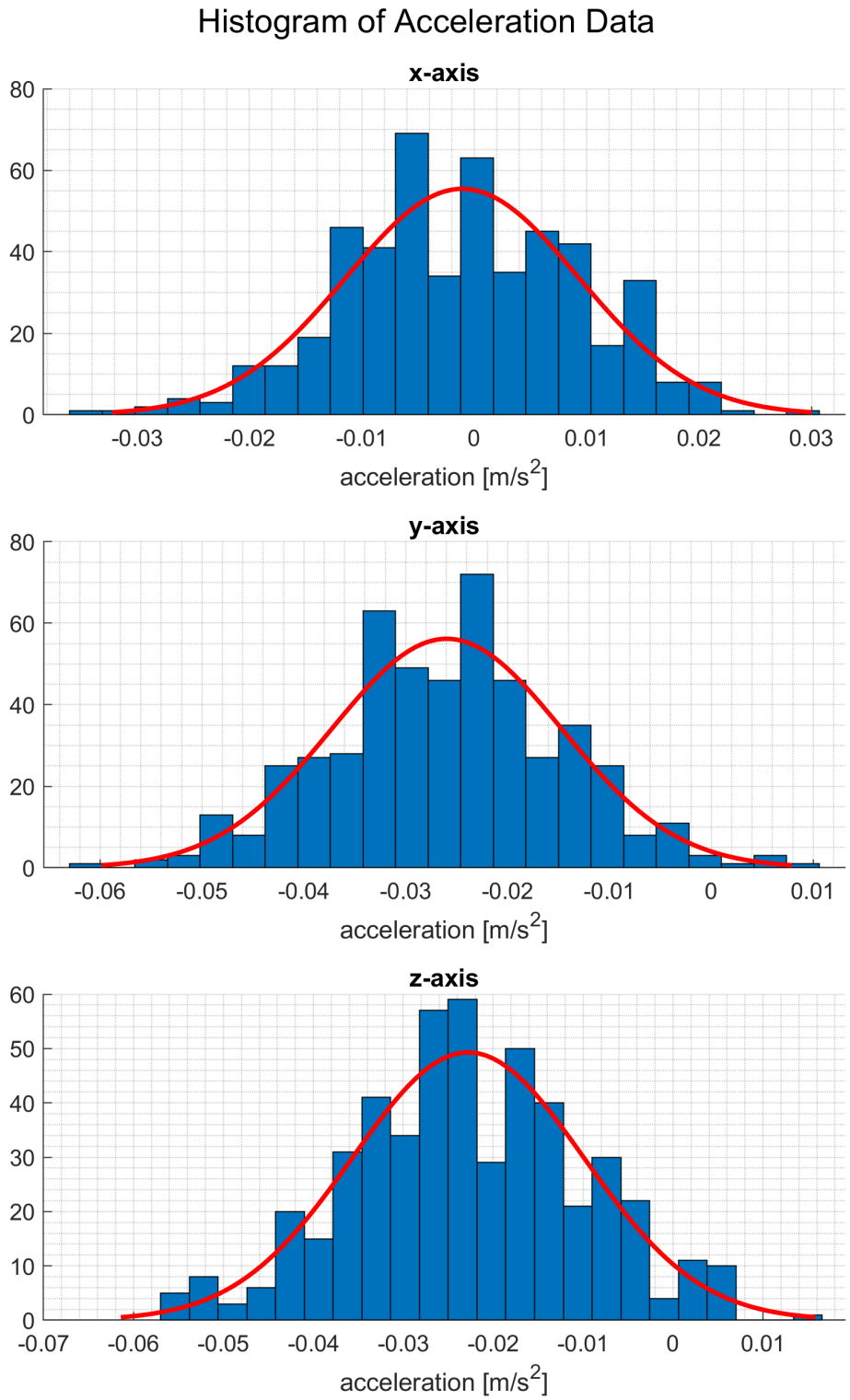

Figure A.40: MMR IMU experiment, steady state, calibrated linear acceleration, histogram with Gaussian fit. Offset from ideal zero measurements is shown, noise appears to be Gaussian.

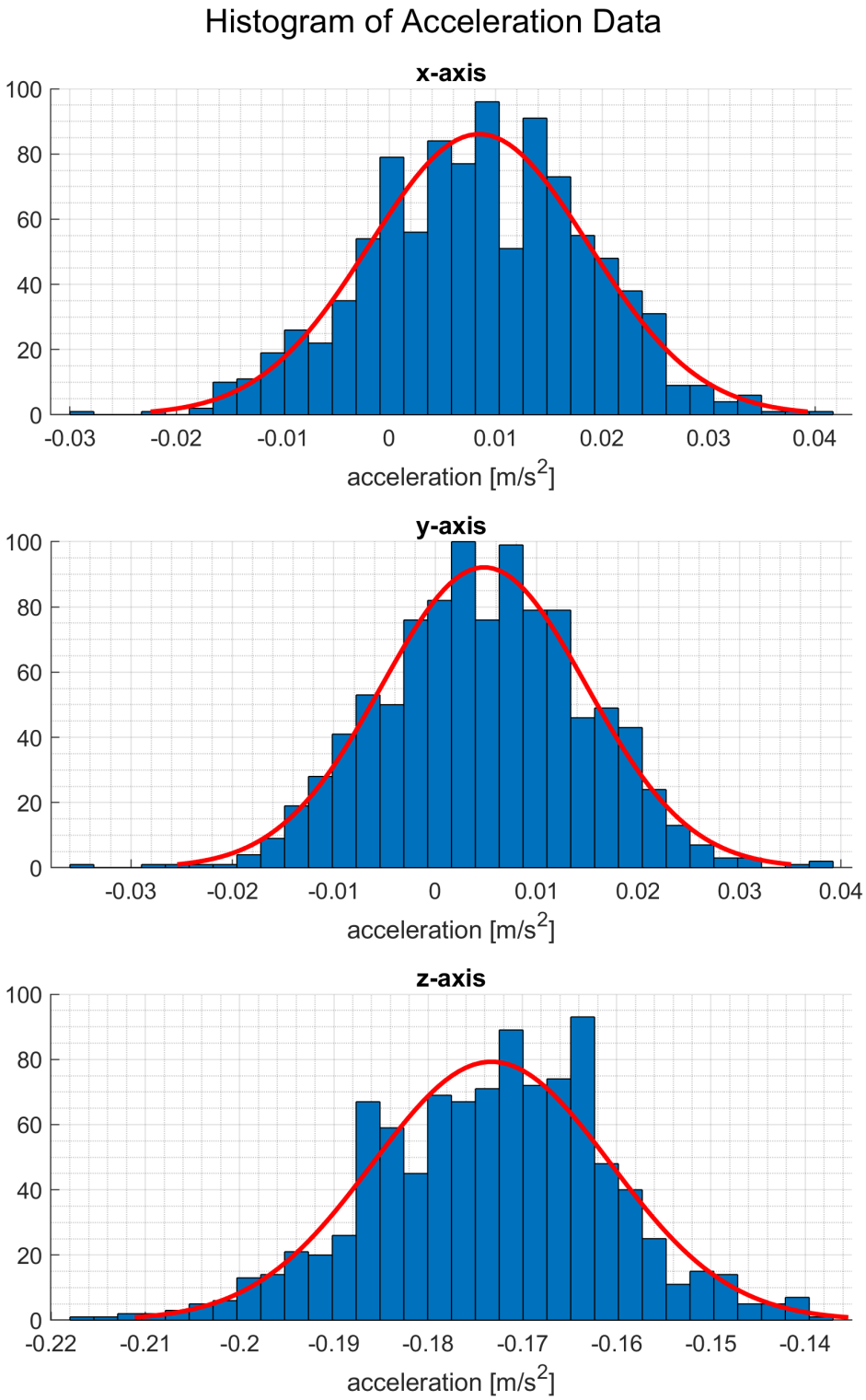

Figure A.41: MMR IMU experiment, steady state, not calibrated linear acceleration, histogram with Gaussian fit. Offset from ideal zero measurements is shown, noise appears to be Gaussian.

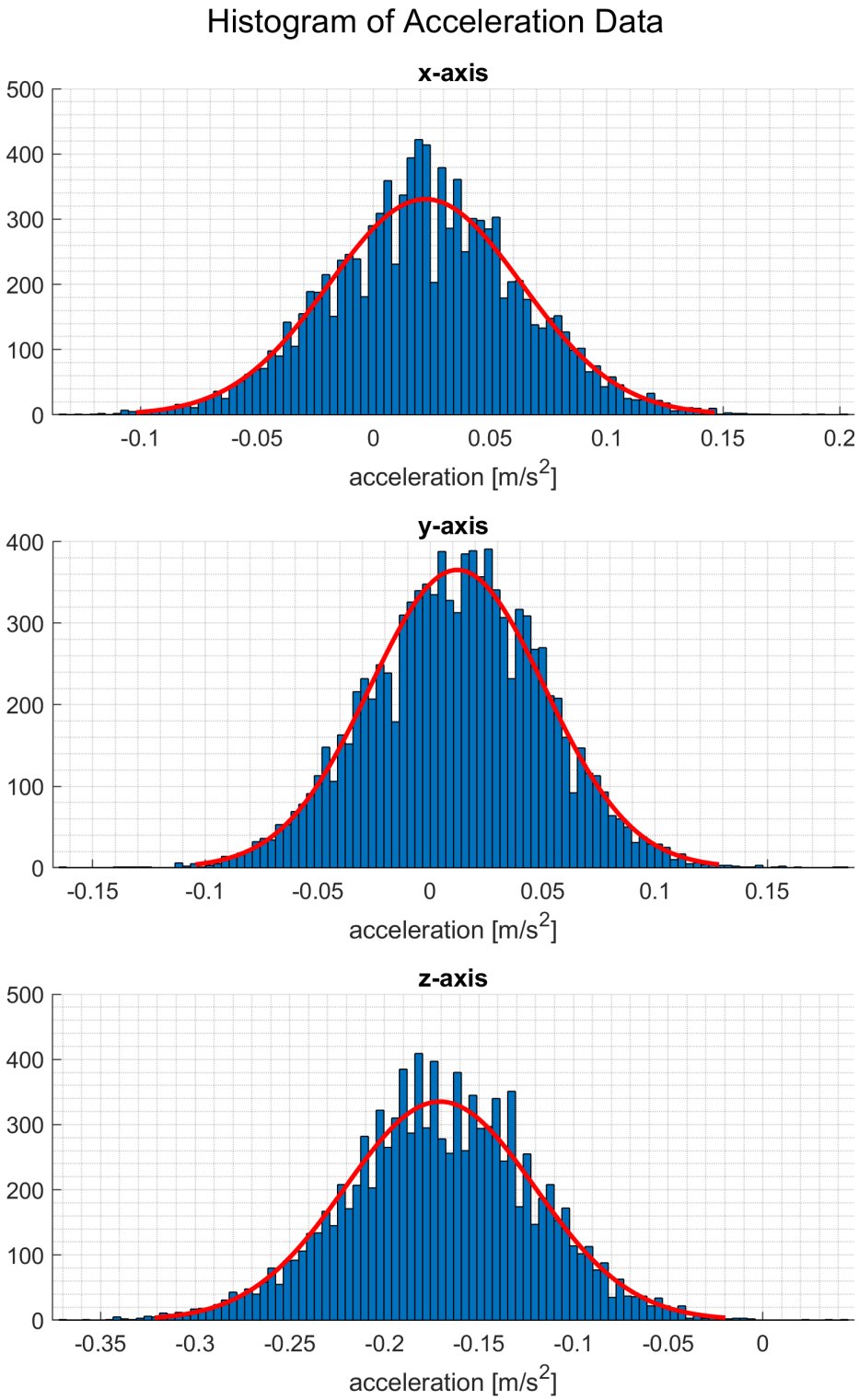

Figure A.42: MMR IMU experiment, steady state, raw acceleration, histogram with Gaussian fit. Offset from ideal zero measurements is shown, noise appears not Gaussian.

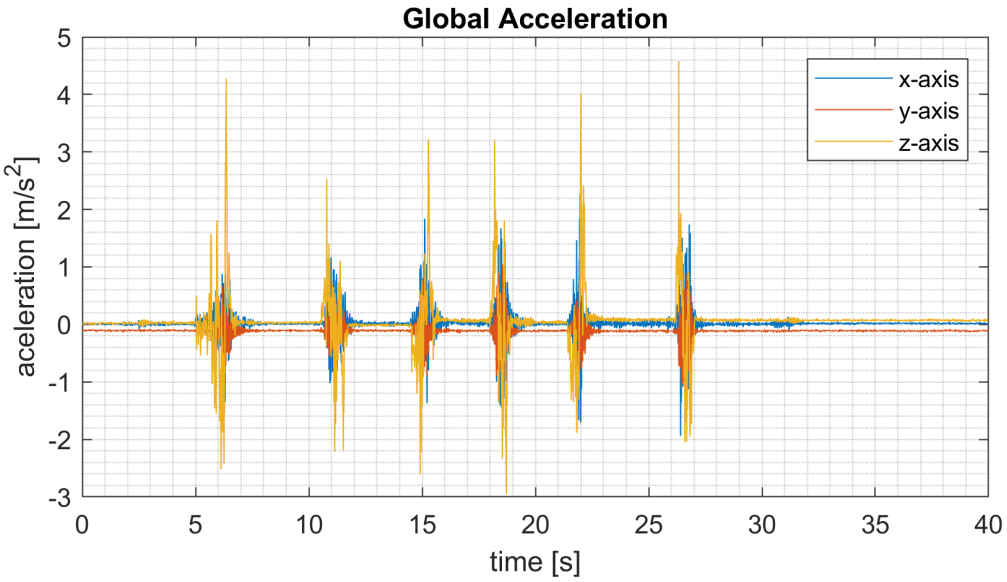

Figure A.43: MMR IMU experiment, repeated translation in z-axis, linear acceleration, global acceleration. The undesirable bias increases with time.

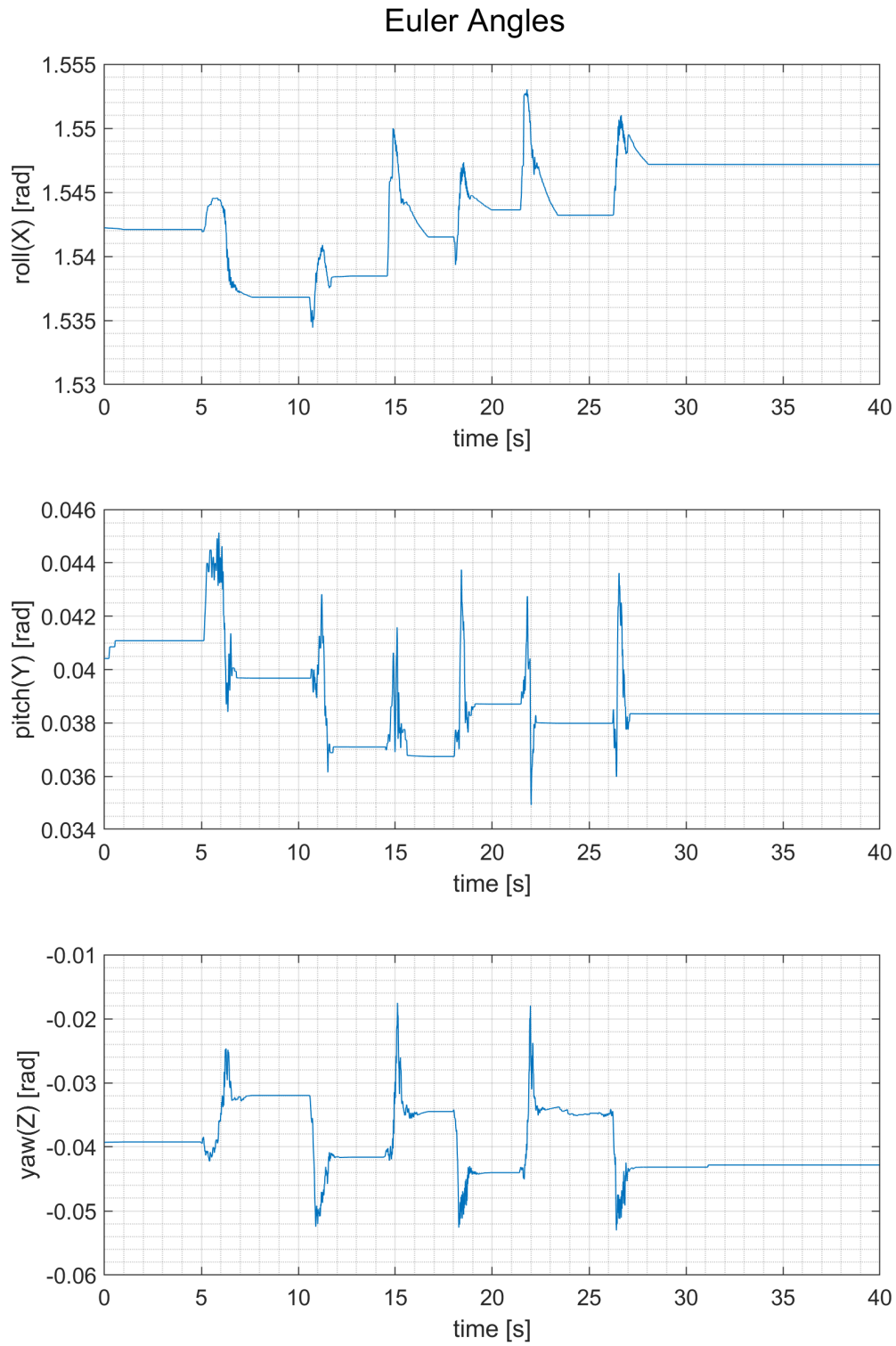

Figure A.44: MMR IMU experiment, repeated translation in z-axis, linear acceleration, Euler angles. Visible drift and deviations are sufficiently small.

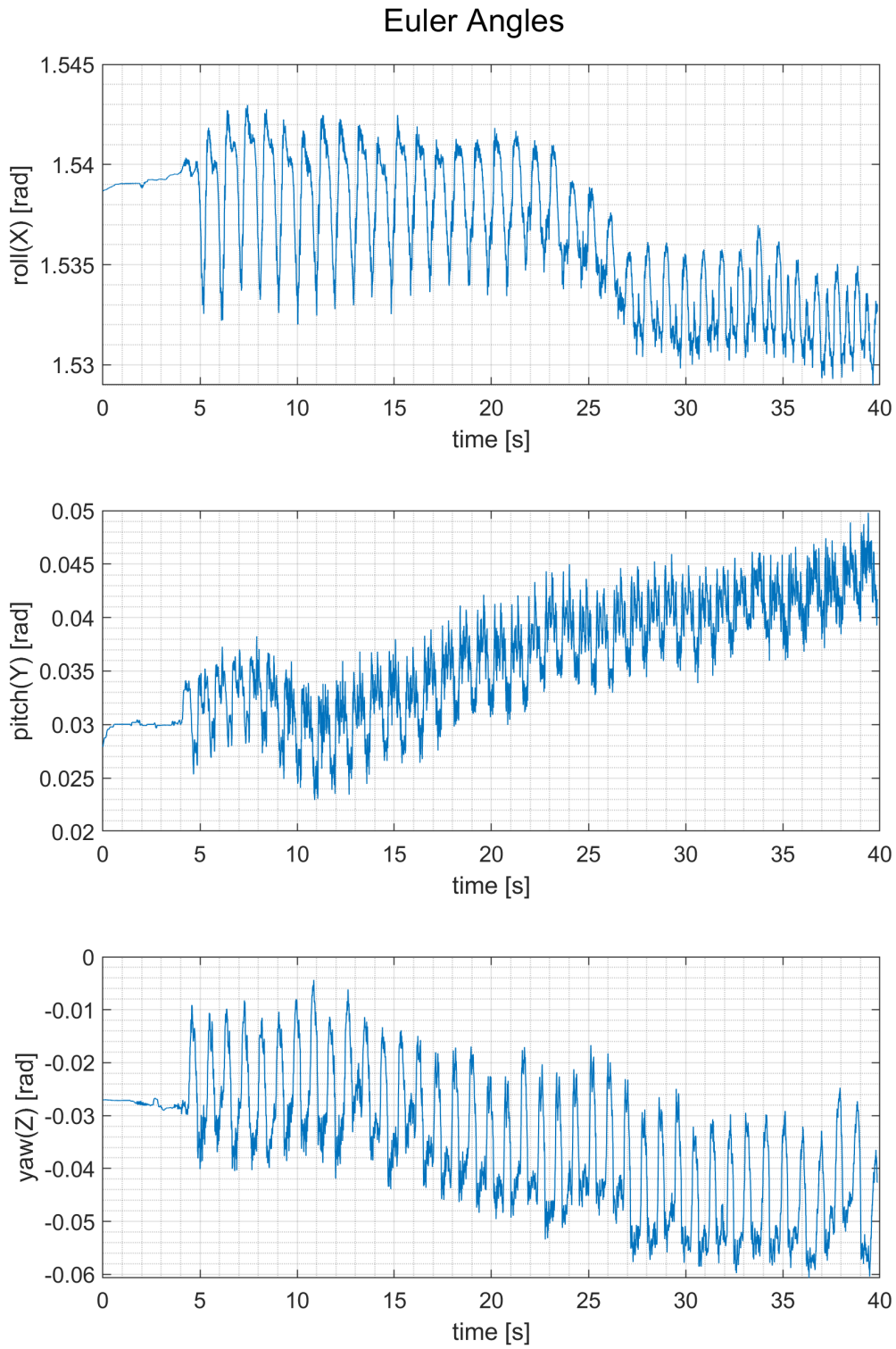

Figure A.45: MMR IMU experiment, harmonic motion in z-axis (fast), linear acceleration, Euler angles. Visible drift and deviations are sufficiently small.

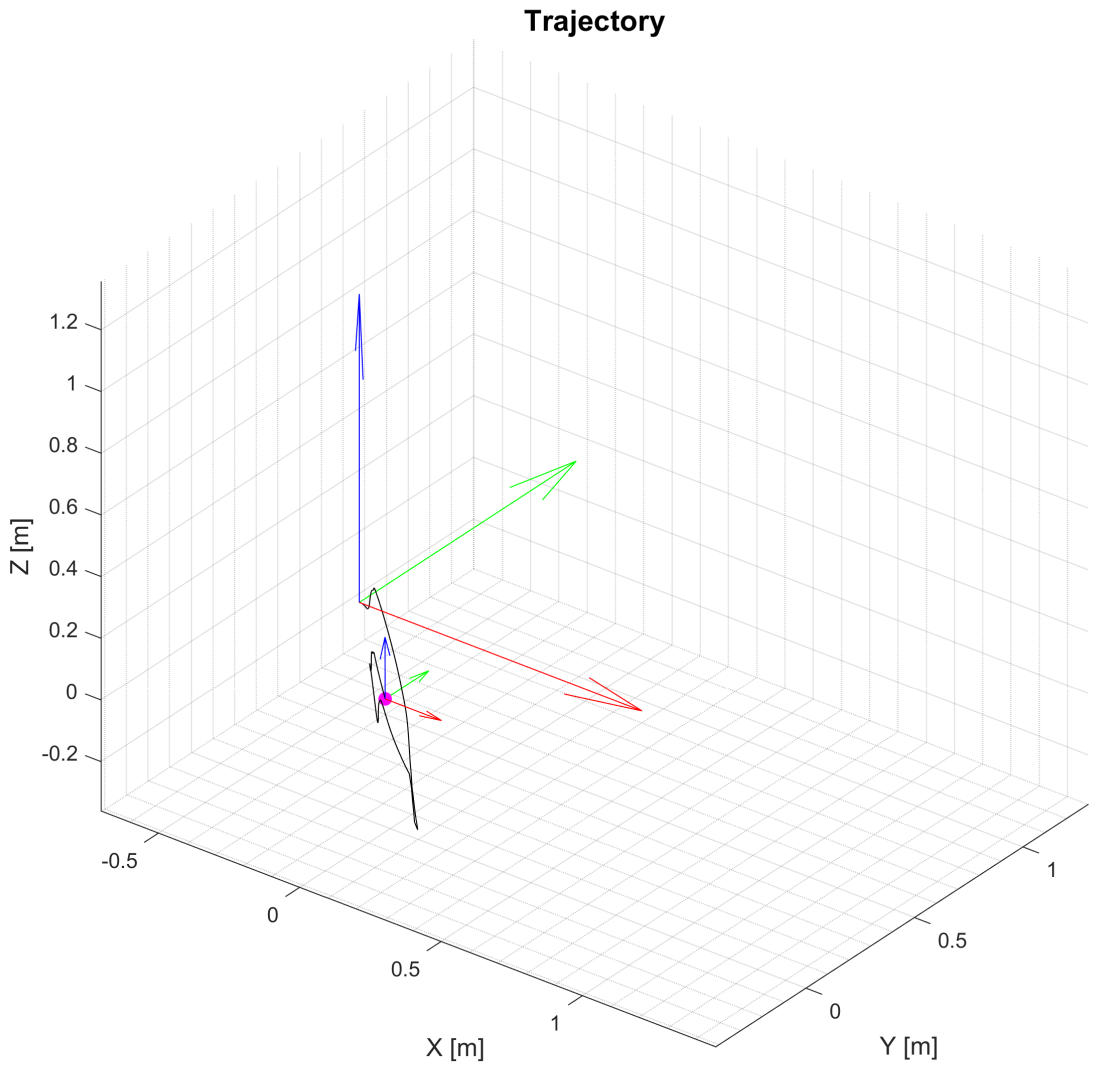

Figure A.46: MMR IMU experiment, repeated translation in z-axis, calibrated linear acceleration, traveled trajectory. Even when filtered, the trajectory does not reflect real motion.

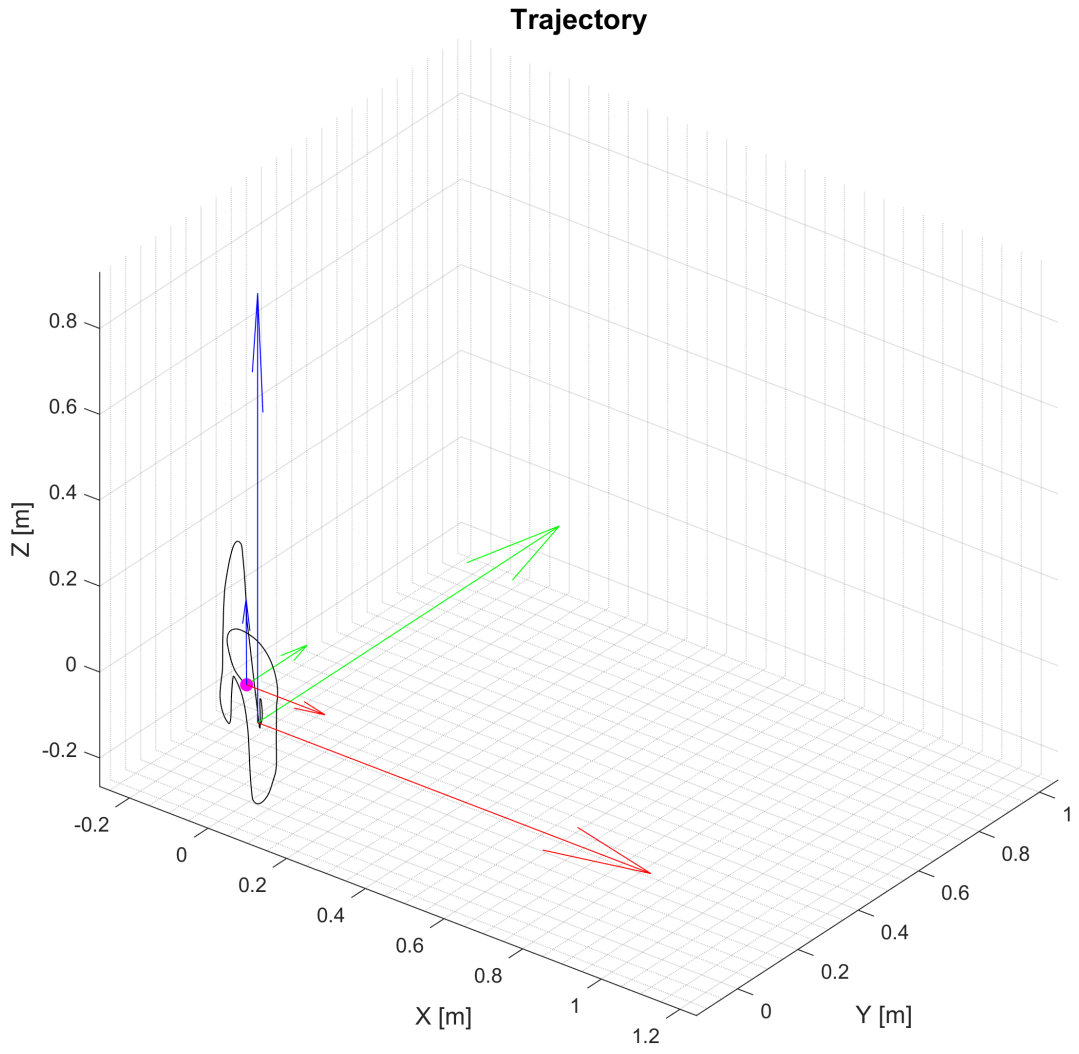

Figure A.47: MMR IMU experiment, repeated translation in z-axis, not calibrated linear acceleration, traveled trajectory. Even when filtered, the trajectory does not reflect real motion.

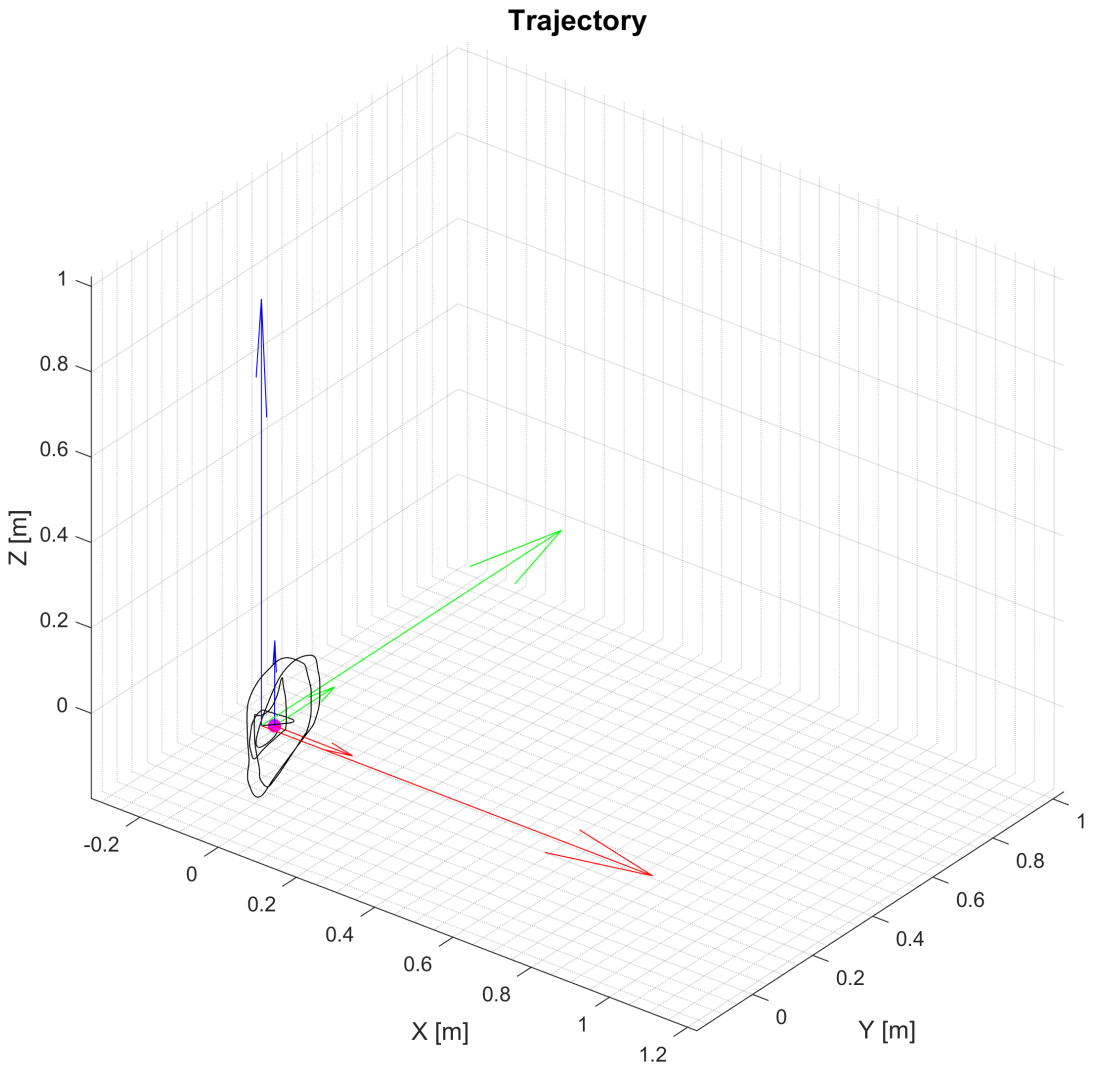

Figure A.48: MMR IMU experiment, repeated translation in z-axis, raw acceleration, traveled trajectory. Even when filtered, the trajectory does not reflect real motion.

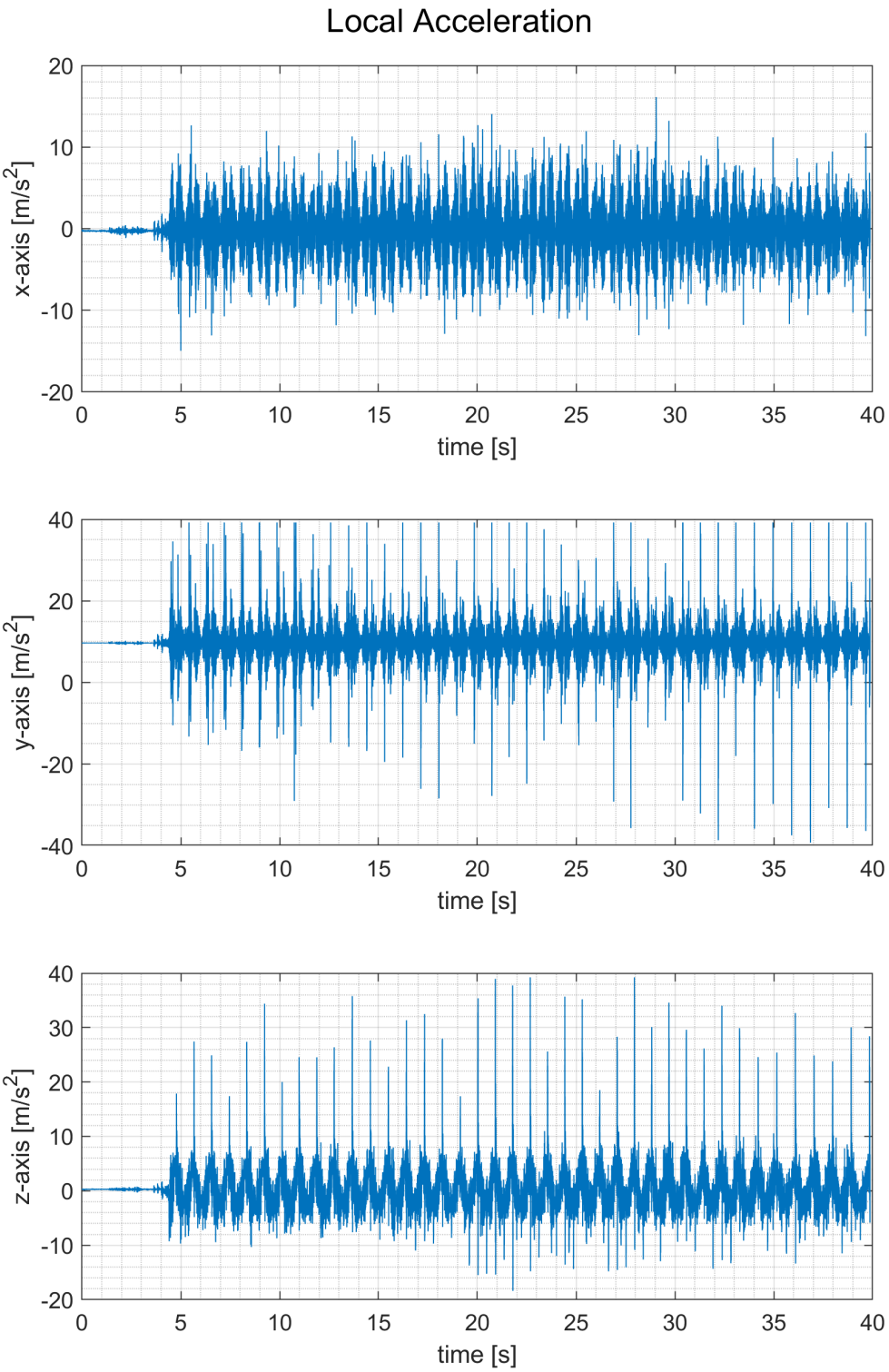

Figure A.49: MMR IMU experiment, harmonic motion in z-axis (slow), raw acceleration, local acceleration.

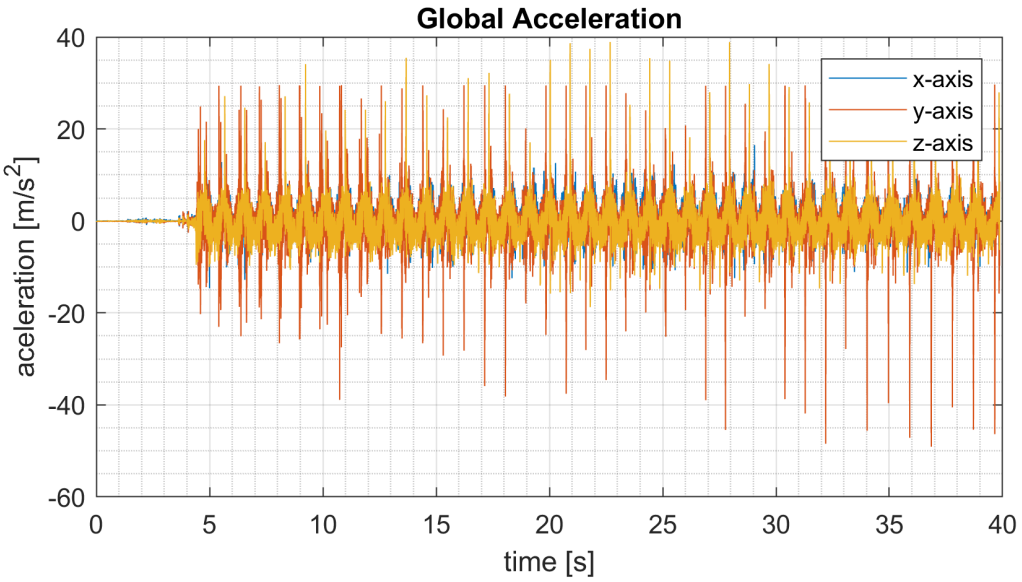

Figure A.50: MMR IMU experiment, harmonic motion in z-axis (slow), raw acceleration, global acceleration.

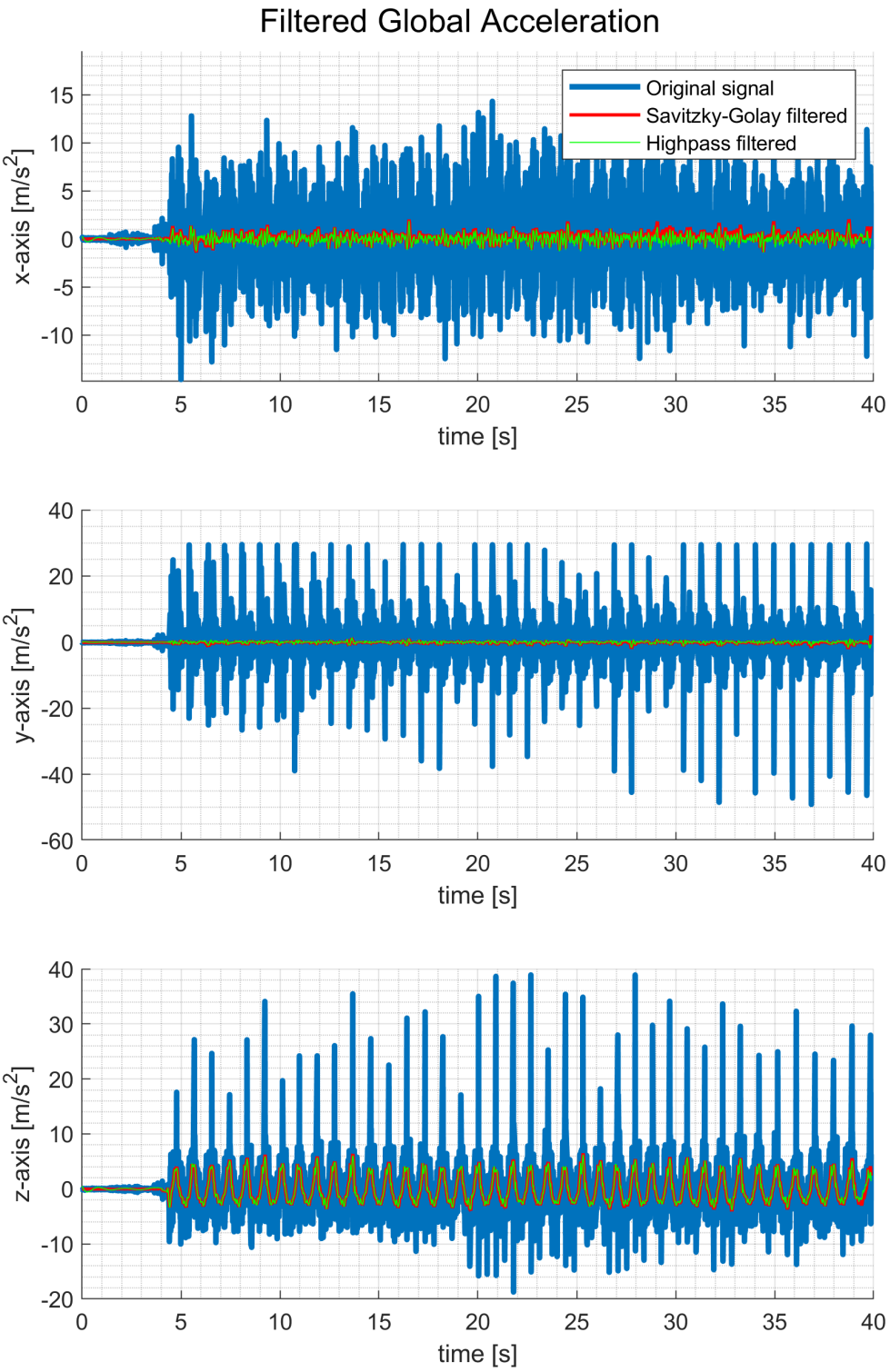

Figure A.51: MMR IMU experiment, harmonic motion in z-axis (slow), raw acceleration, global acceleration. Undesirable oscillation in x- and y-axis is visible, possibly filtered out.

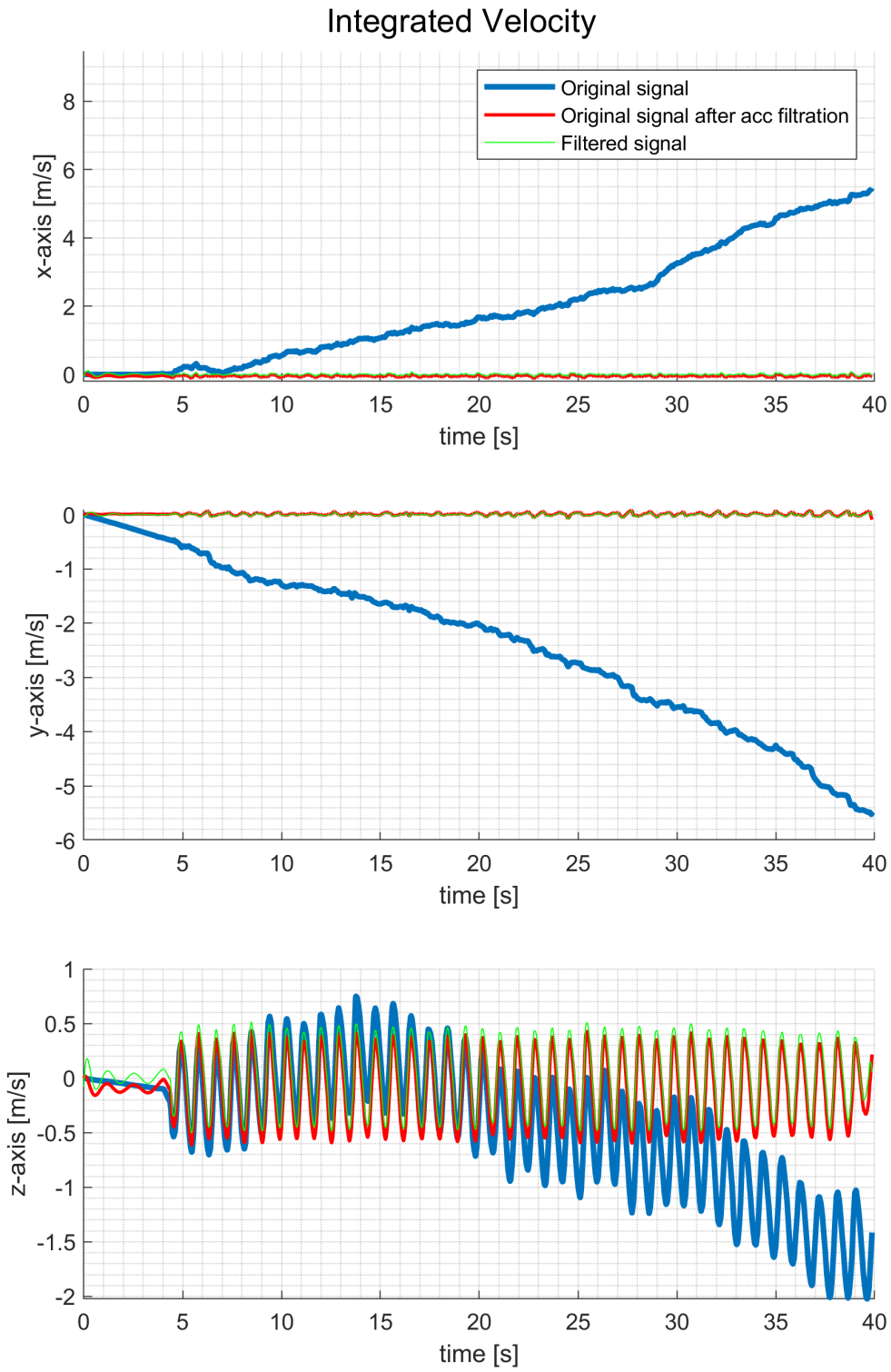

Figure A.52: MMR IMU experiment, harmonic motion in z-axis (slow), raw acceleration, velocity. Original signal diverges, but can be filtered out to show expected values.

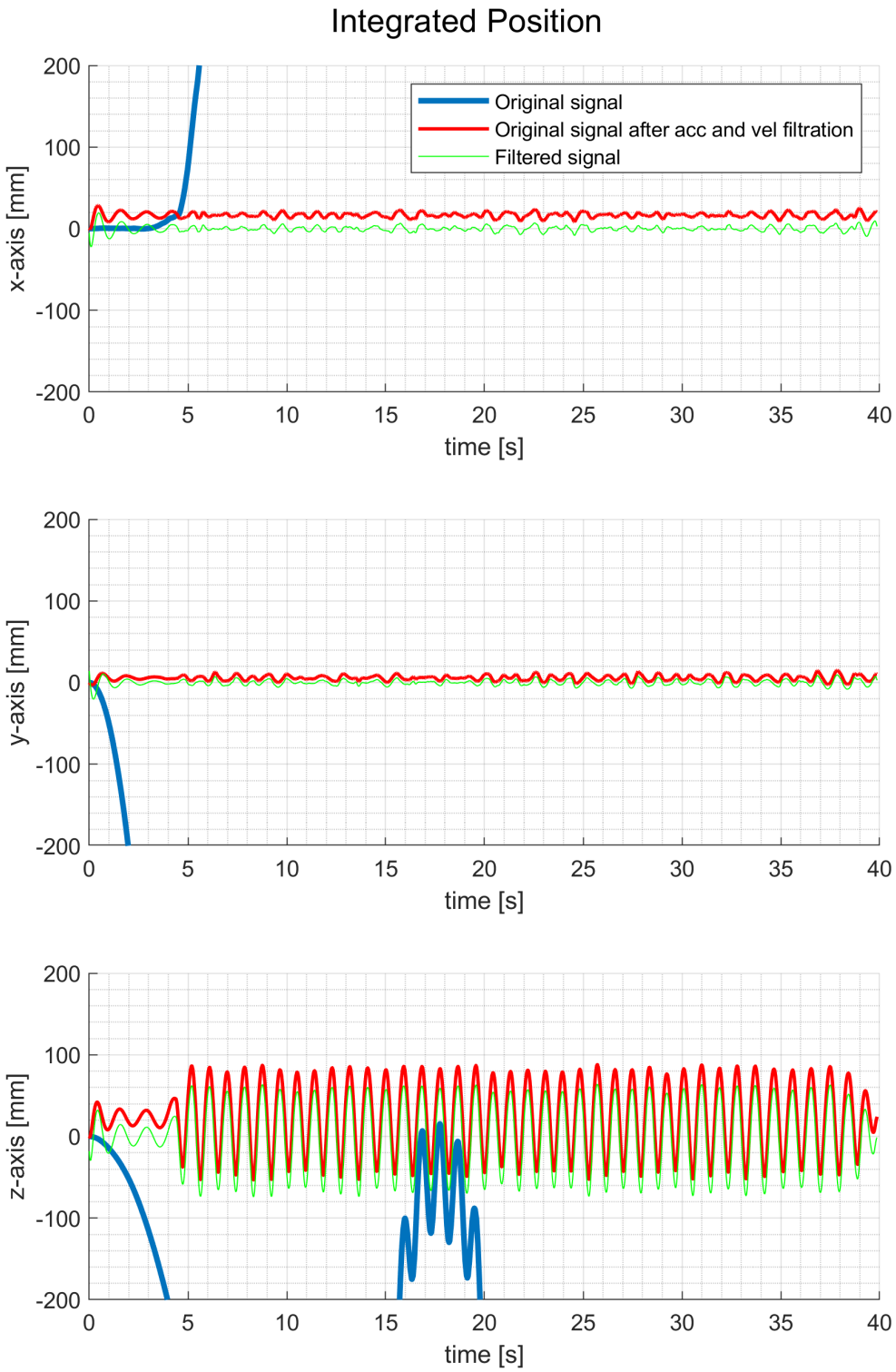

Figure A.53: MMR IMU experiment, harmonic motion in z-axis (slow), raw acceleration, position. Original signal diverges, but can be filtered out to show expected values.

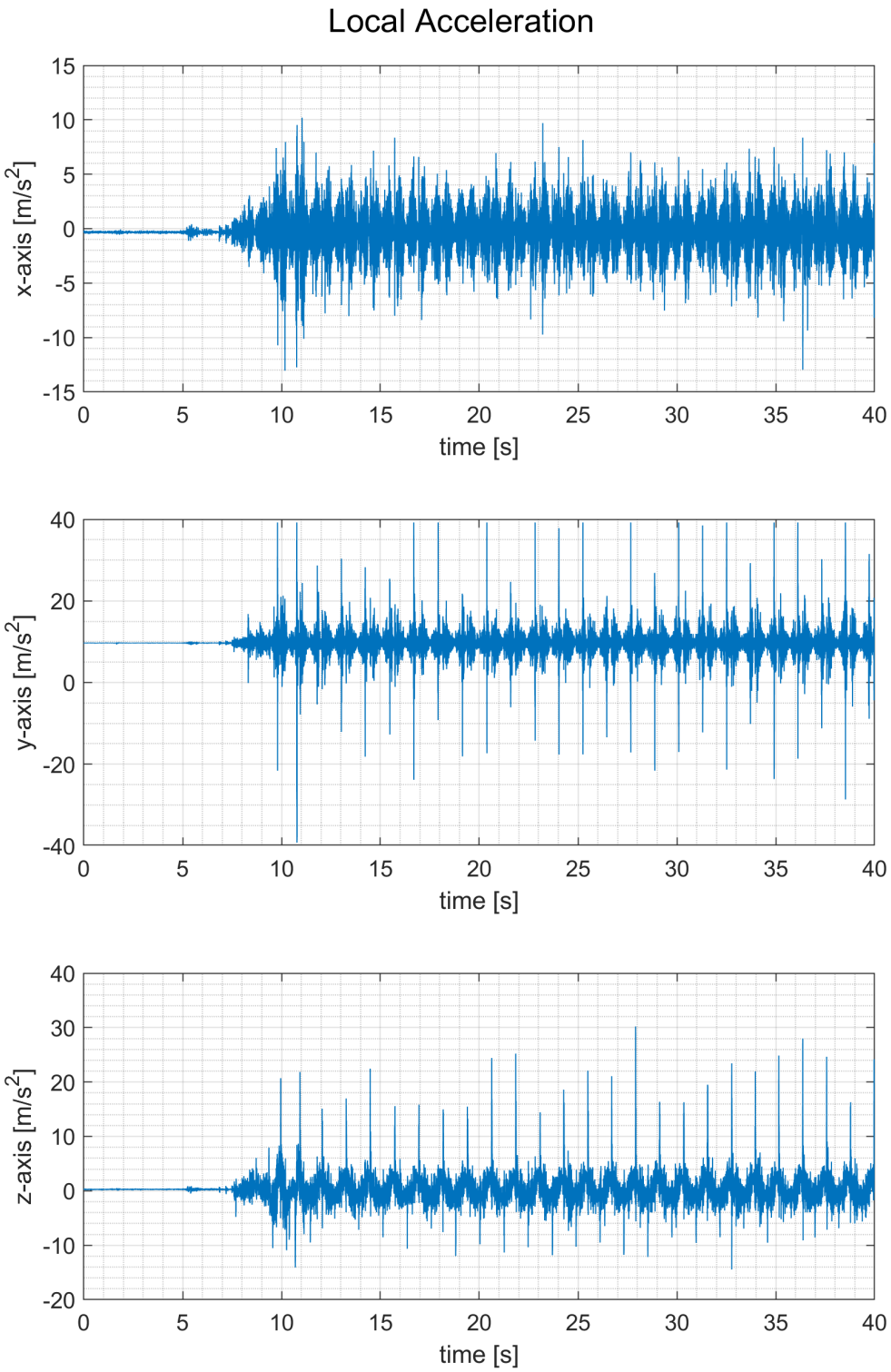

Figure A.54: MMR IMU experiment, harmonic motion in z-axis (fast), raw acceleration, local acceleration.

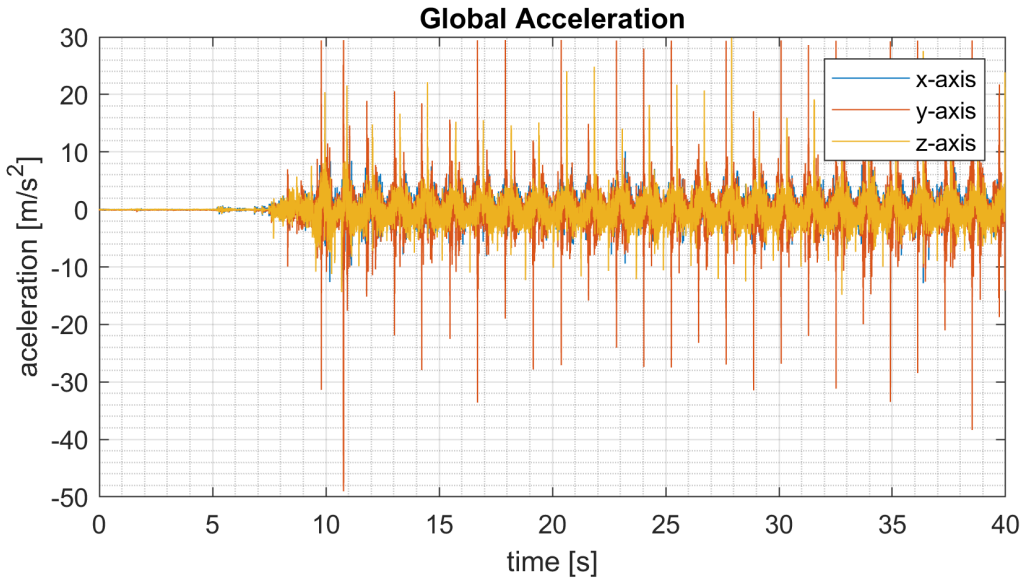

Figure A.55: MMR IMU experiment, harmonic motion in z-axis (fast), raw acceleration, global acceleration.

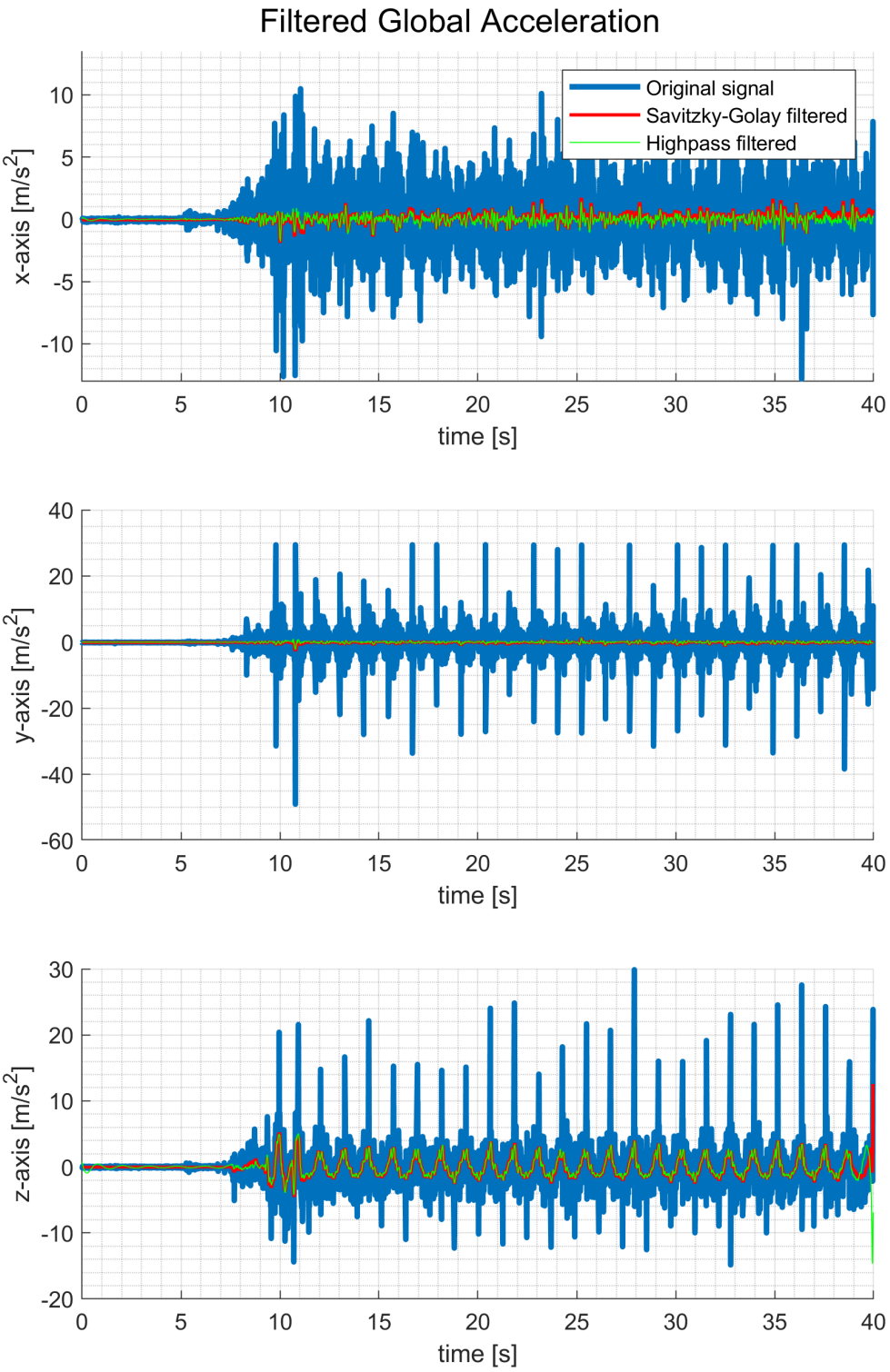

Figure A.56: MMR IMU experiment, harmonic motion in z-axis (fast), raw acceleration, global acceleration. Undesirable oscillation in x- and y-axis is visible, possibly filtered out.

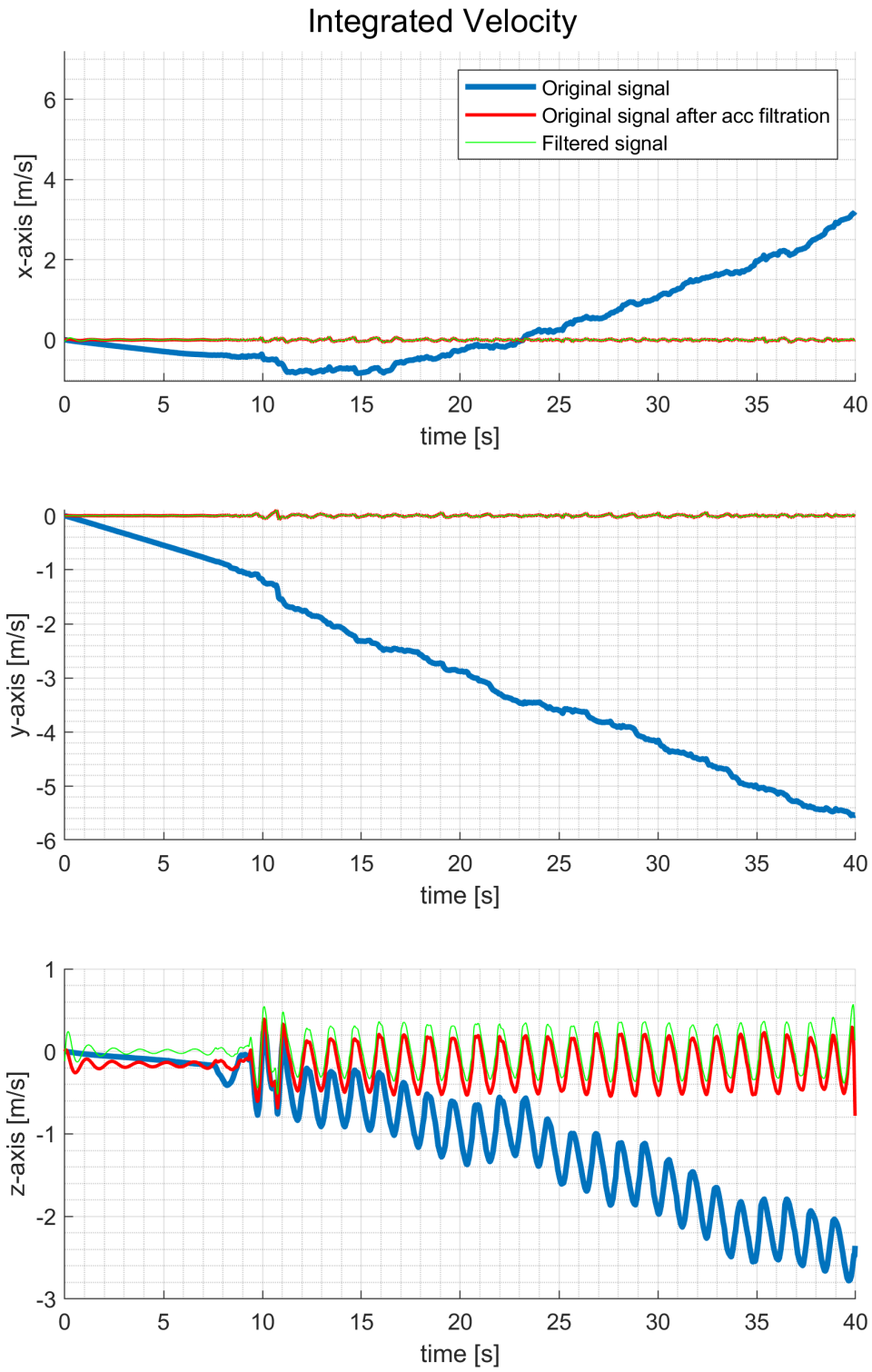

Figure A.57: MMR IMU experiment, harmonic motion in z-axis (fast), raw acceleration, velocity. Original signal diverges, but can be filtered out to show expected values.

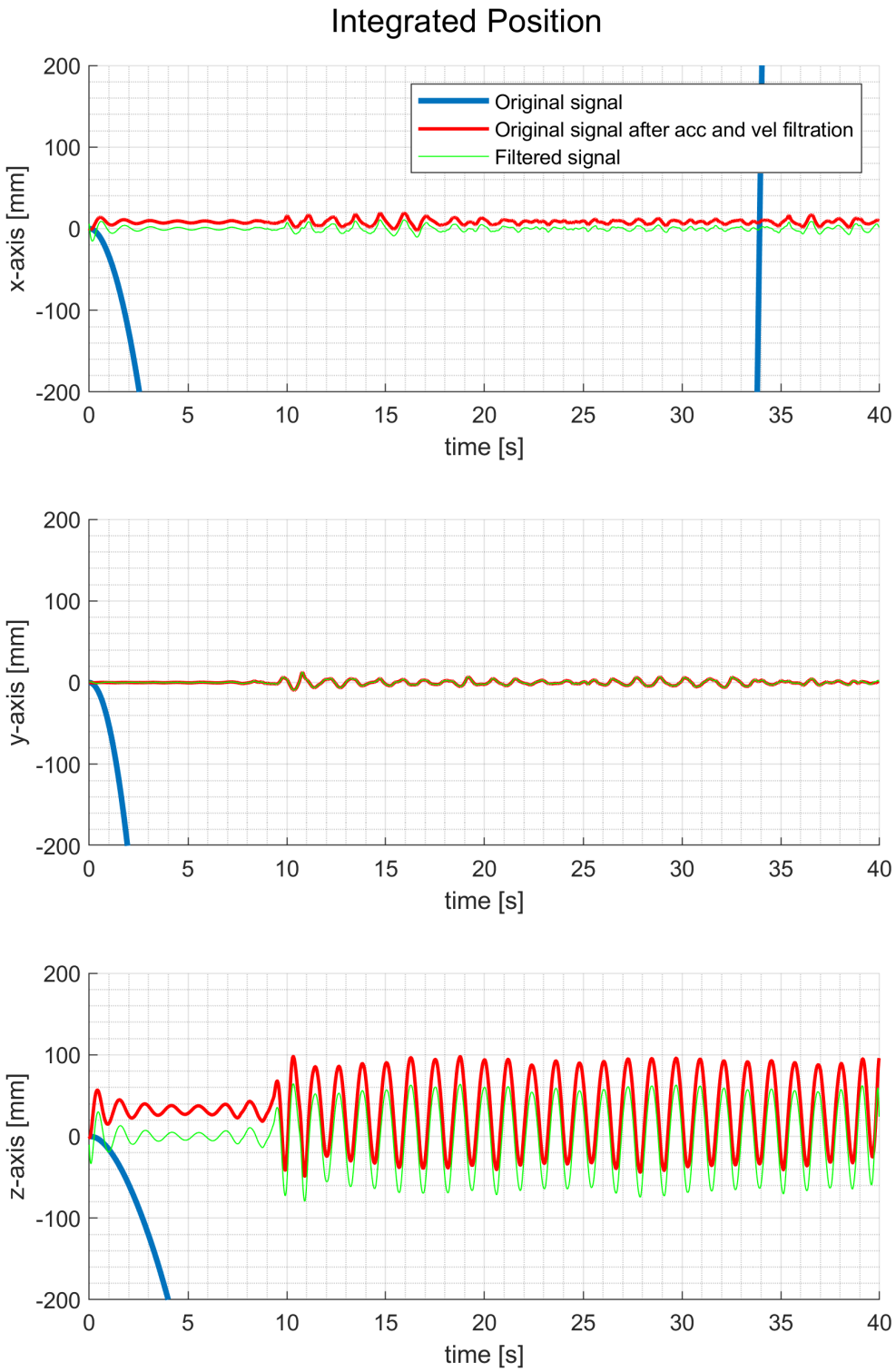

Figure A.58: MMR IMU experiment, harmonic motion in z-axis (fast), raw acceleration, position. Original signal diverges, but can be filtered out to show expected values.

A.3 T 265 tracking camera

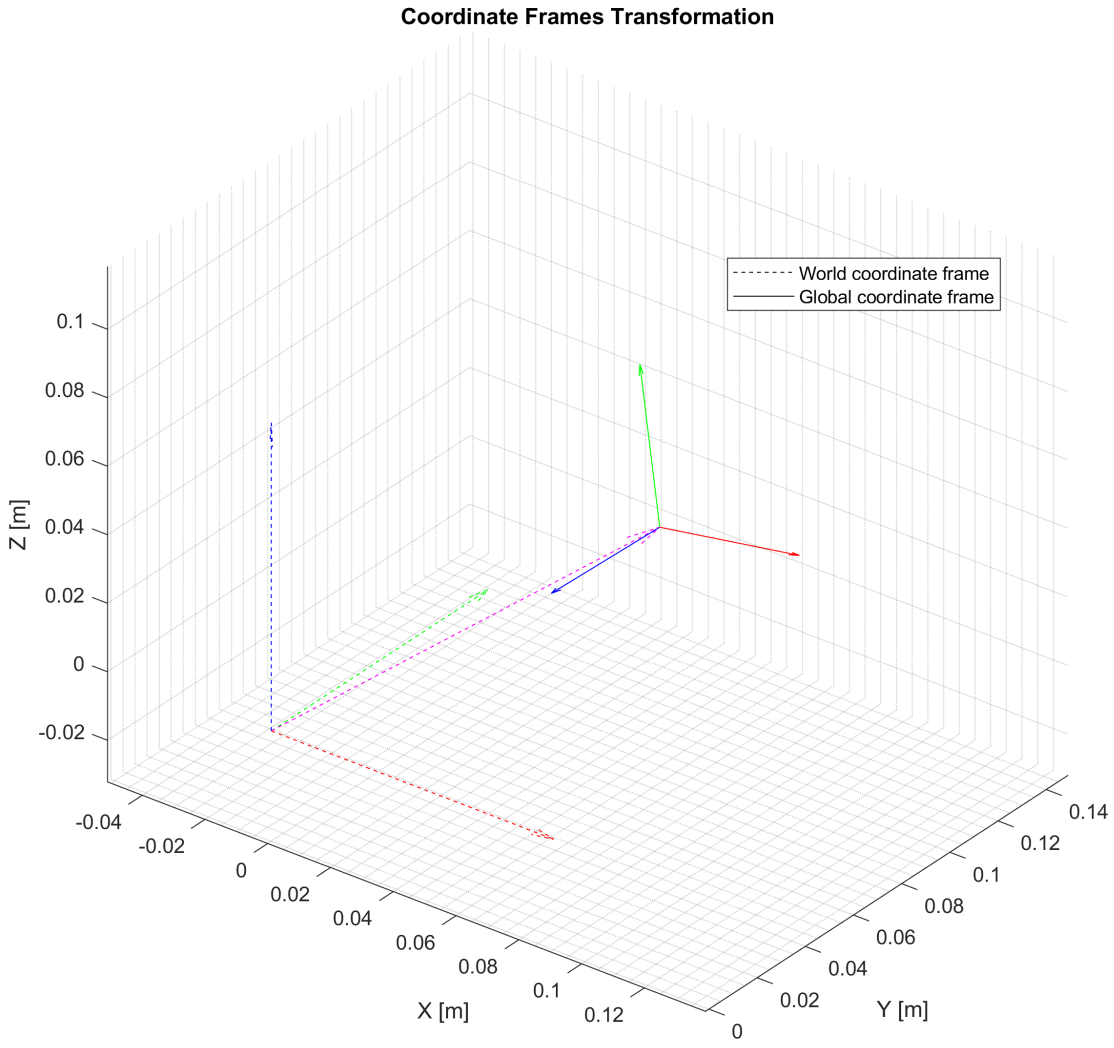

Figure A.59: RealSense T265 experiment, transformation of coordinate frames.

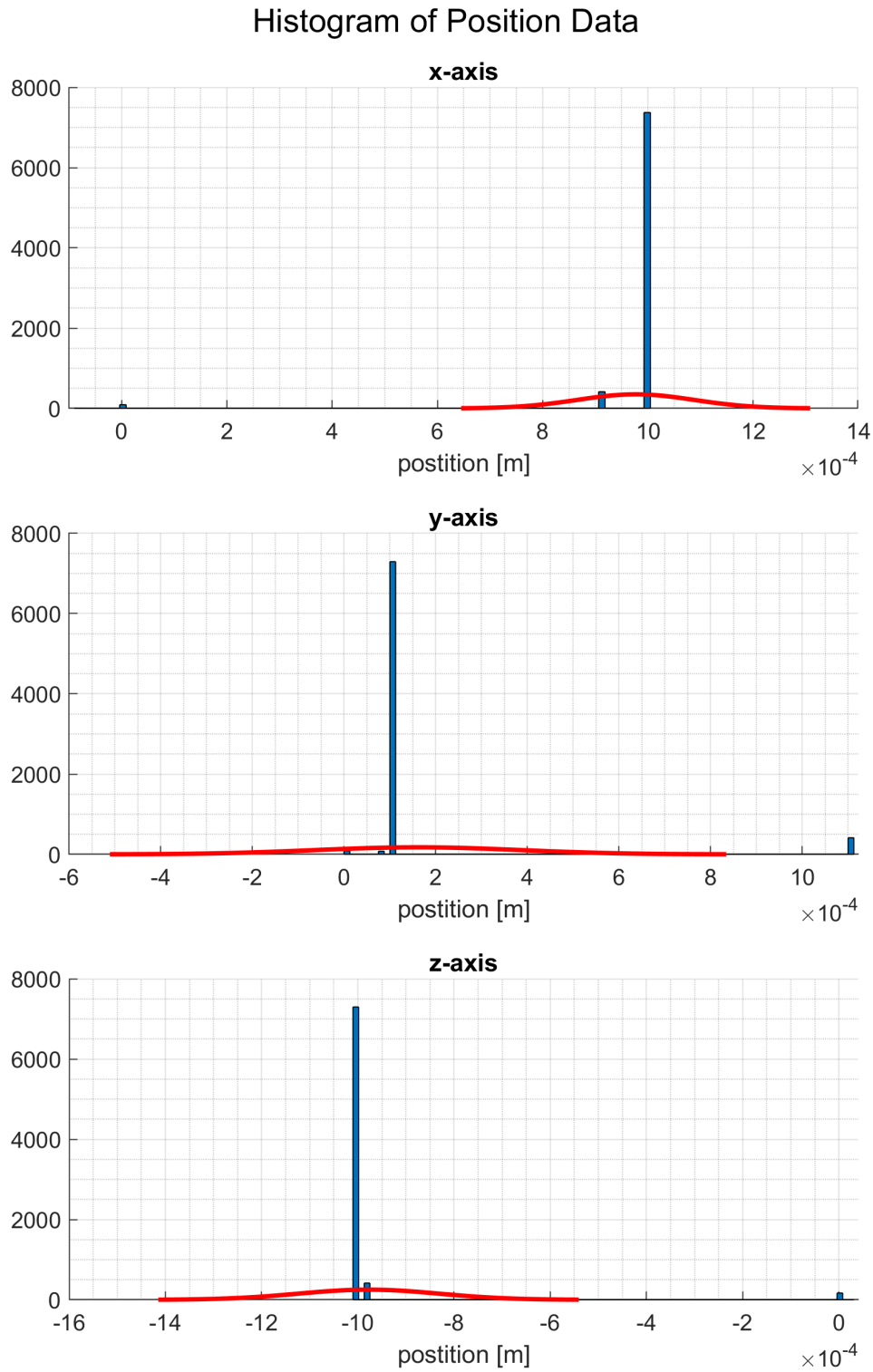

Figure A.60: RealSense T265 experiment, steady state, histogram with Gaussian fit. Offset is visible but sufficiently small, no noise distribution is shown.

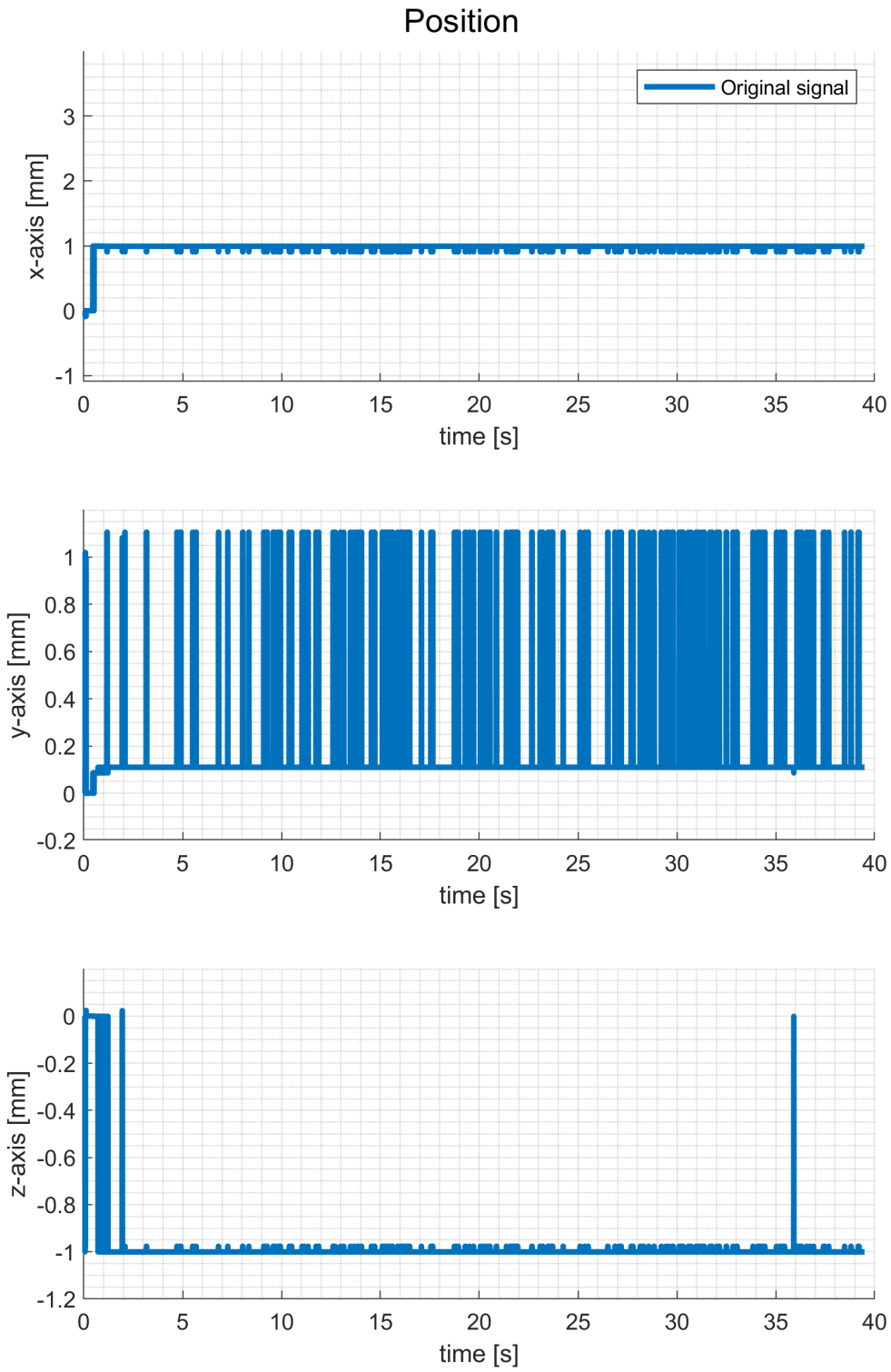

Figure A.61: RealSense T265 experiment, steady state, position. The measured data are stable in sufficient range.

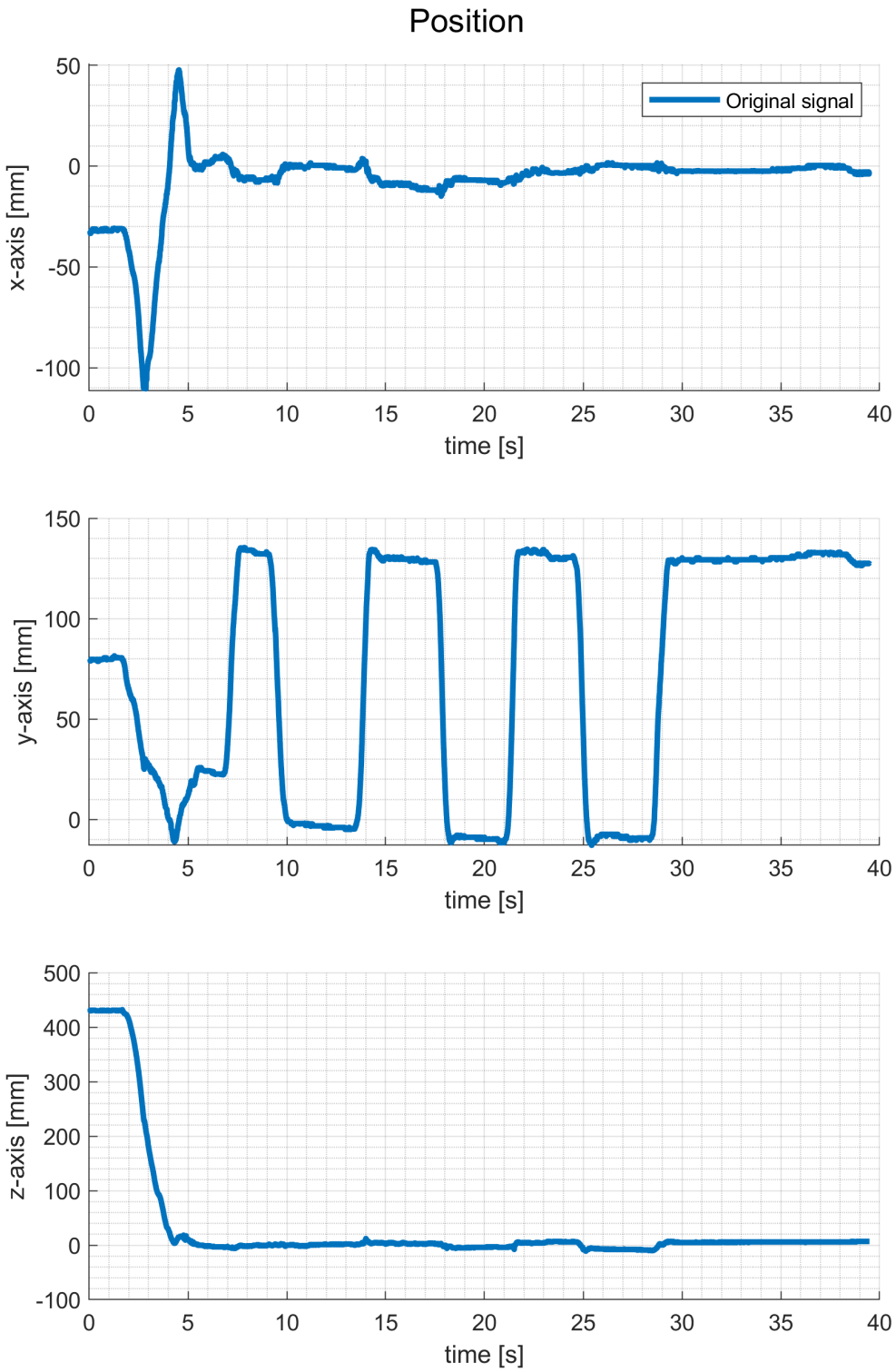

Figure A.62: RealSense T265 experiment, repeated translation in y-axis, position. With coordinate frames initialization part.

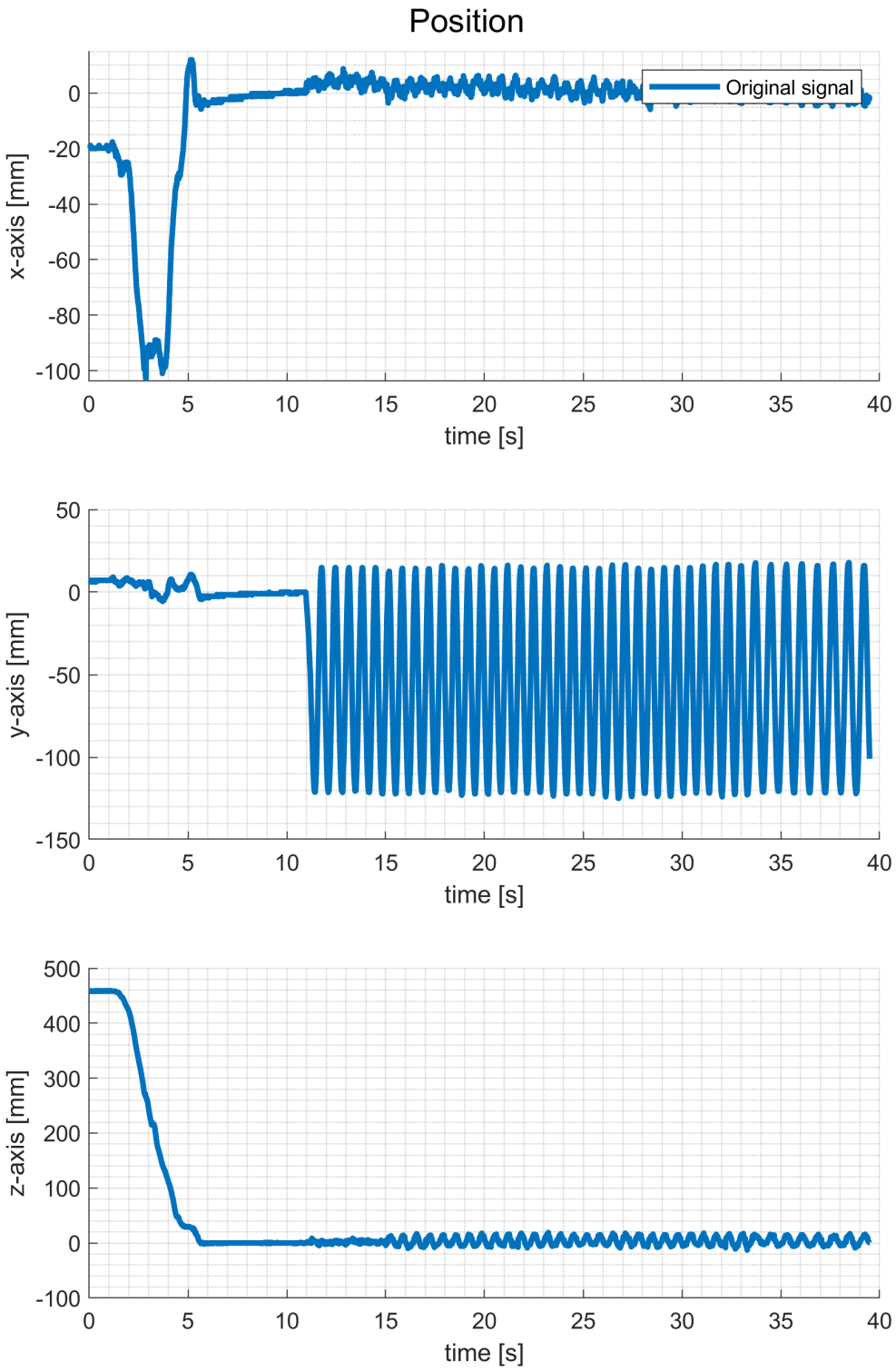

Figure A.63: RealSense T265 experiment, harmonic motion in y-axis (fast), position. With coordinate frames initialization part. Data resemble expected values.

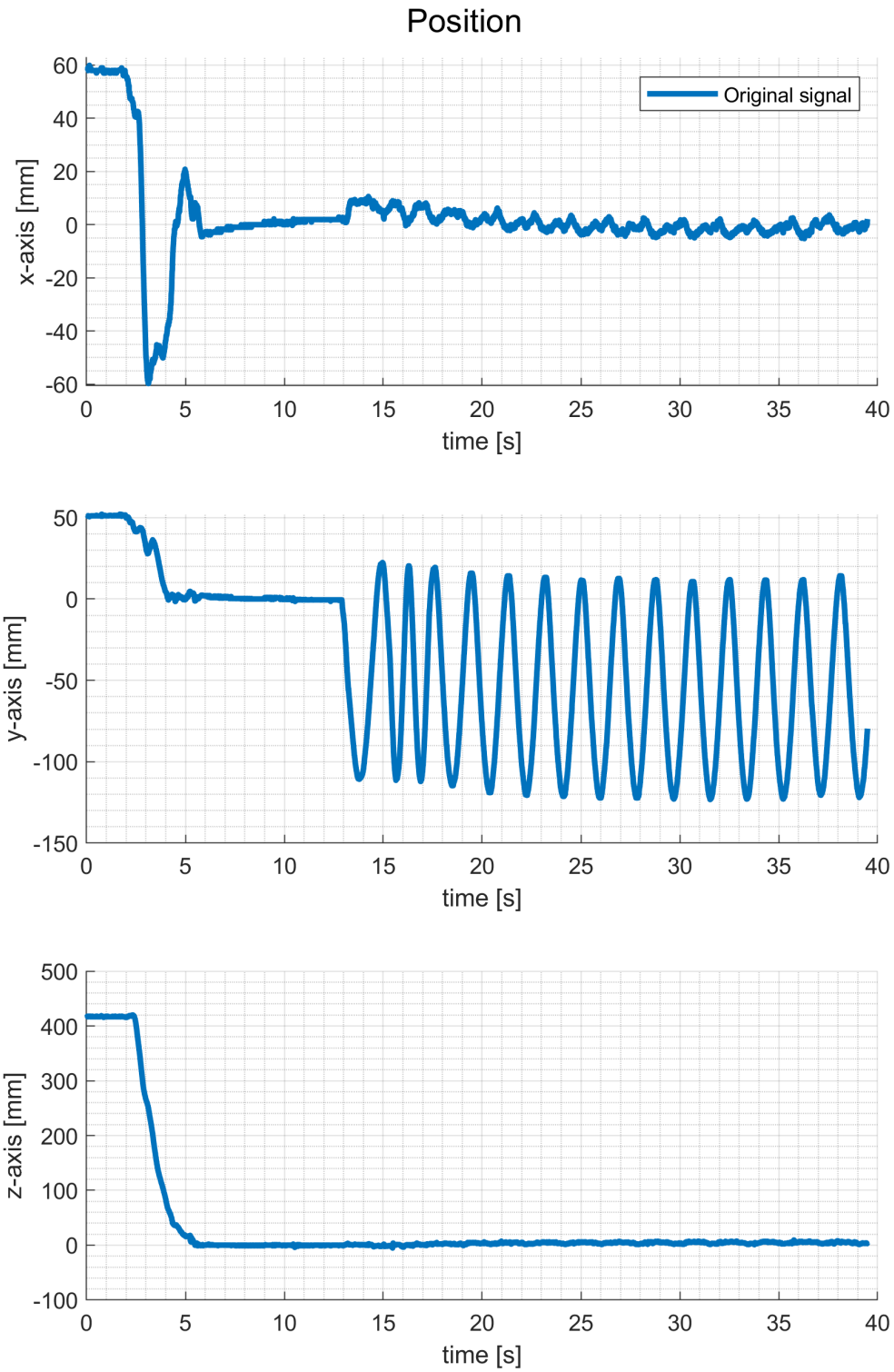

Figure A.64: RealSense T265 experiment, harmonic motion in y-axis (slow), position. With coordinate frames initialization part. Data resemble expected values.

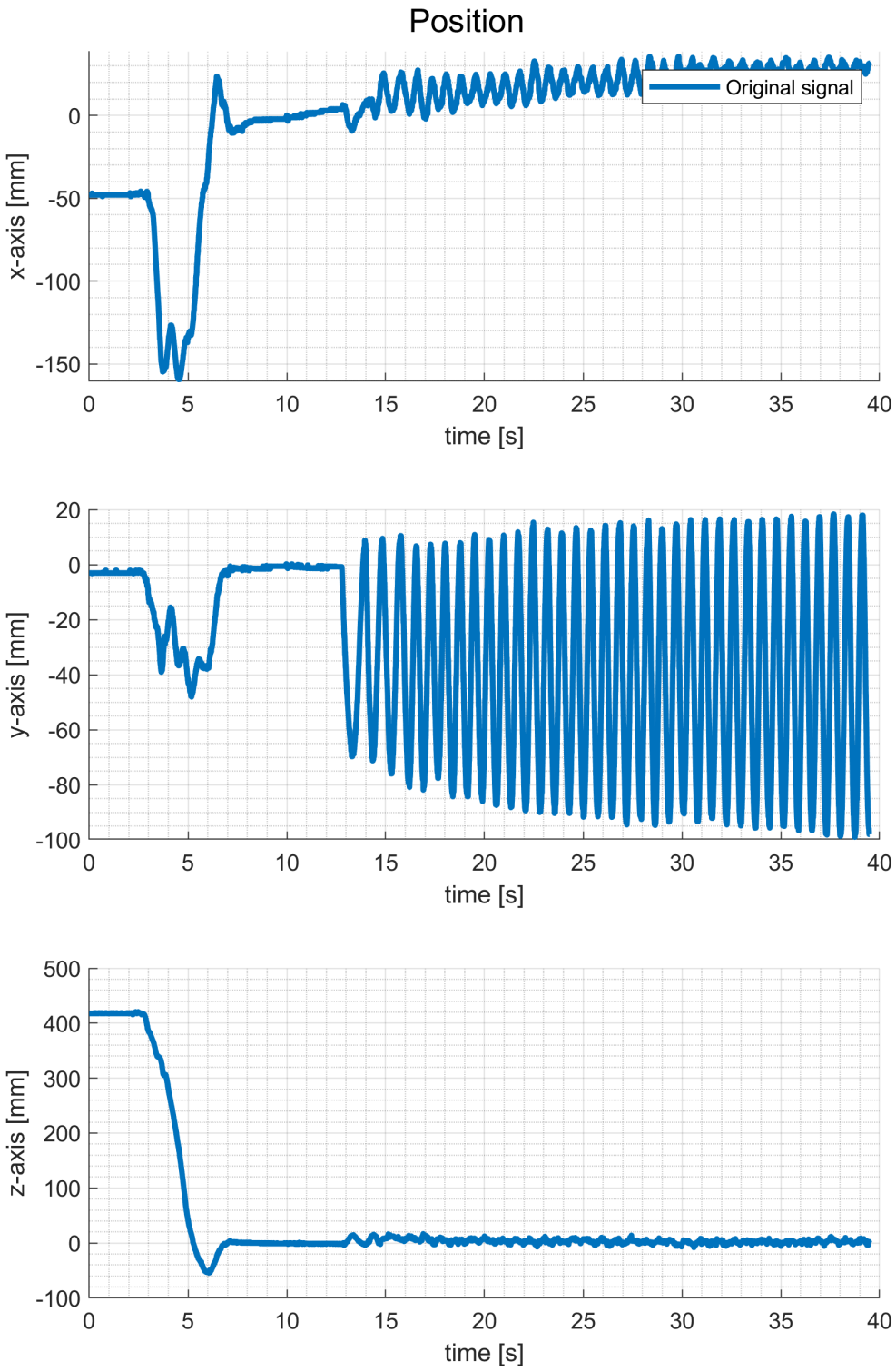

Figure A.65: RealSense T265 experiment, harmonic motion in y-axis (fast), position. With coordinate frames initialization part. Data resemble expected values, but with an observable drift.

A.4 MMR IMU sensor and T265 tracking camera

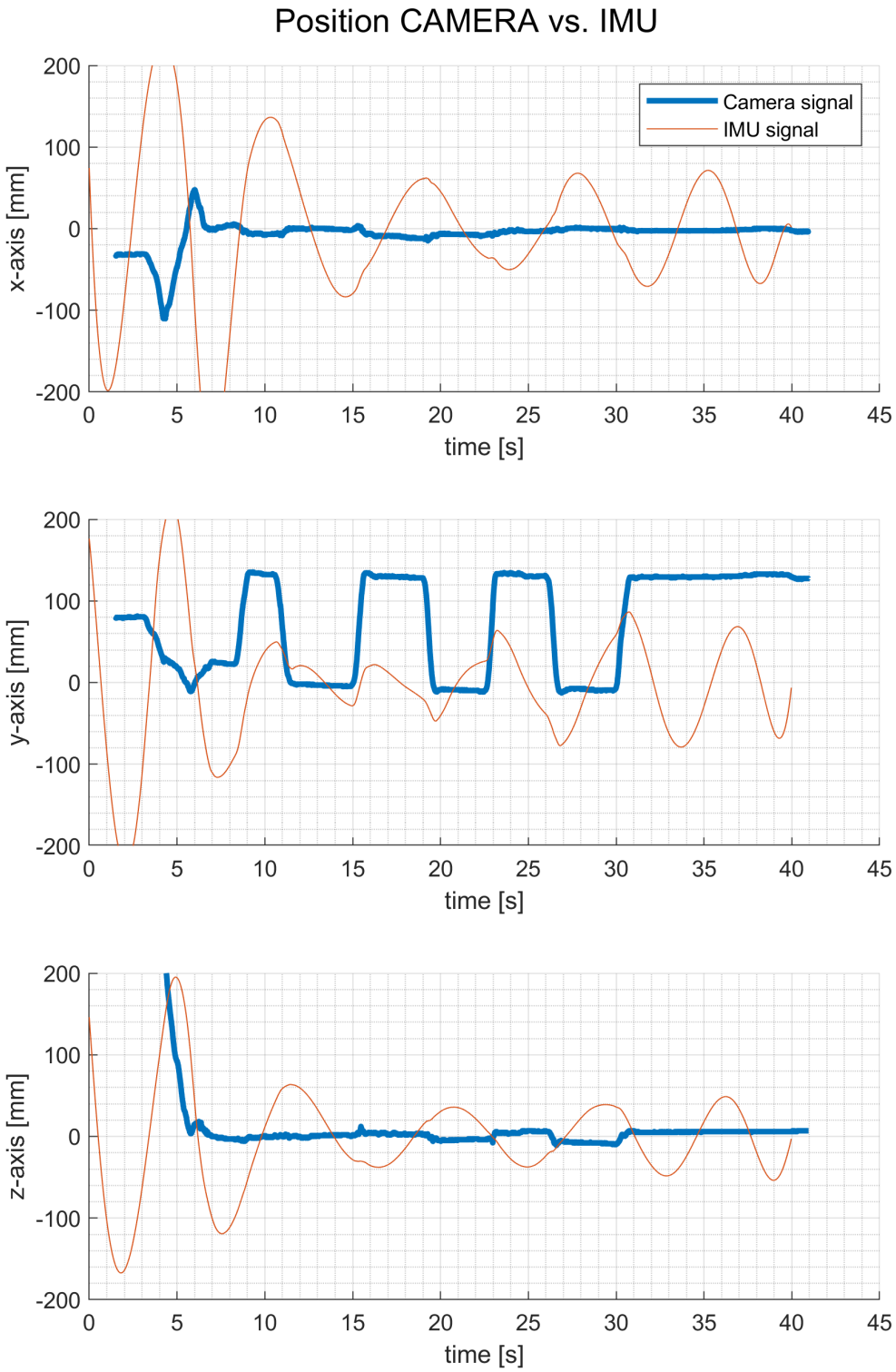

Figure A.66: MMR IMU and RealSense T265 experiment, repeated translation in y-axis, position. T265 shows expected data, MMR follows them only inaccurately.

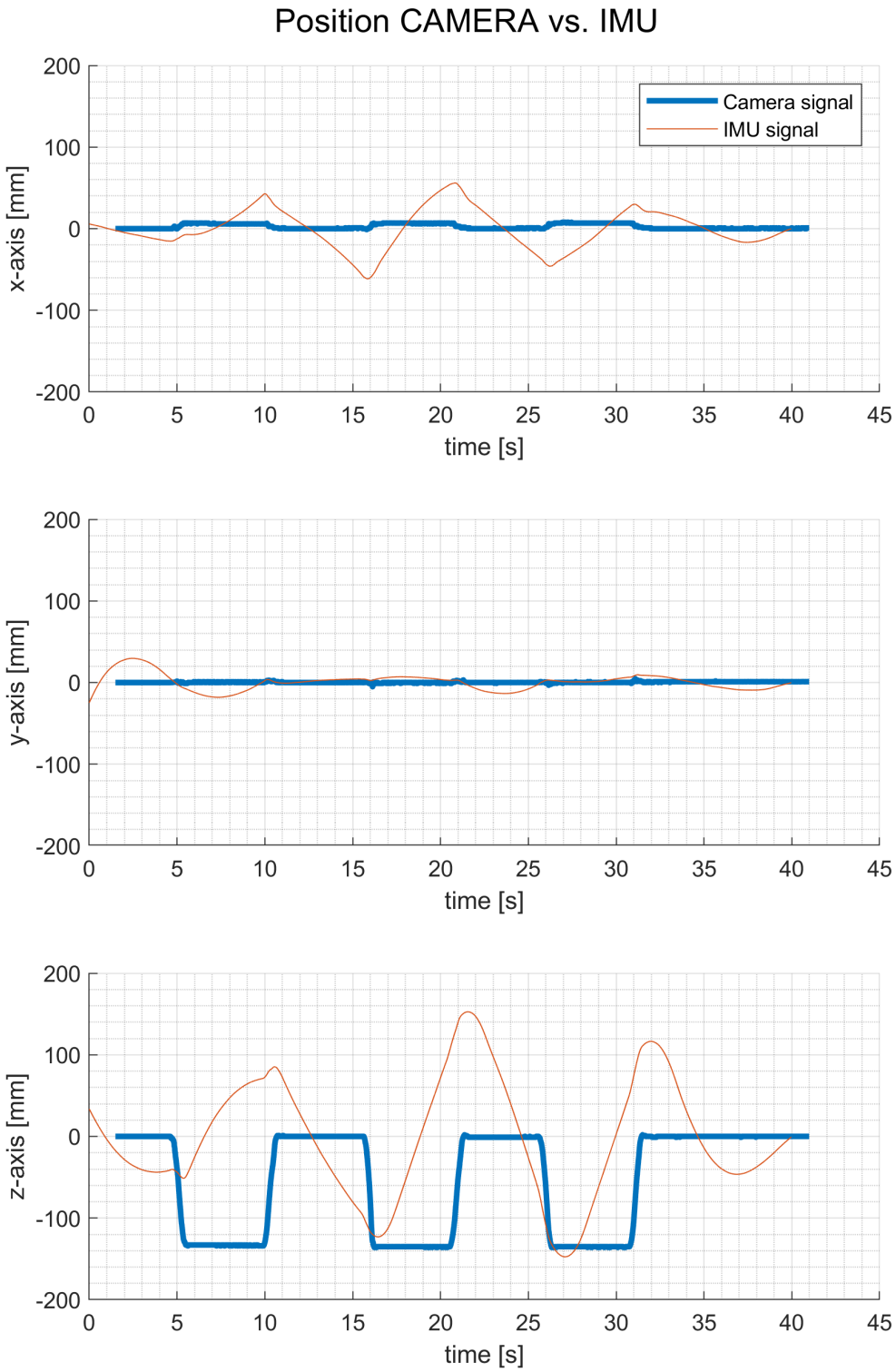

Figure A.67: MMR IMU and RealSense T265 experiment, translation in z-axis, position. T265 shows expected data, MMR follows them only inaccurately.

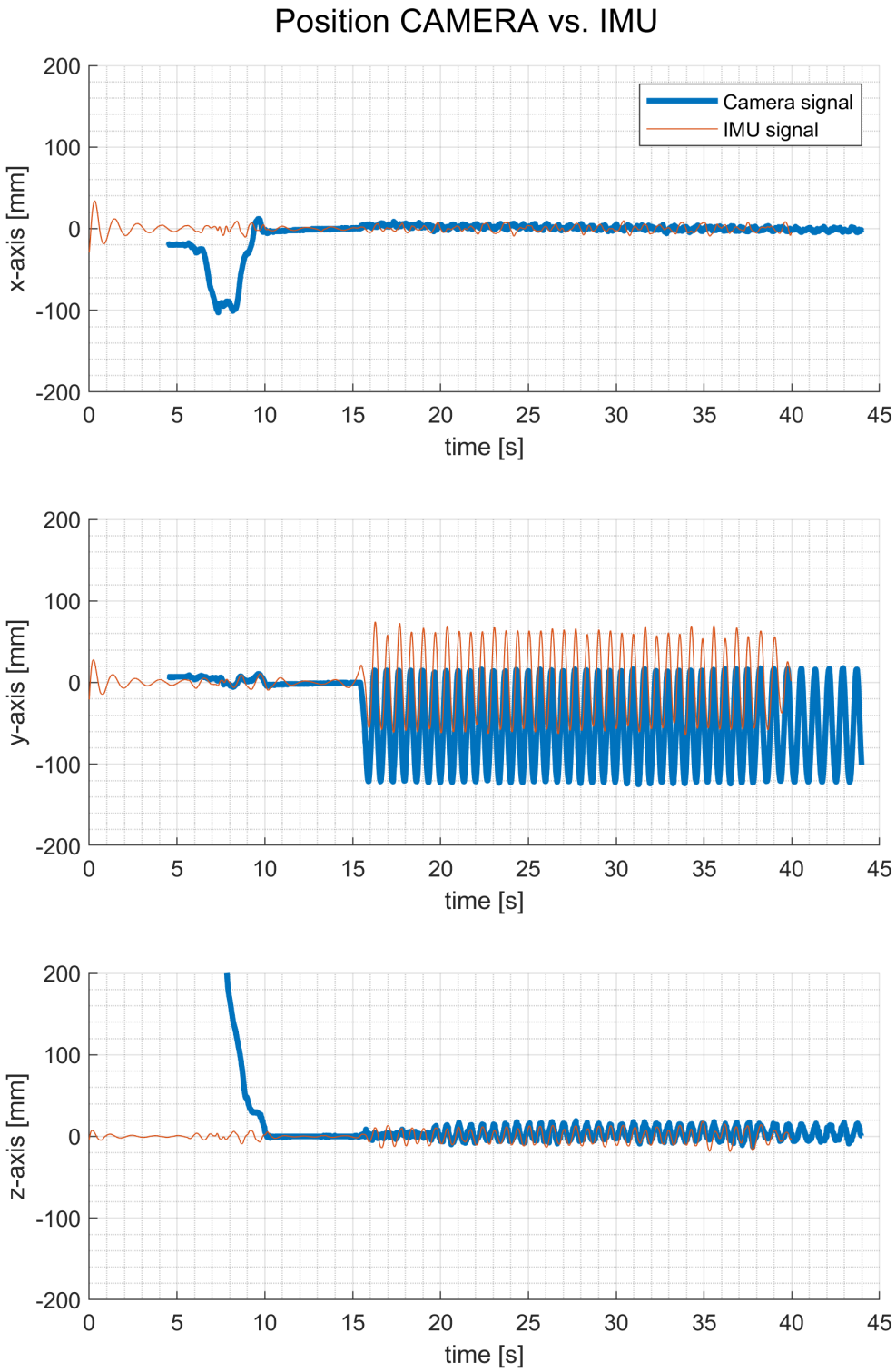

Figure A.68: MMR IMU and RealSense T265 experiment, harmonic motion in y-axis (fast), position. T265 shows expected data, MMR follows them only inaccurately, with offset.

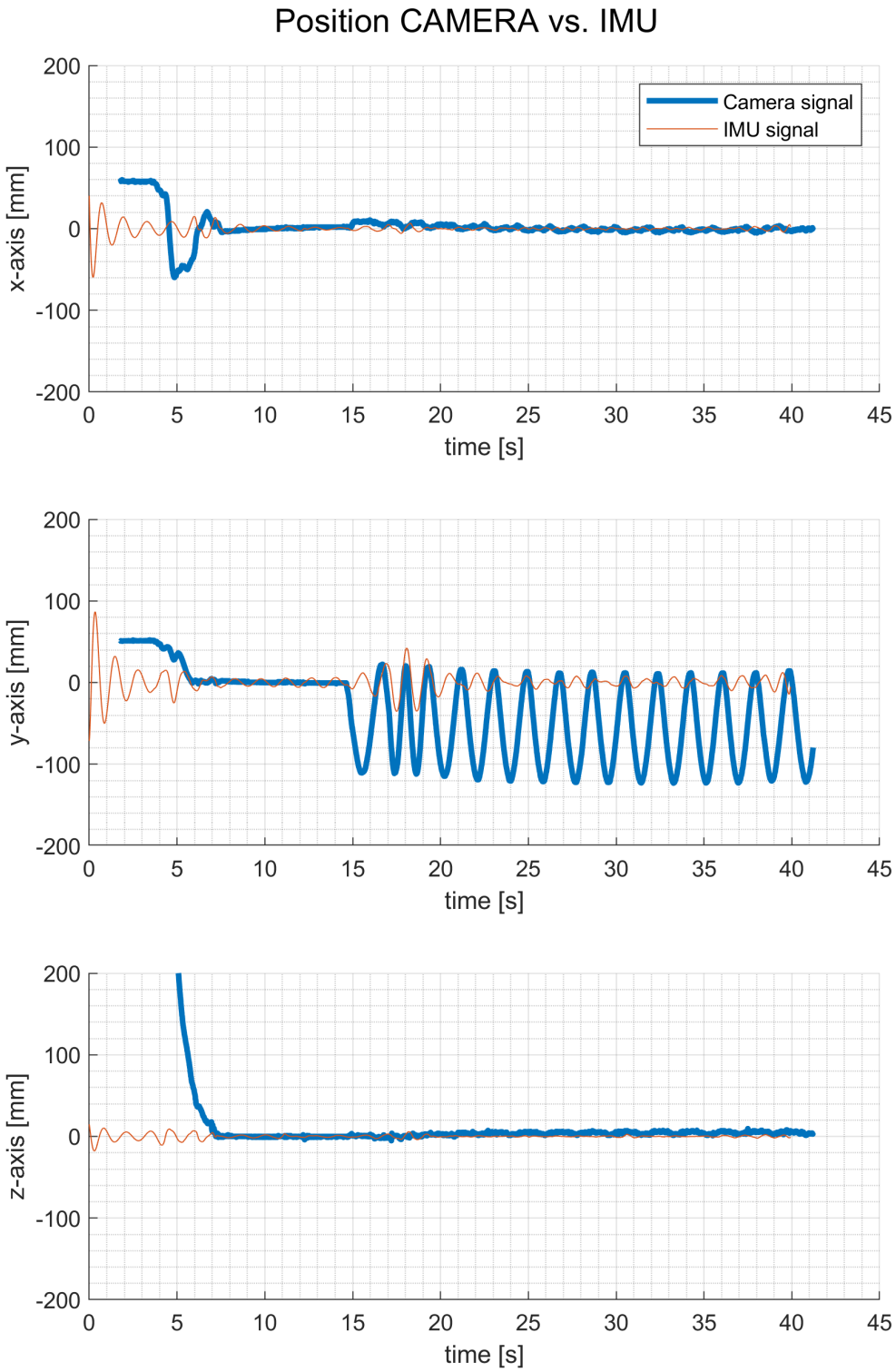

Figure A.69: MMR IMU and RealSense T265 experiment, harmonic motion in y-axis (slow), position. T265 shows expected data, MMR follows them only inaccurately, with offset.

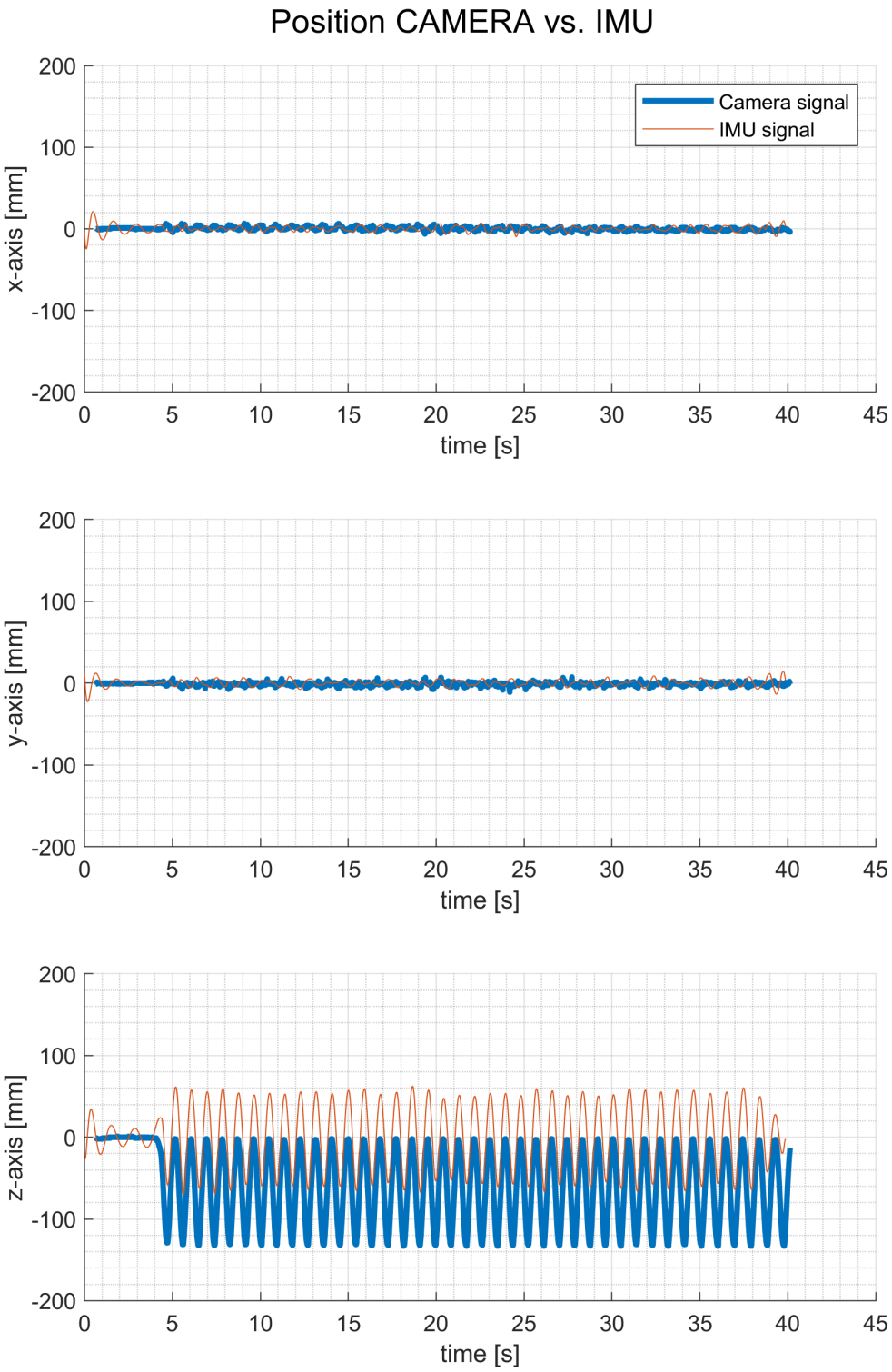

Figure A.70: MMR IMU and RealSense T265 experiment, harmonic motion in z-axis (fast), position. T265 shows expected data, MMR follows them only inaccurately, with offset.

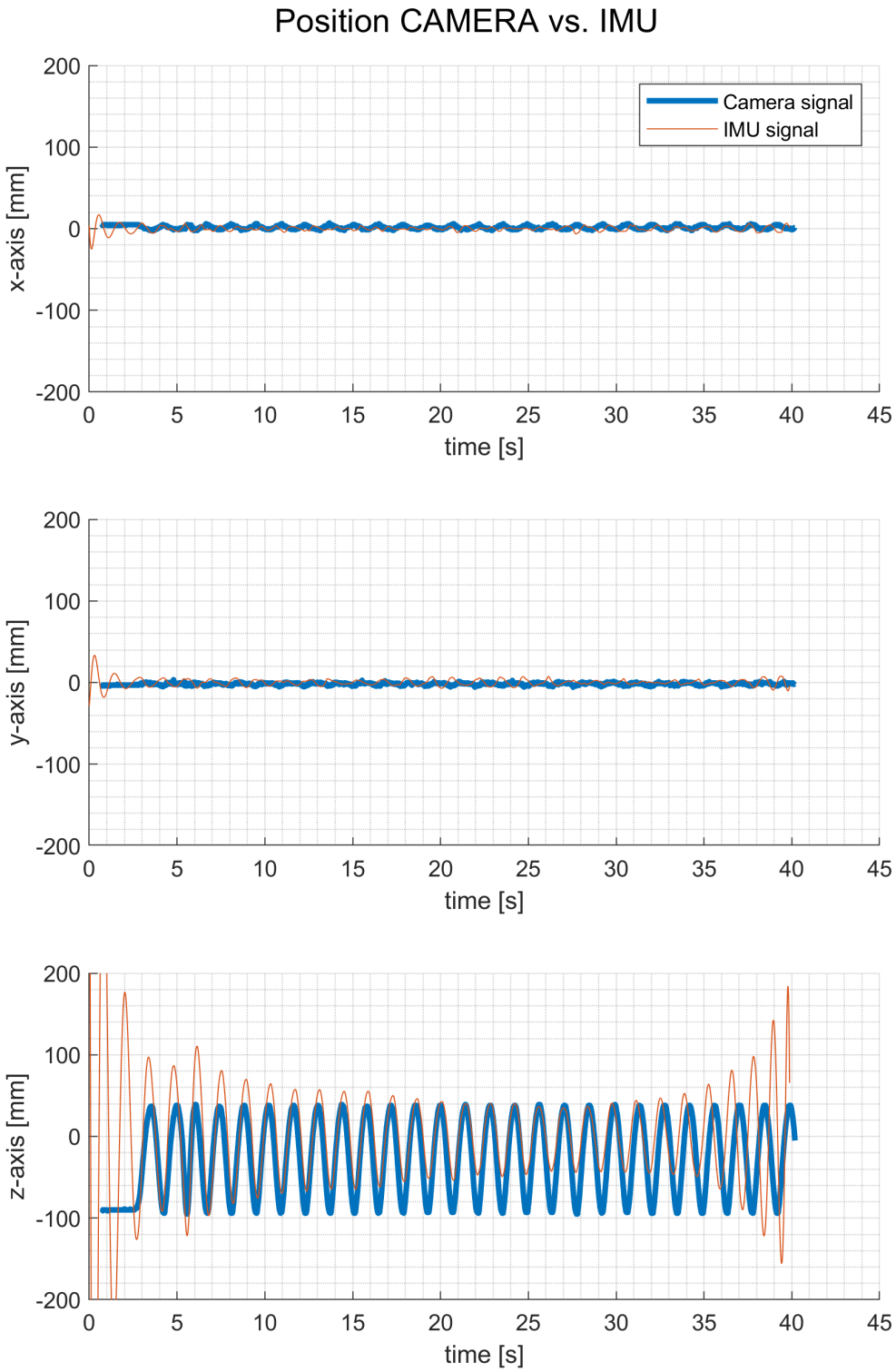

Figure A.71: MMR IMU and RealSense T265 experiment, harmonic motion in z-axis (slow), position. T265 shows expected data, MMR follows them only inaccurately, with offset.